DEVELOPMENT OF MAGNETIC RESONANCE IMAGING BASED DETECTION METHODS FOR BETA AMYLOIDS VIA SIALIC ACID-FUNCTIONALIZED MAGNETIC NANOPARTICLES

By

Hovig Kouyoumdjian

A DISSERTATION

Submitted to
Michigan State University
in partial fulfillment of the requirements
for the degree of

Chemistry – Doctor of Philosophy

2014

ABSTRACT

DEVELOPMENT OF MAGNETIC RESONANCE IMAGING BASED DETECTION METHODS FOR BETA AMYLOIDS VIA SIALIC ACID-FUNCTIONALIZED MAGNETIC NANOPARTICLES

By

Hovig Kouyoumdjian

The development of a non-invasive method for the detection of Alzheimer's disease is of high current interest, which can be critical in early diagnosis and in guiding preventive treatment of the disease. The aggregates of beta amyloids are a pathological hallmark of Alzheimer's disease. Carbohydrates such as sialic acid terminated gangliosides have been shown to play significant roles in initiation of amyloid aggregation. Herein, we report a biomimetic approach using sialic acid coated iron oxide superparamagnetic nanoparticles for *in vitro* detection in addition to the assessment of the *in vivo* mouse-BBB (Blood brain barrier) crossing of the BSA (bovine serum albumin)-modified ones. The sialic acid functionalized dextran nanoparticles were shown to bind with beta amyloids through several techniques including ELISA (enzyme linked immunosorbent assay), MRI (magnetic resonance imaging), TEM (transmission electron microscopy), gel electrophoresis and tyrosine fluorescence assay. The superparamagnetic nature of the nanoparticles allowed easy detection of the beta amyloids in mouse brains in both *in vitro* and *ex vivo* model by magnetic resonance imaging. Furthermore, the sialic acid nanoparticles greatly reduced beta amyloid induced cytotoxicity to SH-SY5Y neuroblastoma cells, highlighting the potential of the glyconanoparticles for detection and imaging of beta amyloids. Silaic acid functionalized BSA (bovine serum albumin) nanoparticles also showed significant binding to beta amyloids, through ELISA and *ex vivo* mouse brain MRI experiments. Alternatively, the BBB crossing was demonstrated by several techniques such as confocal

microscopy, endocytosis, exocytosis assays and were affirmed by nanoparticles transcytosis assays through bEnd.3 endothelial cells. Finally, the BBB crossing was confirmed by analyzing the MRI signal of nanoparticle-injected CD-1 mice.

To My Dear Parents and Sisters
&
To All of My Suffering Family and Friends in Haleb

ACKNOWLEDGEMENTS

I would like to start my acknowledgments by thanking my advisor Professor Xuefei Huang for his guidance and encouragement throughout my graduate school. It makes me proud to have names like Fujio Egami, Yoshimasa Hirata, Koji Nakanishi, and finally, my advisor Xuefei Huang added to my academic genealogy. Prof. Huang has been a role model to me, and all of my labmates with his persistence and excellence, and it is only a matter of time until we see his name next to the great names in this field.

Then, I would like to thank my doctoral committee members, the late Prof. Gregory Baker, Prof. James Jackson, Prof. Christina Chan, Prof David Weliky and finally Prof. David Zhu. It has been hard to witness Prof. Baker leave us that early. Our department lost a real gentleman and scholar indeed.

A special thank goes to Prof. Zhu for his role in establishing all MRI protocols and scanning the samples and animals. His contribution was not limited to my work only, but also to our whole bio-organic research sub group.

During my stay at MSU, I also had the chance to work on my professional development. Attending many seminars, and workshops; serving on several committees, and receiving various certificates and fellowships shaped my academic character and gave me the required tools to build my scholarly leadership. I would specifically highlight my Future Academic Scholars in Teaching (FAST) fellowship, where I was given that chance to work on a Teaching-As-Research (TAR) project to reform a chemistry course. In particular, I would like to thank the FAST fellowship director, the Associate Dean of Graduate School Prof. Rique Campa for his limitless support, my TAR-P.I. Prof. Melanie Cooper, Lappan-Phillips Chair of Science Education for her valuable guidance and help, and finally the Chair of Chemistry Department, Prof. Robert

Maleczka for trusting and believing in me to implement my TAR project in a class of 400 students.

I also thank those present and past members of the Huang group: Abishek, Anthony, Berm, Bin, Bo, Dino, Gilbert, Gopinath, Herbert, Hongguang, Isaac, Jason, Jia, Jicheng, Jingguang, Keisuke, Medha, Mehdi, Moe, Peng, Qian, Sherif, Shuyao, Steve, Weizhun, Vivian, Zeren, and Zhaojun, who were more than willing to help me in my research. In addition to these group members, undergraduate researchers Sarah Daniels and Kelly Lorenz gave me the opportunity and the pleasure to teach and learn from them. It goes without saying to thank the chemistry department staff, Bill, Bob, Dan, Jeanne, Marvey, Nancy, Kermit, Sherry and others.

I would like to thank my parents and sisters who provided me with the much needed love and care especially that I was not able to stand by them during the hard times of losing my niece and the operations of my mom and dad. I especially would like to mention my beloved grandma, who has just got diagnosed with a terminal cancer, for her encouragement and prayers. Also, I cannot forget to thank my family and friends in Haleb especially that they are passing through very hard days. I would like to thank Ali, Samar, Dina and Ramey for their constant support and encouragement.

And lastly, I would like to apologize to everybody who I might have hurt by my actions or by my words during my years at the graduate school.

THANK YOU...

TABLE OF CONTENTS

LIST OF TABLES

LIST OF FIGURES

LIST OF SCHEMES

KEY TO ABBREVIATIONS

Aβ	Beta Amyloid
AD	Alzheimer's Disease
BSA	Bovine serum albumin
cat.	Catalytic
conc.	Concentrated
d	Day
DLS	Dynamic light scattering
EDC. HCl	1-Ethyl-3-(3-dimethylaminopropyl) carbodiimide hydrochloride
ELISA	Enzyme-linked immunosorbent assay
EtOAc	Ethyl acetate
FACS	Fluorescence-assisted cell sorting
FITC	Fluorescein isothiocyanate
h	Hour
H_2O	Water
H_2SO_4	Sulfuric acid
HCl	Hydrochloric acid
HMBC	Heteronuclear multiple bond correlation
HMQC	Heteronuclear multiple quantum coherence
HRMS	High resolution mass spectrometry
HRP	Horseradish peroxidase
KDa	Kilodalton

NHS	N-Hydroxysuccinimide ester
MeOH	Methanol
MFI	Mean FITC fluorescence
NMR	Nuclear Magnetic Resonance
OAc	Acetate
PBS	Phosphate buffered saline
PBST	Tween 20 surfactant in Phosphate Buffered Saline
RPM	Revolutions per minute
rt	Room temperature
sec	Second
TMB	3,3',5,5'-Tetramethylbenzidine

Chapter 1 Review of Interactions of Sialic Acid Modified Nanoparticles with Beta Amyloid

1.1 Introduction

Nanotechnology is a recent part of science that deals with the fabrication and functionalization of nanoparticles (1-100nm) to be used in many disciplines including those in disease detection and therapeutic applications. These advances made synthesizing many variations of new nano-sized structures with different optical, mechanical, and electrical properties achievable. One of their most important characteristics is the high surface area-to-volume ratio. This high ratio is the key in increasing the ligand density on the surface of these nanoparticles to provide a larger surface for functionalization with different compounds and macromolecules by way of different surface functional groups (for example, carboxylic and amino groups). Different nanoparticles were used as basis of new methods for effecting molecular changes within cells both for diagnostic and investigational purposes. Nanoparticles such as gold and iron oxide, quantum dots, dendrimers, graphenes, fullerenes, and carbon nanotubes were successfully integrated in biological applications as diagnostic and therapeutic tools and in drug-delivery systems.

Alzheimer's disease (AD) is a progressive, irreversible neurodegenerative disorder characterized by the destruction of brain cells and neural connections. In 2014, 5.2 million people in the United States had AD with an estimated cost of $214 billion in medical care.[1] It is forecasted that the number of AD patients and medical care cost will triple by 2050.[2] This trajectory suggests the urgent need for research into the diagnosis, treatment, and possible

prevention of AD. For early detection of AD before any clinical manifestation, biomarker-detection based strategies are gaining momentum.

Today, there is no consensus on the root cause or the exact etiology of AD. However the pathology of AD is consistently characterized by neuronal cell death mainly in the neocortex and limbic structures by amyloid plaques and neurofibrillary tangles (NFTs).[3] Research determined the appearance of neurofibrillary tangles in the limbic system (entorhinal cortex, hippocampus, dentate gyrus) and their progression to the cortical region directly correlated with neuronal dysfunction.[4]

A considerable amount of research has also been directed toward studying the cause and function of amyloid plaques in AD. According to the Amyloid Cascade Hypothesis, the amyloid-β peptide (Aβ) accumulates in the frontal cortex and then spreads over the entire cortical region.[5] Aβ peptide has many forms and it ranges from 36 to 42 amino acids. The length of the peptide is governed by the cleavage of amyloid protein precursor (APP) in specific patterns. APP is a transmembrane protein ranging in size from 695 to 770 amino acids and is produced by proteolytic cleavage of the amyloid precursor protein in the central nervous system by β-secretase (also known as BACE) and γ-secretase.[6]

Although Aβ can contain varying numbers of amino acids, the most abundant forms are Aβ(1−40) **(Figure 1.1)** and Aβ(1−42) **(Figure 1.2)**.[7] Aβ is prone to aggregating to form plaques and the extra two hydrophobic residues in the C-terminus of Aβ(1−42) render it capable of aggregating faster than Aβ(1−40).[7b] The accumulation of the Aβ is due to an imbalance between its production and clearance mechanisms.[8] The production and accumulation of Aβ is mainly associated with familial determinants and the early onset of AD,[6c] and the decreased clearance of Aβ is associated with the more commonly observed late onset AD.[6b]

Figure 1.1: Aβ (1-40) peptide sequence

Figure 1.2: Aβ (1-42) peptide sequence

Although there is a massive debate about the exact cause of AD, one hypothesis presents the most acceptable explanation.[4] As previously mentioned, the increased production and reduced clearance of Aβ peptides result in aggregation and hence formation of more complex structures. These structures include oligomers, protofibrils, and fibrils whose formations result in a cascade of deleterious changes. These cause neuronal death and thus cause AD. This process is known as the Amyloid Cascade Hypothesis.

The role of Aβ aggregation as the primary cause of events has been evaluated several times and it was noted that the Aβ fibrils were shown to be less important in terms of pathogenicity. These reevaluations were due to studies that confirmed the load of the Aβ plaques do not correlate well with extent of dementia and, additionally, are due to numerous advanced AD patients showed no plaques in their brains upon post-mortem analysis.[9]

Moreover, many AD mouse models showed that plaques were observed in the brains long after the memory was affected.[10] This fact was further established by *in vivo* neuroimaging where healthy brains clearly showed the occurrence of Aβ plaques.[11] These results triggered a new wave of criticism about the hypothesis which in turn led to the possibility that insoluble fibrils are not the ones involved in triggering the pathological events. Subsequent studies came up with new findings where the responsible form of the peptide was determined to be the soluble oligomer. The amphiphilic Aβ peptides aggregate to form higher order aggregates, namely oligomers. Several groups isolated those oligomeric Aβ forms from culture media,[12] AD mice,[13] and patient brains.[14] Oligomers isolated from human AD brains potently inhibited long-term potentiation and enhanced long-term depression with IC_{50} values in the picomolar range.[15] Disruption in memory of a learned behavior in normal rats, was also proved to be caused by soluble Aβ from AD-like rat brains. Potential *in vivo* oligomerization pathways are summarized in Scheme 1.1. Scheme 1.1**A** depicts a single linear oligomerization pathway with Aβ monomers initially forming low molecular weight soluble aggregates (step 1). In step 2, aggregation into insoluble protofibrils and fibrils occur. Both soluble and insoluble aggregates are considered to be cytotoxic. In part B, two distinct pathways were proposed. A pathogenic pathway (step 1) and a non-pathogenic pathway (step 2). In the first one, the formation of soluble oligomers is hypothesized to cause the disease. In the latter one, the direct formation of insoluble aggregates and plaques is proposed. Step 3 indicates the leachy nature of benign insoluble aggregates to form pathogenic soluble oligomers.[16]

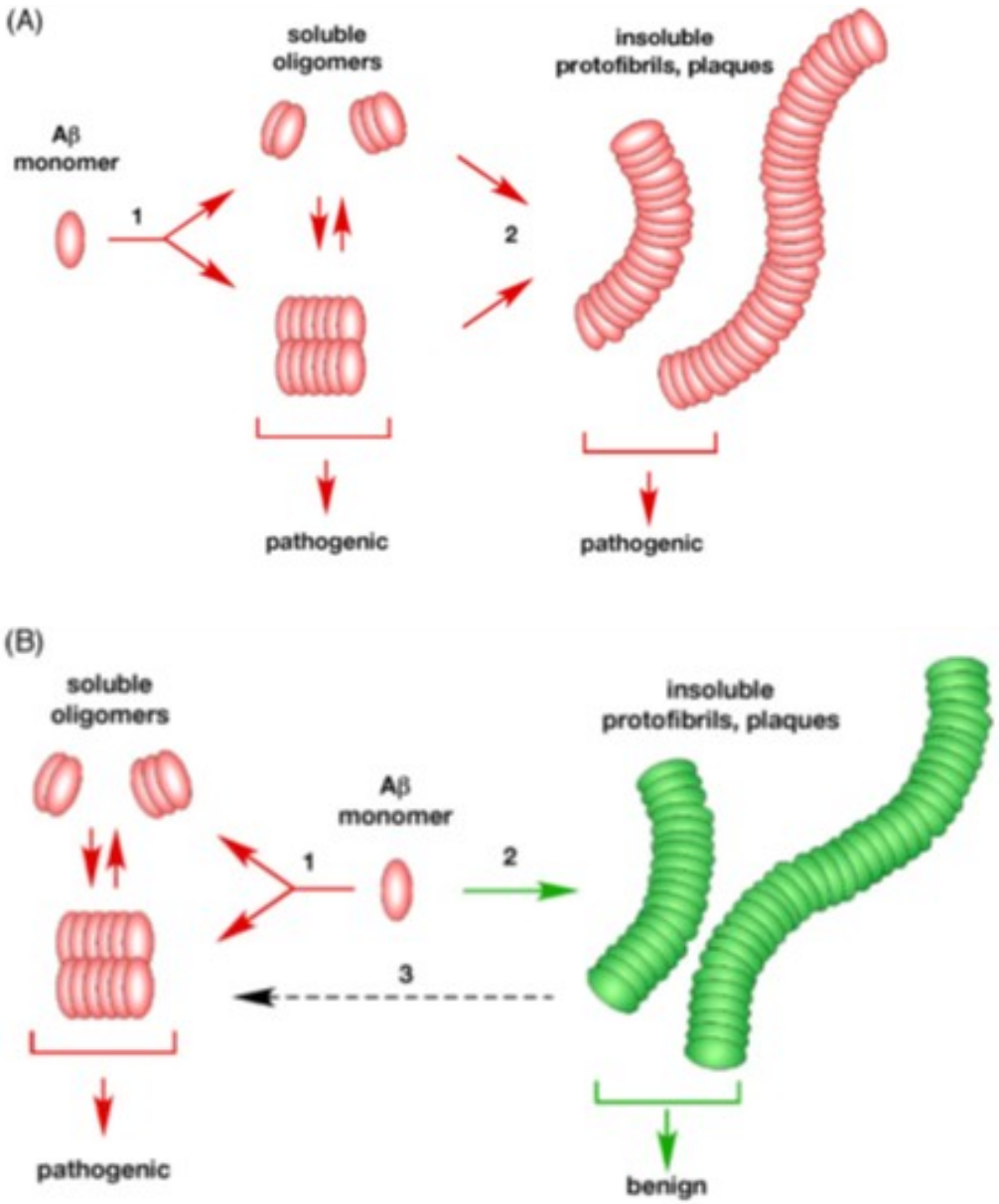

Scheme 1.1: Potential pathways of *in vivo* Aβ oligomerization (Adopted from *Pimplikar et. al.*)[17]

Interestingly, circular dichroism spectroscopy (CD), X-ray diffraction (XRD), and nuclear magnetic resonance (NMR) studies were conducted that observed the time-dependent secondary structure changes of the two most abundant peptides, Aβ (1-40) and Aβ (1-42),. These

experiments showed that oligomers' secondary structure transition from random coil to α–helix to the β–sheet structure and thus concluded that the formation of an oligomeric α-helix-containing assembly is a key step in Aβ fibrillogenesis.[18]

1.2 Role of Carbohydrates in Beta Amyloid Binding

1.2.1 Sialic Acid

Sialic acids (N-Acetylneuraminic acid or Neu5Ac) are a family of sugar units with a nine-carbon backbone that are typically attached to the terminal ends of these saccharide chains. This location gives sialic acid the opportunity to influence numerous physiological and pathological processes. For instance, sialic acids serve as components of binding sites for various pathogens and toxins.[19] Examples of these include Human Influenza A, Avian Influenza A, Human Influenza C, *Vibrio cholera*, *Plasmodium falciparum*, *Clostridium botulinum*, and *Helicobacter pylori*.[20]

There are many important structural and physical roles of sialic acid. For instance, extended polysialic acid chains play an important role in cell plasticity.[21] Also, due to its negative charge and hydrophilicity, they can contribute to preventing undesired interaction between human erythrocytes and other cell types mainly through cell charge repulsion. Moreover, they are found in abundance in the glomerular basement membrane and were determined to be critical in maintaining the normal filtering function of the organ.[22] It is noteworthy that the loss of sialic acid on those membranes can be accompanied by naturally occurring diseases such as 'minimal change' nephrosis.[20]

Sialic acids play an important role in cell adhesion. They are considered the primary ligands for the Sialic acid-binding immunoglobulin-type lectins (Siglecs). Mostly found on immune cell surfaces, the primary function of Siglecs is to bind glycans containing sialic acids. They are a subset of I-type lectins that are responsible for leukocyte regulation during immune responses.[23]

1.2.2 GM1

One of the most abundant gangliosides in the brain is GM1 which constitutes 20% of brain gangliosides **(Figure 1.3)**.[24] GM1 is an acidic glycosphingolipid that is involved in synaptic signaling and transmission and it is abundant in the plasma membrane of neurons.[25] Additionally, it has been considered to be involved in the pathology of AD.[26]

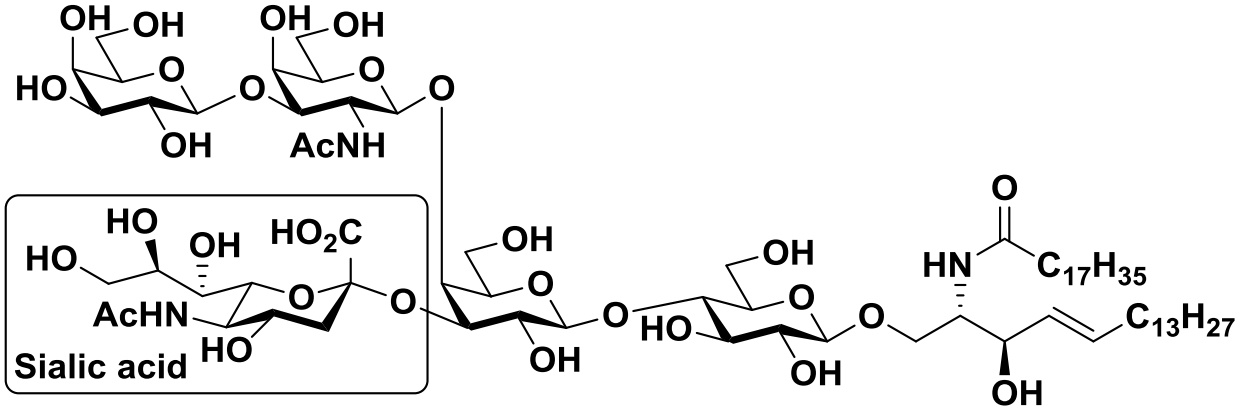

Figure 1.3: The structure of GM1 ganglioside with sialic acid moiety shown in the box

There is evidence to show that the first step of peptide/cell interaction is the association of the aggregates to the cell membrane.[27] This association was suggested to be through membrane gangliosides or glycoproteins containing sialic acid.[28] Notably, it was shown that Aβ binds to gangliosides on the neuronal membrane forming a GM1-Aβ moiety, which further acts as an endogenous seed for amyloid fibril formation.[29] The Aβ -GM1 ganglioside interactions involved in this process GM1-bound Aβ (GM1- Aβ) were discovered in brains of patients with AD as well as Down syndrome using sucrose density gradient centrifugation and western blotting techniques.[26b, 30]

Yanagisawa's group was the first to discover monosialoganglioside GM1-bound Aβ in the brains of patients with AD.[30] After those early studies indicated a binding pattern between GM1 and Aβ, a huge amount of interest in the AD research field was generated. As a result, researchers demonstrated that gangliosidic micelles stimulated aggregation of Aβ to form GM1-Aβ species.[31] This aggregation, which occurs on the cell membrane, plays the role of a seed for other Aβ peptides to further aggregate and hence induce neuronal cytotoxicity.[32] It is noteworthy that the extent of Aβ aggregation on the neurons was enhanced by the presence of high density clustering gangliosides or by increased degree of sialylation.[28d, e, 28l, 33]

The acidic character of GM1 can be attributed to the sialic acid moiety, which is believed to have an imperative role in binding.[34] Protein and carbohydrate interactions are usually mediated by hydrophobic and hydrogen-bonding interactions.[35] The interactions between the carbohydrate ring and the two exposed aromatic residues of Aβ (Phe-4, Tyr-10) in addition to the hydrogen bonding of carbohydrate hydroxyls with residues such as His-13 are believed to be the most important interactions.

Using NMR on N^{15}-labelled Aβ (1–40) and Aβ (1–42), Williamson's group revealed that the chemical shifts changes of Aβ (1-40) upon incubation with GM1 confirmed the binding of Aβ to GM1 micelles. Aβ-peptide's His-13 residue was significantly involved in binding with gangliosidic micelles. His-13 has also been identified as having an important role in fibrilization of Aβ.[18] Upon comparing chemical shift changes in Aβ (1–40) and Aβ (1–42), the binding to GM1 micelles is located at the N-terminal end. The C-terminal does not play any role in binding, but is important for oligomerization in solution.[28h]

1.3 Proteoglycans and Beta Amyloids

Another aspect of carbohydrate-Aβ interaction is the involvement of some proteoglycans in the binding. Proteoglycans are a diverse family of large molecules that are composed of glycosaminoglycans (GAGs) bonded to the protein backbone. They are mostly found in the extracellular matrix (ECM) and on the cell surface. They are mainly responsible for regulatory and functional processes in the brain.[36] Negatively charged GAG chains have different forms: hyaluronan (HA), heparan sulfate (HS), chondroitin sulfate (CS), keratan sulfate (KS), and dermatan sulfate (DS). Each one of them is composed of disaccharide units, containing iduronic and glucuronic acids, glucosamine, *N*-acetyl-glucosamine, galactose, galactosamine, and *N*-acetyl-galactosamine. These repeating disaccharides can also exhibit different O- and N-sulfation patterns **(Scheme 1.2)**.

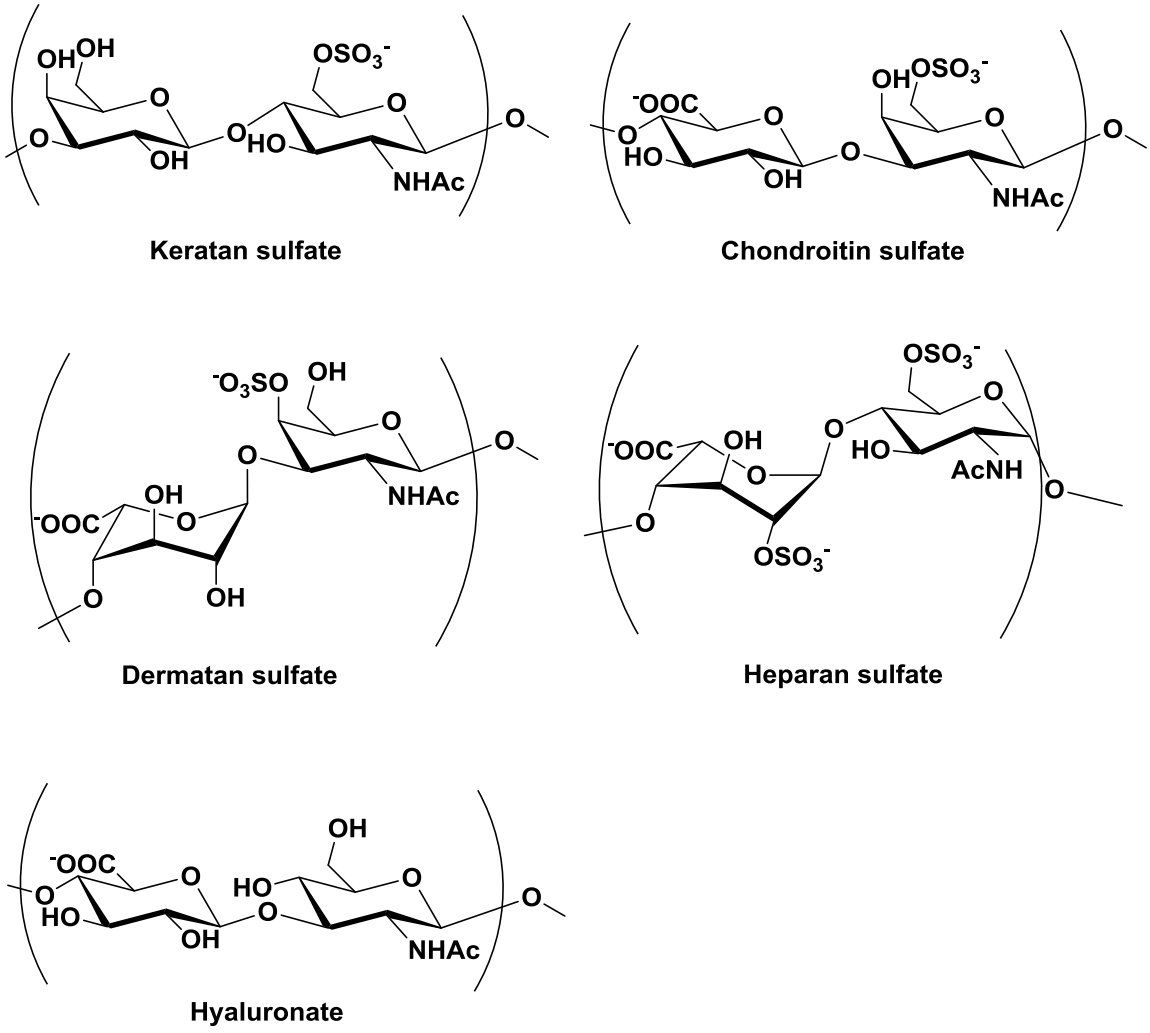

Scheme 1.2: Structure of disaccharide units of different GAGs

GAGs like heparan sulfate, keratan sulfate, or chondroitin sulfates were found to be associated with amyloid plaques.[37] Several *in vitro* studies demonstrated that those GAGs accelerate the aggregation of monomeric Aβ to result in β-sheeted Aβ fibrils.[38] Specifically, HS proteoglycans were shown to be associated with amyloid plaques of the hippocampus in AD brain .[39] Evidence shows that, both HS chains and core proteins can bind to the N-terminal region of Aβ.[40] Moreover, it has been demonstrated that residues 13–16 of the N-terminal region

play an important role in the HS/Aβ interaction.[41] It is noteworthy that this interaction is pH sensitive where acidic conditions favor stronger HS/Aβ binding.[42]

1.4 Different NPs Used in AD

It has been demonstrated that nanoparticles constitute a versatile vehicle to interact with Aβ peptides. Numerous groups conducted research to study the influence of nanoparticles on protein folding and aggregation through binding to different forms of Aβ, namely monomers, oligomers and fibrils. Inorganic nanoparticles such as gold[43] and iron oxide[44] nanoparticles, in addition to quantum dots,[43b, 45] showed promising therapeutic functions due to their longer bioavailability and longer shelf lives.

Other types of nanoparticles used to study Aβ aggregation and binding were polymeric nanoparticles. Dendrimers,[33d, e, 46] biomolecular[33g, 47] and copolymeric[48] nanomaterials constitute multipurpose vehicles in terms of flexibility of the design and ease of surface modification.

In addition studies were conducted to highlight the importance of carbon-based nanomaterials and their functions in interacting with amyloid fibrils, such as graphenes[49], fullerenes[50], and carbon nanotubes[51].

1.5 Sialic Acid Functionalized Nanoparticles

In this section we will discuss the different sialic acid conjugated nanomaterials that have been used to detect Aβ. Silaic acid conjugated nanomaterials such as dendrimers, gold nanoparticles and sugar polymers showed considerable attenuation of Aβ-induced cytotoxicity in addition to significant binding to Aβ.

1.5.1 Dendrimers-Sia

Many *in vitro* studies investigated specific binding of Aβ peptides to truncated gangliosides, namely clustered sialic acids to mimic neuronal cell surfaces. Theresa Good's group performed pioneering research on Aβ binding as well as Aβ-induced cytotoxicity attenuation by sialic acid-functionalized platforms.[33d, 52] The approach of mimicking the clustered-sialic-acid cell surface was achieved by synthesizing sialic acid-conjugated dendrimer (Scheme 1.3). Radiochemical methods were applied to measure the binding of sialic acid-conjugated dendrimers to Aβ, where the dissociation constant (K_d) was found to be in the order of 10^{-8}M. Because multivalency plays an important role in binding to Aβ, it was demonstrated by the improved $K_{A\beta}$ values with increased numbers of sialic acid moieties on differernt generations of dendrimeric platform, namely second, third and fourth generation dendrimers **(Table 1.1)**.

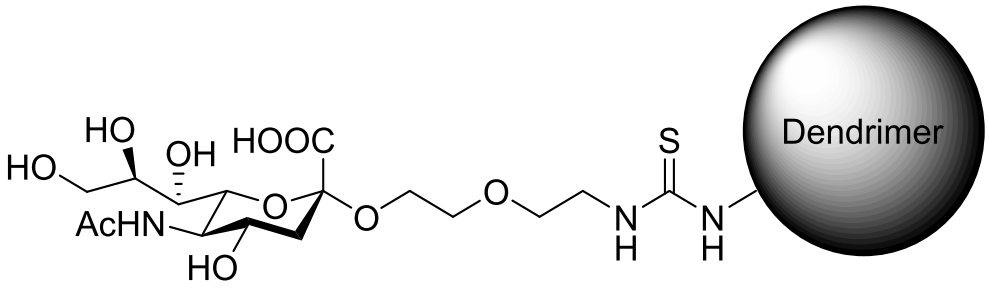

Scheme 1.3: Sialic acid-conjugated dendrimer used for Aβ binding and inhibition

Table 1.1: Equilibrium dissociation constant for Aβ to different dendrimer generations with sialic acid modification

Generation	$K_{Aβ}$ (μM)
2.0	0.25 ± 0.02
3.0	0.02 ± 0.01
4.0	0.009 ± 0.005

The specificity of binding is another aspect of testing for such constructs. For instance, isotherms of sialic acid-conjugated third generation dendrimer with radioiodinated Aβ, insulin, and lysozyme **(Figure 1.4)** showed high selectivity of Aβ. The choice of insulin, and lysozyme was due to the fact that they are known to form amyloid fibrils under some experimental conditions.

In these dendrimeric systems, the increased multivalency, hence improved Aβ binding properties come with a major drawback, which is the intrinsic cytotoxicity of the larger dendrimeric platforms. It is noteworthy that fourth generation dendrimers showed relatively high intrinsic toxicity, which is a potential limitation of using this platform for *in vivo* detection.

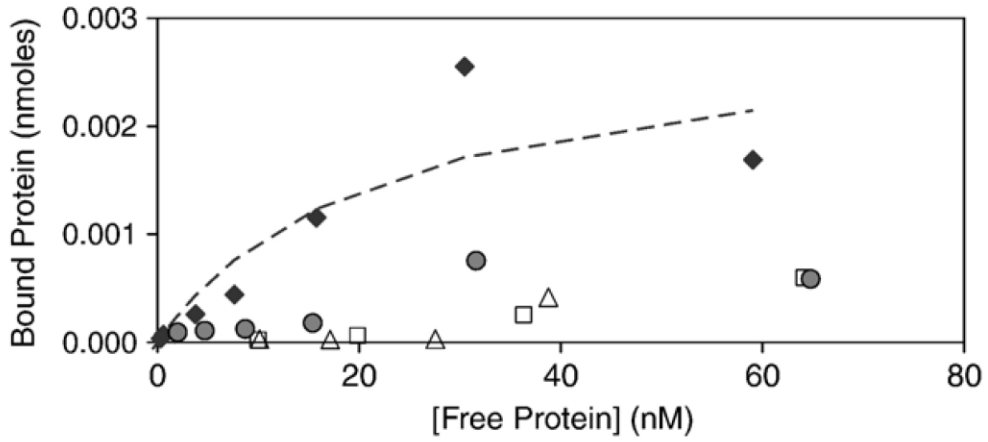

Figure 1.4: Equilibrium binding isotherms of Aβ (solid diamonds) insulin (open squares) and lysozyme (open triangles) to sialic acid third generation dendrimer complex.The solid circles represent the binding isotherm of unmodified dendrimer to Aβ

Assessing cytotoxicity of dendrimeric sialic acid constructs can be performed via methods like Methyl Thiazolyl Tetrazolium (MTT), and propidium iodide (PI) assay. In dendrimer studies, the cytoxicity was assessed by performing PI assay, on SH-SY5Y neuroblastoma cells. As indicated in **Figure 1.5**, the attenuation of the sialic acid-conjugated and unconjugated dendrimers' toxicity of Aβ were studied. After treating all cells with a constant concentration of Aβ (50μM) for 24 hours (Dashed line in **Figure 1.5**), only 60% of the cells were alive. At that point the cell viability was assessed by varying concentration of dendrimers. **Figure 1.5** demonstrates the varying protective effects of dendrimers on the cells. For instance, this data indicates that second generation sialic acid dendrimers showed better protective effect than the third generation ones. However the fourth generation protective effect increased up to

1.5 μM then decreases quickly. As established above, the phenomenon of decreased protection ability of the higher generation dendrimers can be explained by the intrinsic toxicity of those higher order dendrimers.

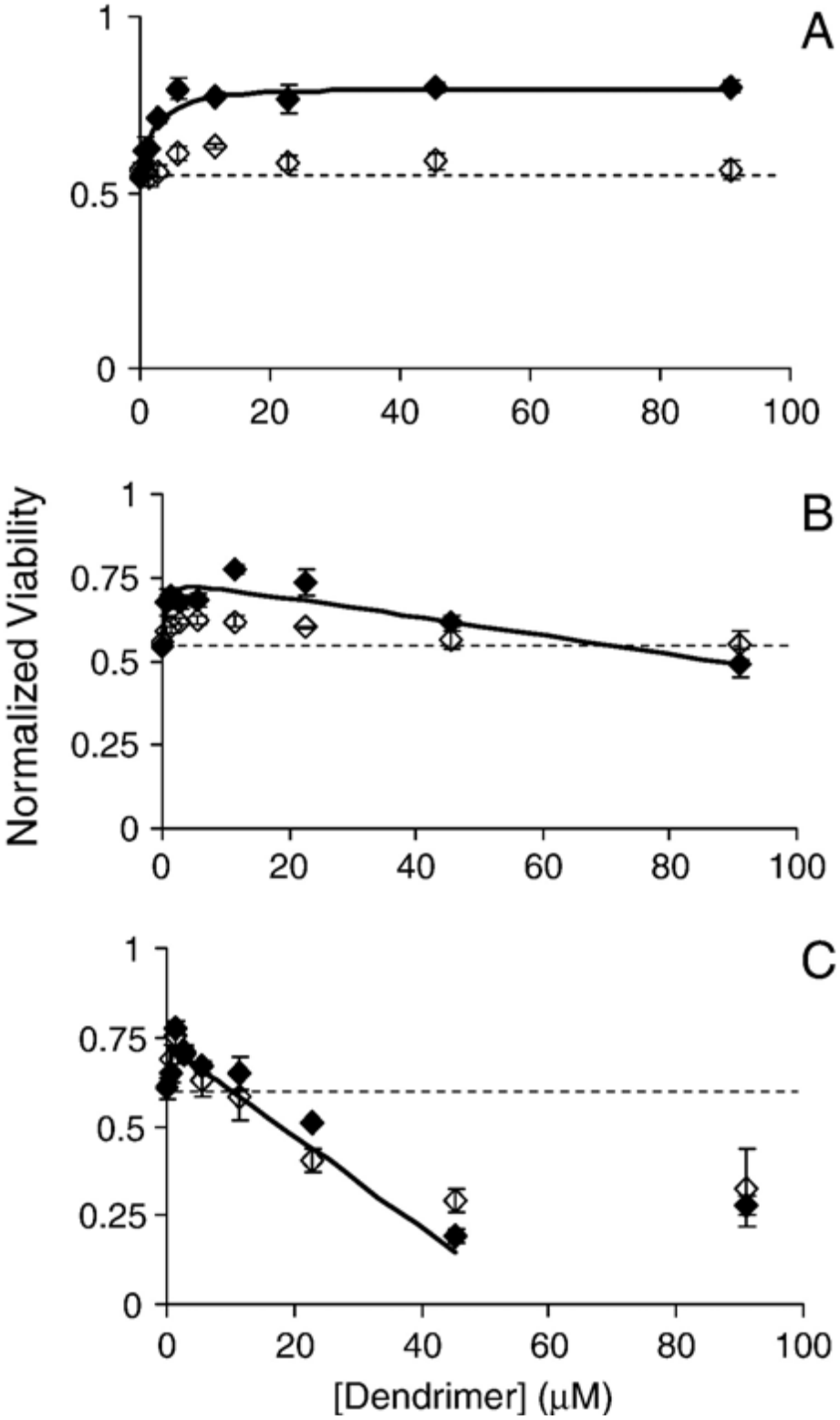

Figure 1.5: Normalized cell viability upon treatment of SH-SY5Y cells with sialic acid conjugated dendrimers (filled diamonds) and unmodified dendrimers (open diamonds) when treated with Aβ. (A) 2.0 (B) 3.0 (C) 4.0 generation dendrimers

1.5.2 Au-Nanoshells-Sia

Gold nanoparticles have been extensively used in nanoresearch due to their versatility to be used in various detection methods. Its metallic properties and the large surface area make those platforms an attractive choice. For instance, carbohydrate-immobilized gold nanoparticles were used as large glycol-clusters that are shown to be useful several analytical methods.[53]

The method of Surface-Enhanced Raman Spectroscopy (SERS) was one of the analytical methods utilized to detect Aβ by monitoring the signal from the Congo Red dye (CR) bound to aggregated beta amyloids.[54] The platform involved depositing a monolayer of Si-core and Au-shell nanoshells that are optimized for excitation laser wavelengths, with a specific chemistry for Aβ binding. It is noteworthy that the multivancy in this case was achieved by using the gold nanoshell film due to its easily modifiable surface with the direct conjugating of the thiol functional groups. To facilitate the binding between these nanoshells and Aβ, nanoshells were functionalized with thiol-terminated sialic acid (Scheme 1.4).

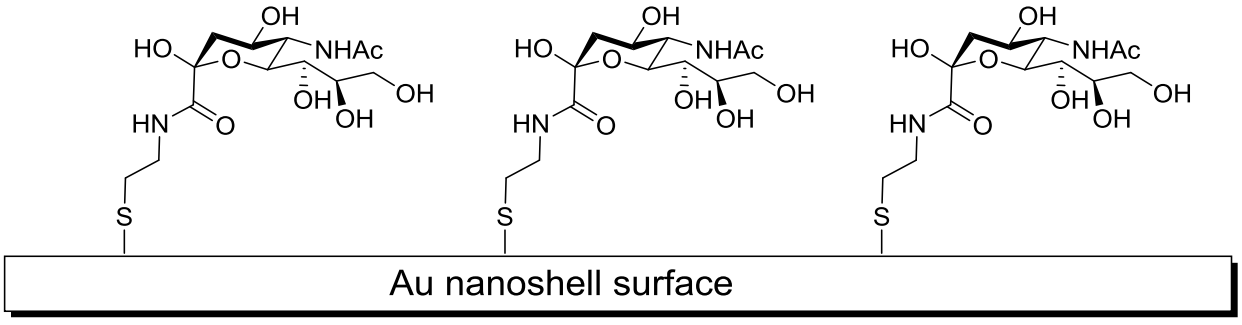

Scheme 1.4: Scheme showing the self-assembled monolayer bound to the nanoshells. By functionalizing the nanoshells with sialic acid, a platform was created for the selective binding of Aβ with limited interactions with other nonspecific proteins

The use of Raman spectroscopy is an alternative technique that employs an optical fingerprint of the desired molecules. Surface-Enhanced Raman Spectroscopy (SERS) is a powerful method for detection of trace concentrations. This is due to its ability to provide significant enhancement of the Raman intensity on the order of 10^6 to 10^{14} times through electromagnetic field enhancement and chemical enhancement.[55]

The sialic acid coated nanoshell and Aβ binding was tested by performing equilibrium-binding isotherms using 125-I radio-iodinated Aβ via IodoBead catalyst. The equilibrium dissociation constant of the Aβ with the surfaces was found to be 14±8 nM **(Figure 1.6)**. This value was comparable to the affinity values obtained in sialic acid-conjugated dendrimer study.[33d]

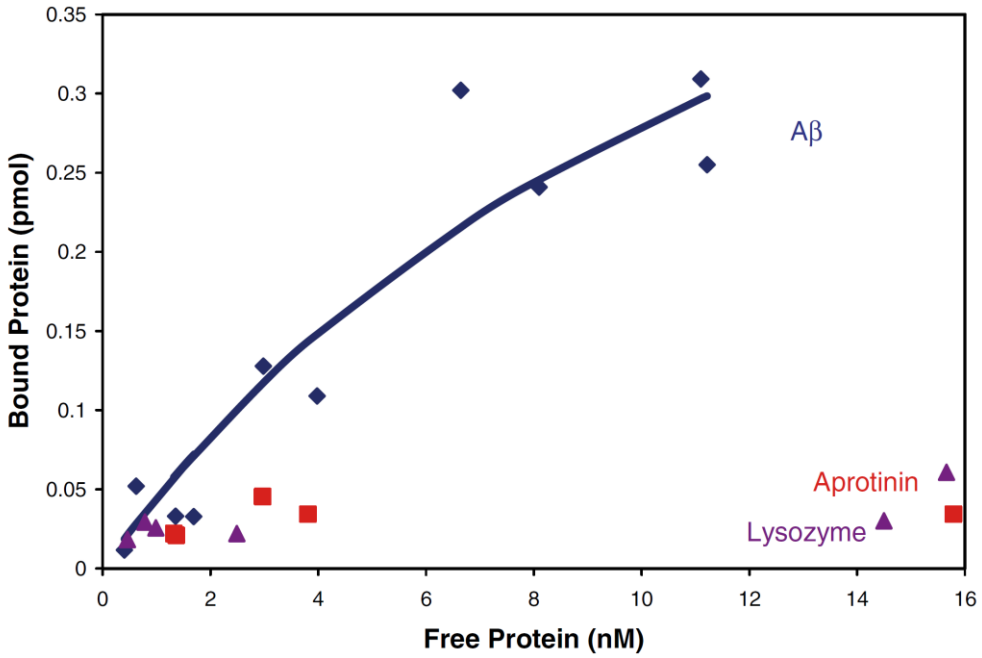

Figure 1.6: Equilibrium binding isotherm of I-125-labeled Aβ bound to the sialic acid SAM. The equilibrium dissociation constant of Aβ was determined to be 14±8 nM, and the maximum amount of Aβ bound to the surface was 0.7±0.3 pmol/cm2 of nanoshell covered area.

Furthermore, the SERS experiments confirmed the sialic acid-nanoshells binding to Aβ via CR signals. **Figure 1.6** shows the spectra generated by the CR signal corresponding to several concentrations of Aβ. The lowest concentration of Aβ that was detected by CR was found in a remarkably small picomolar range (1 pM) **(Figure 1.7)**.

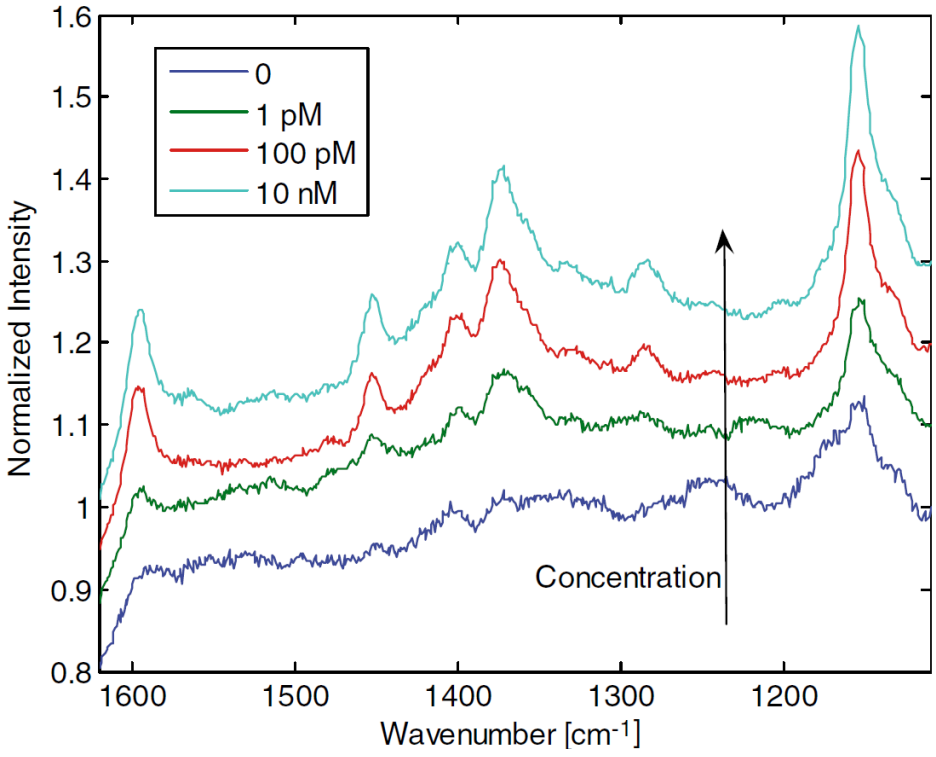

Figure 1.7: Congo red spectra showing the intensity dependence on concentration of Aβ applied to the nanoshells. The concentration of 1 pM of Aβ plus Congo red showed some spectral features.

Gold (Au) nanoparticles were also used in the electrochemical sensing of saccharide–protein interaction.[56] This analytical method involved depositing densely-packed glyco-functionalized gold nanoparticles on a carbon electrode to measure electric responses for Aβ

recognition purposes. Sialic acid moieties were conjugated to a self-assembled monolayer (SAM) of gold nanoparticles via click chemistry **(**Figure 1.8**)**. Those nanoparticles were electrochemically deposited on the carbon screen **(Scheme 1.5)**.

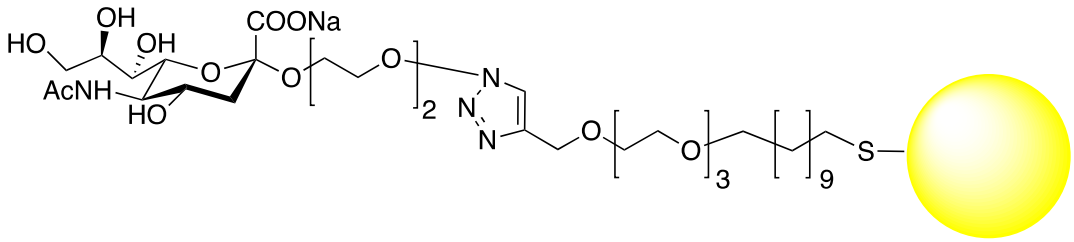

Figure 1.8: Click chemistry-linked sialic acid functionalization of the Au nanoparticles

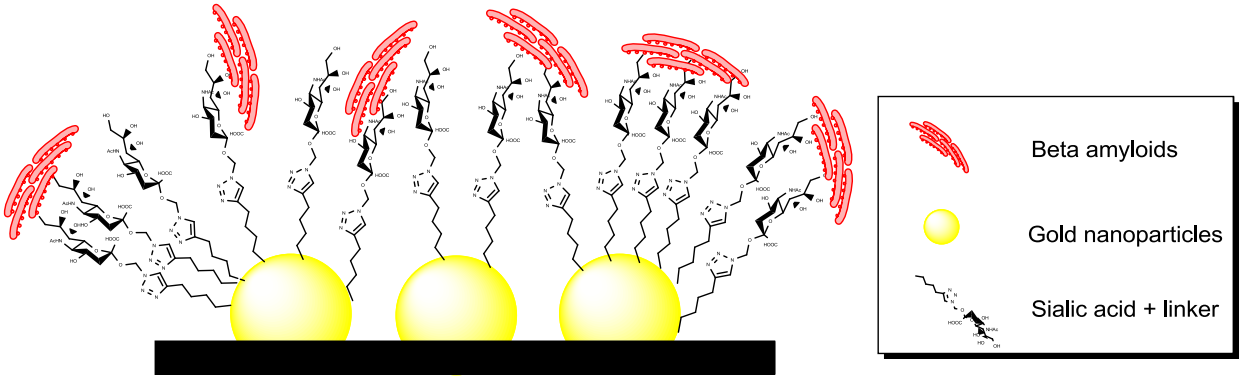

Scheme 1.5: Sialic acid-conjugated gold nanoparticles used for Aβ binding.

Upon subsequent introduction of the Aβ peptide, the attachment to the sialic acid layer was confirmed by atomic force microscopy. A slight roughness was observed on the Au substrate after modification with sialic acid **(Figure 1.9B)**. However, upon incubation of Aβ with

the surface electrode surface, an increased roughness was noticed, signifying the successful attachment to the sialic-acid conjugated gold-monolayer **(Figure 1.9C and D)**.

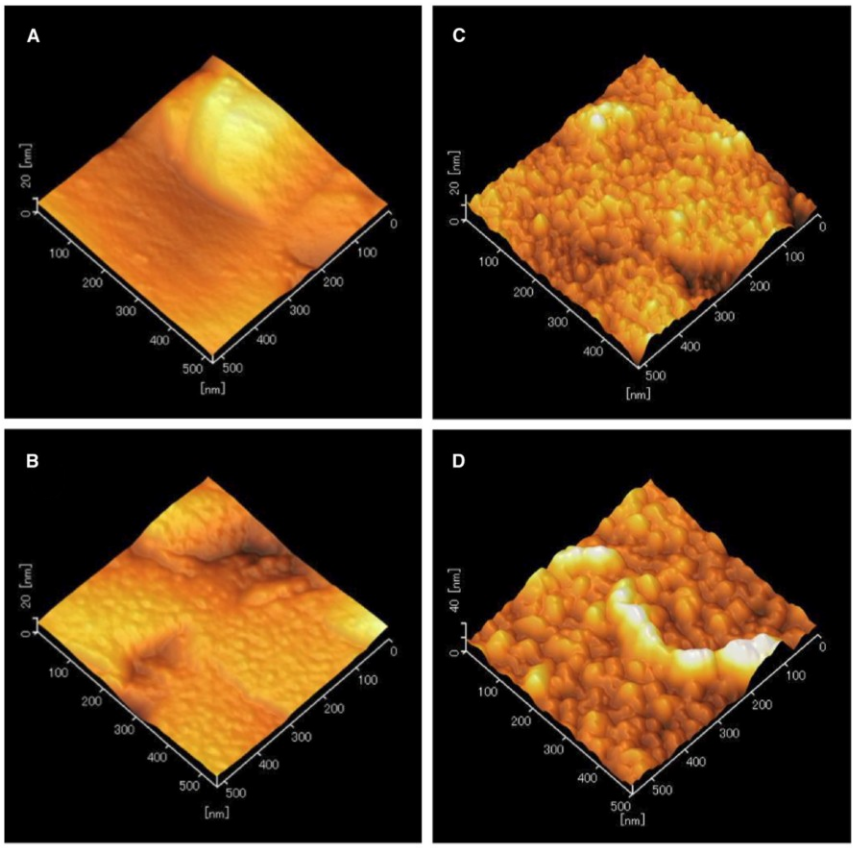

Figure 1.9: AFM images of the bare gold substrate (A); after sialic acid conjugation (B); the attachment of Aβ after incubation; Aβ(1-40) (C) and Aβ(1-42) (D).

Those atomic force microscopic images indicate that the sensitivity for Aβ detection was further improved by the sialic acid modification on screen-printed Au strip (SPGS) based on the sugar-Aβ interaction. This result is in agreement with the literature where GM1-Aβ interaction and the effect of acidic group immobilized substrate on Aβ aggregation is well established.[57] To test the detection specificity of this binding, the electric response of the tyrosine (Tyr) oxidation

signal was measured. The obtained signal showed strong affinity of Aβ for the sialic acid modified Au electrode. However, other proteins like insulin, showed no oxidation signal. This indicates that the insulin-sialic acid interaction was too weak to be detected, despite insulin's four Tyr residues **(Figure 1.10)**.

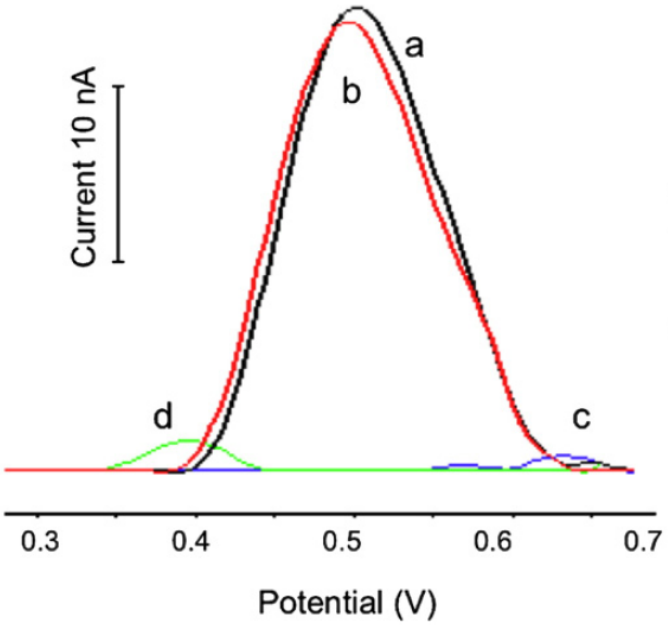

Figure 1.10: Electric responses of the Aβ sensor applied the Aβs. Aβ(1-40) (a), Aβ(1-42) (b), insulin (c) from 5 μM solutions, and PBS only (d) (A).

1.5.3 Polysaccharides-Sia

The cationic polysaccharide, chitosan is another nanoplatform that was used to detect beta amyloid. Due to its excellent biodegradability, biocompatibility, and biosecurity, and overall nontoxic characteristics,[58] chitosan has been used as a conjugation vehicle for sialic acid analogs.

The approach proposed by Dhavale et. al. demonstrated the ability of sialic-acid-analog conjugated chitosan polysaccharides to attenuate Aβ toxicity.[33g] The sialic acid (N-acetylneuraminic acid) and four other analogs: keto-deoxynonulosonic acid (KDN), D(+)-galacturonic acid (GA), tetrahydropyran-2-carboxylic acid (Pyran), and cyclohexanecarboxylic acid (CHC) were conjugated on chitosan via EDC chemistry.[33g33g] These analogs were substructures of sialic acid (Scheme 1.6).

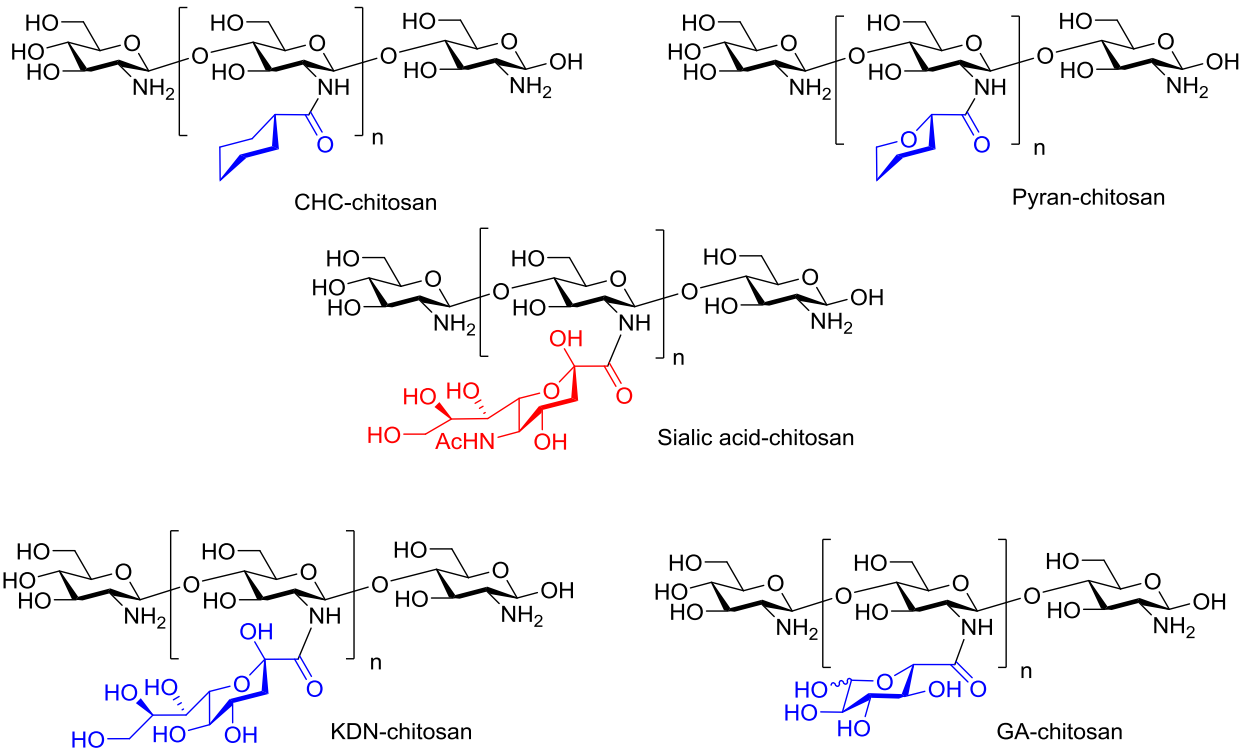

Scheme 1.6: The sialic acid in red and four other analogs; Cyclohexanecarboxylic acid (CHC), Tetrahydropyran-2-carboxylic acid (Pyran), D(+)-Galacturonic acid (GA), Keto-deoxynonulosonic acid (KDN) chitosan-conjugated complexes in blue.

Upon assessing the toxicity of the pure (free) sugar analogues and sugar/chitosan complexes, most analogues and complexes, except the CHC ones, showed intrinsic toxicity. However Pyran analog and complex was an outlier in terms of toxicity, which suggested the role of the ring oxygen in the process **(**Figure 1.11**)**.

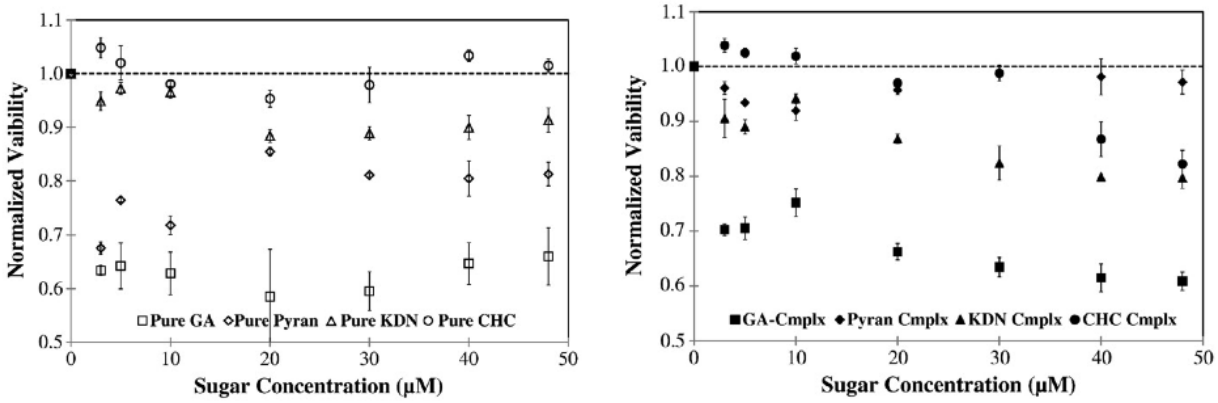

Figure 1.11: Toxicity of (a) pure sugars analogs, and (b) sugar/chitosan complexes. Dashed line represents the normalized control viability with no analog or complex in the system

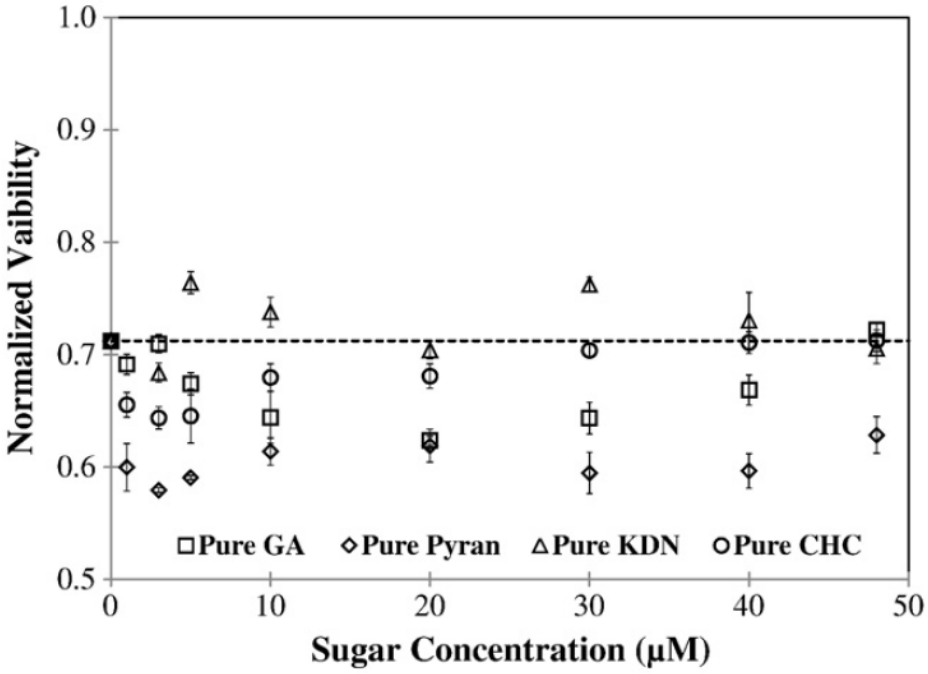

Figure 1.12: Attenuation of Aβ toxicity by pure sugar analogs. Pure sugar analogs incubated with 50 μM Aβ. Pure GA, square; pure Pyran, diamond; pure KDN, triangle; and pure CHC, circle; dashed line represents the normalized control viability with no analog/complex.

The Aβ toxicity attenuation assays are designed to assess the protective role that those analogues (pure or complexed) exhibit. The importance of sialic acid clustering was demonstrated when most of pure sugar analogs did not show significant levels of Aβ toxicity attenuation on human neuroblastoma SH-SY5Y cells **(Figure 1.12)**. It was noticeable that KDN was able to moderately attenuate the toxicity. These findings support previous research focusing on the significant role the clustering of sugars in Aβ binding.

On the other hand, chitosan conjugated analogs (complexes) showed pronounced attenuation of Aβ toxicity on the SH-SY5Y cells but mostly at lower concentration. The increased attenuation of Aβ toxicity by the chitosan conjugates is indicative of stronger Aβ binding. This can be especially observed in the case of the KDN analogs. This is the only analog, besides sialic acid, that has the multi-OH tail that is known for its role Aβ binding **(Figure 1.13)**. That being said, Pyran, which showed a considerably lower toxicity in the direct toxicity assays, showed contradicting behavior in the Aβ toxicity attenuation assays. These observations led to hypothesis that the oxygen ring substitution allows for either cellular or Aβ binding in a competitive, and interfering manner. It is noteworthy that the observed Aβ toxicity attenuation effects or the sialic acid analogs were rather small, which may pose a challenge in terms of using those analogs in an *in vivo* set up.

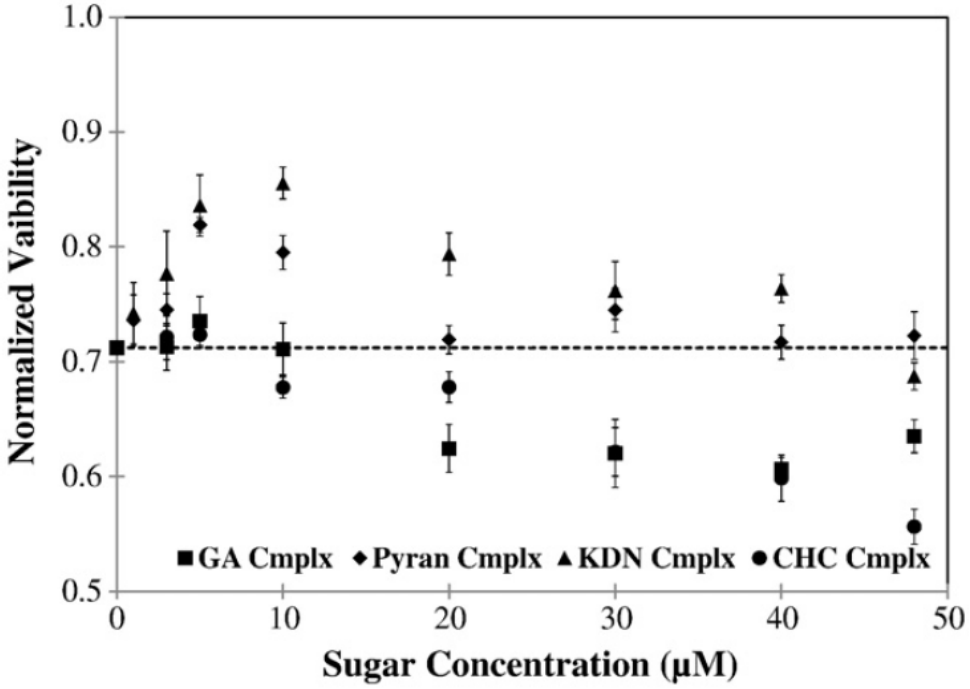

Figure 1.13: Attenuation of Aβ toxicity by sugar-chitosan complexes. Complexes incubated with 50 µMAβ. GA complex, square; Pyran complex, diamond; KDN complex, triangle; and CHC complex, circle; dashed line represents the normalized control viability

Chapter 2 Glyconanoparticle Aided Detection of Beta Amyloid by Magnetic Resonance Imaging and Attenuation of β-Amyloid Induced Cytotoxicity

2.1 Introduction

Traditional diagnostic approaches towards AD rely on the analysis of cognitive abilities and behavior of patients, which are non-specific and prone to false results. Neuroimaging using magnetic resonance imaging (MRI),[59] single photon emission computed tomography (SPECT) or positron emission tomography (PET) has become an important tool to aid in AD detection.[60] These techniques can provide important information on morphological and functional changes of brain, which are more suitable towards imaging advanced stages of AD.

For early detection of AD before any clinical manifestation, biomarker-detection based strategies are gaining momentum. Although the etiology of AD is not yet well understood, Aβ peptide, the major constituent of amyloid plaques, is one of the most prominent pathological hallmarks of AD.[5] Aβ peptide is produced by proteolytic cleavage of the amyloid precursor protein in the central nervous system by β and γ-secretases. Although Aβ can contain varying numbers of amino acids ranging from 36 to 42, the most abundant forms are the Aβ (1-40) and the Aβ (1-42).[7a] Aβ is prone to aggregation to form plaques and the extra two hydrophobic residues in the C-terminus of Aβ (1-42) render it aggregate faster than Aβ (1-40).[61]

Due to its important role in AD, Aβ imaging has been actively pursued *in vivo* using non-invasive techniques including PET,[62] MRI[63] and near IR fluorescence imaging.[64] Multiple PET reagents that can selectively bind with Aβ have been developed for determination of plaque burden in human patients with several undergoing late stage clinical trials.[62] Although PET can

give high sensitivities, MRI is a complementary approach due to its high spatial and temporal resolution. Furthermore, MRI does not require ionizing radiation thus is suitable for longitudinal studies. To better detect Aβ by MRI, MRI contrast agents have been developed using full length or fragments of Aβ as targeting ligands.[63a-c] As Aβ has the inherent affinity with amyloid plaques, these targeted agents could selectively bind with amyloid plaques, thus enhancing the contrast from surrounding tissues and enabling plaque visualization by MRI. In addition to the usage of Aβ peptide, ground breaking ^{19}F-MRI studies have been performed using a fluorine-containing Congo red derivative to image amyloid plaques in mice.[63e] Besides these targeted versions of contrast agents, a non-specific commercially available gadolinium based agent was explored for Aβ imaging by intracerebroventricular injection.[63d] Presumably due to the hydrophobicity of the Aβ plaques, the hydrophilic gadolinium agent avoided Aβ plaques while staining the rest of the brain well, thus enhancing the contrast between Aβ plaques and surrounding tissues. These innovative studies have revealed the potential power of MRI for Aβ imaging and continual development of contrast agents is necessary to realize the full potential of this technique.

Due to the ubiquitous existence of carbohydrates, they can influence Aβ aggregation. Glyco-conjugates including gangliosides and anionic glyco-polymers (e.g., glycosaminoglycans and nucleic acids) have been reported to bind Aβ.[65] Gangliosides such as GM1 (a sialic acid containing glycosphingolipid)[26b, 66] are abundant in neuronal plasma membranes and involved in synaptic signaling and transmission.[25] GM1-bound Aβ has been found in the brains of AD patients,[26b] with GM1 shown to serve as nucleation sites on neuronal cell membrane for Aβ aggregation.[66b] The negatively charged sialic acid moiety of GM1 is critical for Aβ interactions[67] through hydrogen bonding with His13 and clustering of sialic acid can significantly enhance the

binding with Aβ.[33b, c, 46a, 67-68] Based on these findings, we became interested in exploring whether carbohydrates can be utilized for Aβ detection and imaging.

Nanotechnology has been introduced to Aβ research with the majority of the studies focusing on the effects of nanoparticles on Aβ aggregation.[45, 69] The nanoparticle platform is very useful for our study, as it can display multiple copies of ligands that can potentially interact with Aβ leading to enhanced avidity. Herein, we report the development of magnetic glyconanoparticles, where the magnetic cores of the nanoparticles are coated with carbohydrates. The glyconanoparticles can selectively bind with Aβ and the magnetic properties of these nanoparticles enable the Aβ detection *in vitro* and *ex vivo* by MRI. Furthermore, these nanoparticles can expedite the aggregation of Aβ and mitigate Aβ induced cellular toxicity.

2.2 The Preparation and Characterization of NP-Sia.

Our study started from the synthesis of magnetic glyconanoparticles with magnetite (Fe_3O_4) cores. The superparamagnetic magnetite nanoparticles (SPIONs) were prepared by co-precipitating ferric chloride and ferrous sulfate under basic condition in the presence of the polysaccharide dextran **(Figure 2.1a)**.[70] Dextran coats the external surface of the nanoparticles forming a stable colloidal suspension. Dextran coating was crosslinked with epi-chlorohydrin, which was followed by ammonia treatment to introduce amine groups (SPION-NH_2). Sialic acid methyl ester derivative **1**[71] was partially deprotected under the Zemplén condition producing sialic acid **2**, which was subsequently linked to SPION-NH_2 via amide coupling mediated by 1-

ethyl-3-(3-dimethylaminopropyl) carbodiimide (EDC) **(Figure 2.1b)**. The methyl ester of sialic acid was removed by saponification leading to sialic acid coated NPs (NP-Sia).

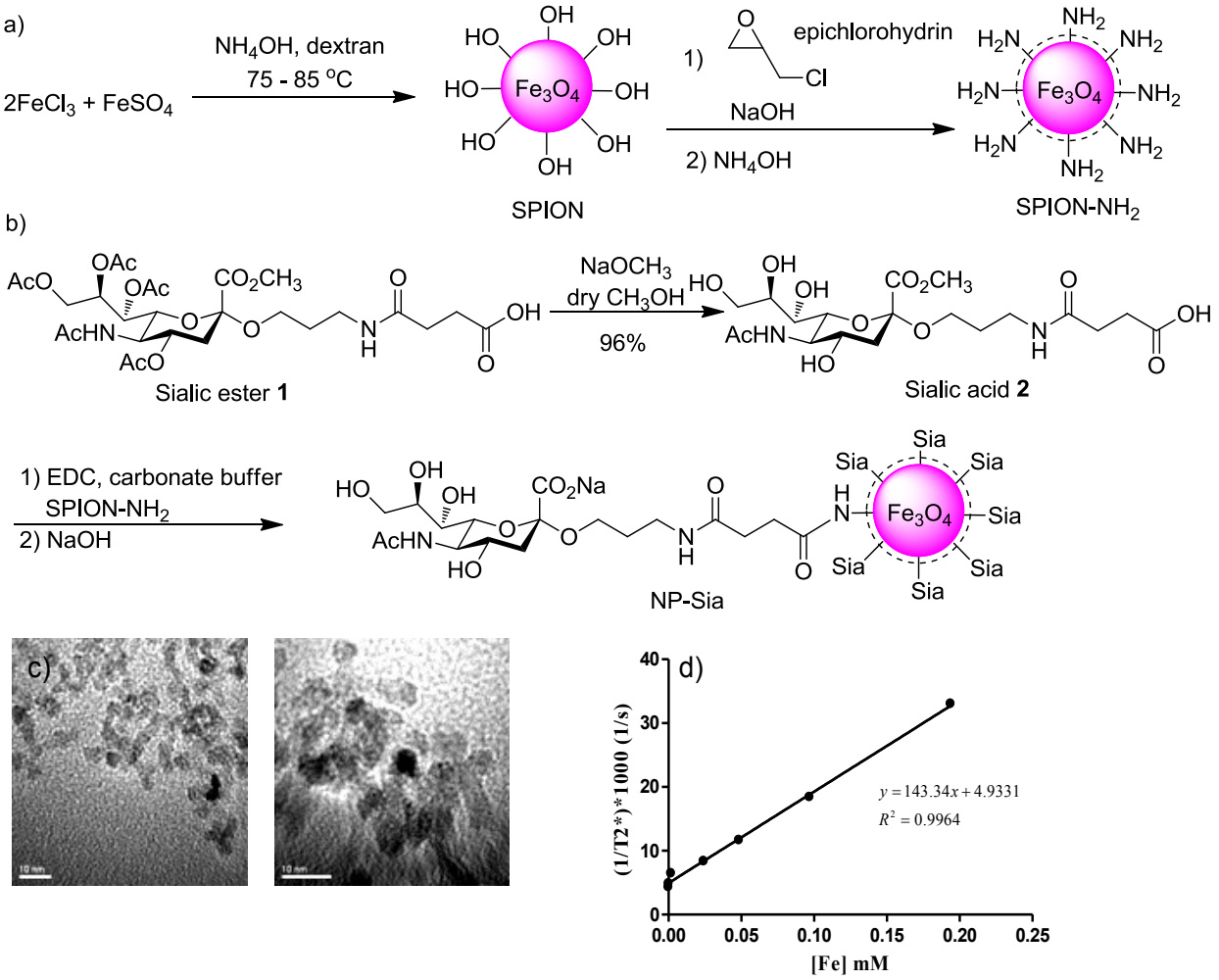

Figure 2.1: Synthesis of a) SPION and b) NP-Sia. c) TEM (The scale bar is 10 nm) and d) T2* relaxivity characterization of NP-Sia

NP-Sia was characterized via a variety of techniques, including transmission electron microscopy (TEM), high-resolution magic angle spinning nuclear magnetic resonance (HRMAS

NMR), thermogravimetric analysis (TGA), zeta potential, dynamic light scattering (DLS), thiobarbituric acid assay (TBA), and MRI **(Figure 2.1**and **Figure 2.2)**. TEM images indicated that the diameters of NP core were around 5 nm **(Figure 2.1c)**. Both SPIONs and NP-Sia have close to neutral zeta potentials in PBS buffer (-1.8 mV and 2.5 mV respectively). The total carbohydrate content represented 80% weight of NP-Sia as determined by TGA **(Figure 2.2a)**. To analyze the amount of sialic acid on NPs, sialic acid was selectively cleaved under a mild acidic condition and the amount of sialic acid was quantified by TBA showing that sialic acid accounted for 4% weight of the NPs **(Figure 2.2b)**. This suggested on average there were 98 copies of sialic acid on each NP. The presence of dextran and sialic acid was also confirmed by HRMAS NMR with their characteristic chemical shifts observed in ^{1}H-NMR spectrum of the NP-Sia **(Figure 2.2c)**. The NP-Sia was an excellent contrast agent with high magnetic relaxivity (The R2* magnetic relaxation rate (R2* = 1/T2*) of NP-Sia was measured to be 143 mM^{-1} s^{-1} at 3T **Figure 2.1d**. The R1 and R2 values for NP-Sia were 3.5 and 198 mM^{-1} s^{-1} respectively as shown in **Figure 2.2d,e)**.

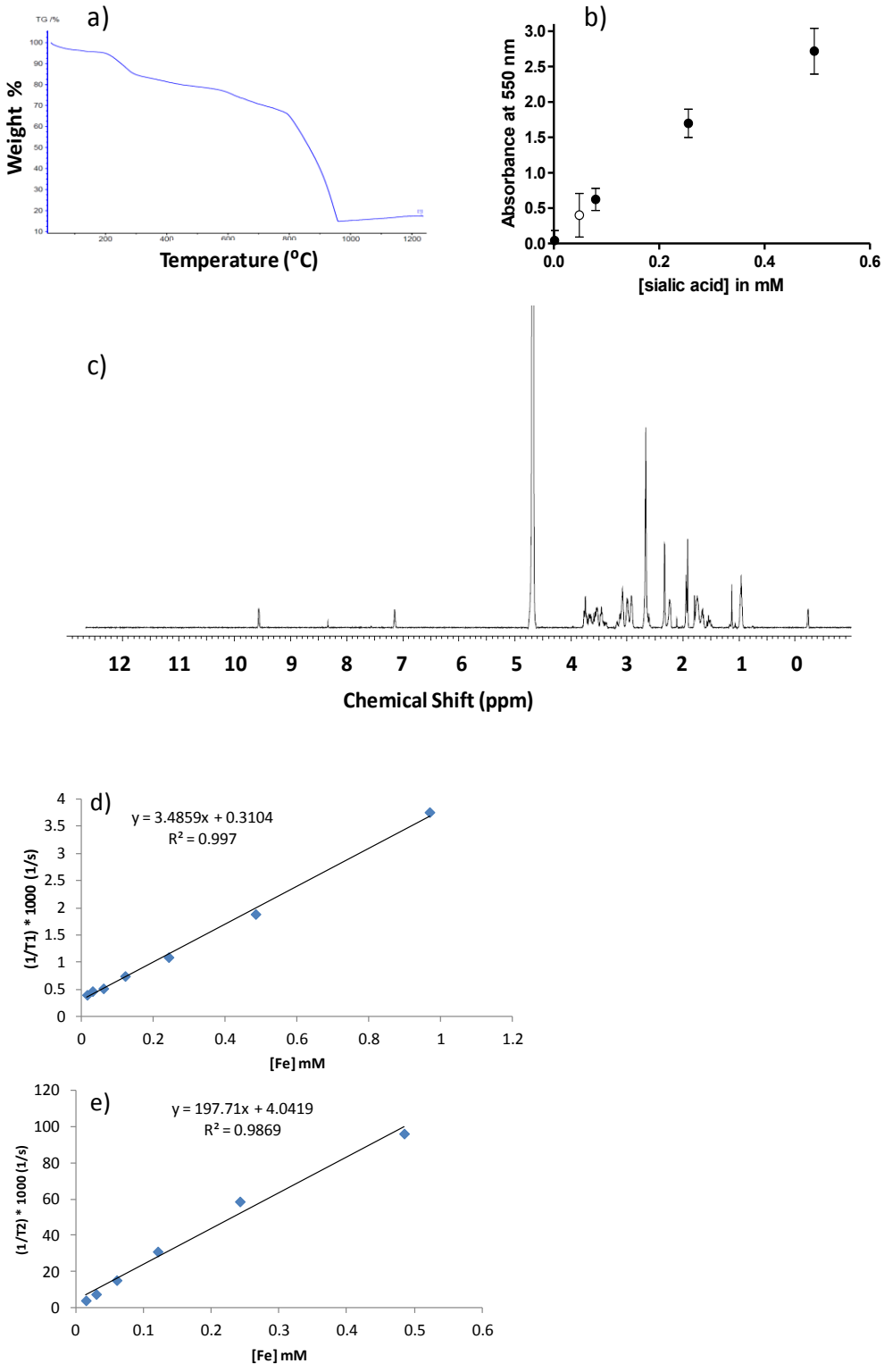

Figure 2.2: Characterization of NP-Sia a) thermogravimetric analysis; b) thiobarbituric acid assay; c) high-resolution magic angle spinning nuclear magnetic resonance; d) T1 and e) T2 relaxivity characterization of NP-Sia

2.3 Assessment of NP-Sia Binding with Aβ via ELISA and Prussian Blue Staining

In order to study NP interactions with Aβ, we selected Aβ (1-42) since it is a major component of amyloid peptides in the senile plaques in AD brains[72] and considered as the most toxic Aβ forms.[73] The Aβ peptide was dissolved in 10 mM NaOH solution, which was diluted in PBS buffer to the desired final concentration. The Aβ monomer solution was incubated at 37 °C for 48 hours without stirring to form fibrils. To check the quality of the fibrils, thioflavin (ThT) binding assay was performed. ThT is a cationic benzothiazole salt, which displays enhanced fluorescence and a characteristic red shift of its emission maximum when bound with β-sheet structures.[74] Upon incubation of Aβ fibrils with ThT, significant enhancement of ThT fluorescence and red shift of its emission (489 nm) were observed suggesting that good quality β-sheet rich Aβ fibrils were obtained **(Figure 2.3a).**[75] TEM imaging also showed fibrillar structures of Aβ **(Figure 2.3b)**. In order to visualize Aβ in TEM, 2% uranyl acetate stain on the fibril was needed to provide contrast from the background.

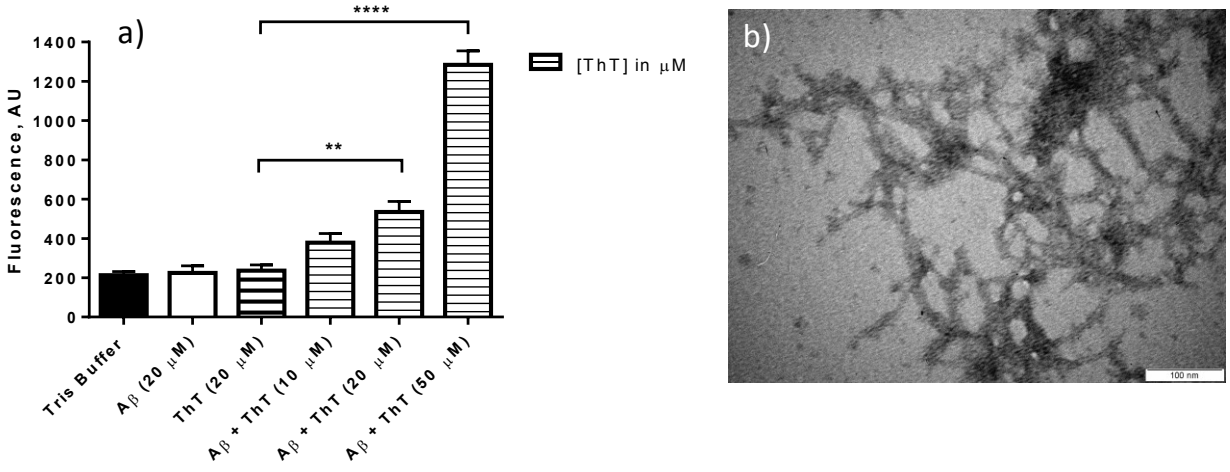

Figure 2.3: a) Enhancement of ThT fluorescence (excitation 440 nm and emission at 489 nm) upon binding to β-sheet rich Aβ fibrils; b) TEM images of Aβ fibrils with 2% uranyl acetate staining

The interactions between NP-Sia and Aβ fibril were investigated first using ELISA. A solution of NP-Sia was added to a microtiter plate. After overnight incubation, NPs adhered to the bottom of the wells. Aβ solutions were added to the NP-Sia coated wells followed by thorough washing and addition of an anti-Aβ IgG primary antibody. The amount of Aβ bound was quantified by the absorbance change of each well upon incubation with an anti-IgG secondary antibody linked with horse radish peroxidase (HRP). As shown in **Figure 2.4a**, a dose dependent increase in absorbance was observed with increasing Aβ concentration (apparent K_d = 0.7 μM). The immobilization of NP-Sia on the plate was important for Aβ binding, as without NP coating, the absorbance of Aβ on naked plates was much lower after washing **(Figure 2.4a)**. Although the dextran coated SPION could be recognized by Aβ presumably due to its negative surface charges,[76] the addition of sialic acid onto the dextran NP (NP-Sia) enhanced NP binding with Aβ **(Figure 2.5a)**. To further ascertain the role of sialic acid, a competitive ELISA was

performed when fixed amount of Aβ was added to NP-Sia coated plates together with free sialic acid. As free sialic acid should compete with NP-Sia for Aβ binding, the amount of Aβ remained on the plate should decrease with increasing amount of sialic acid. This was observed experimentally **(Figure 2.4b)**, supporting the notion that sialic acid plays a considerable role in mediating Aβ binding.[67]

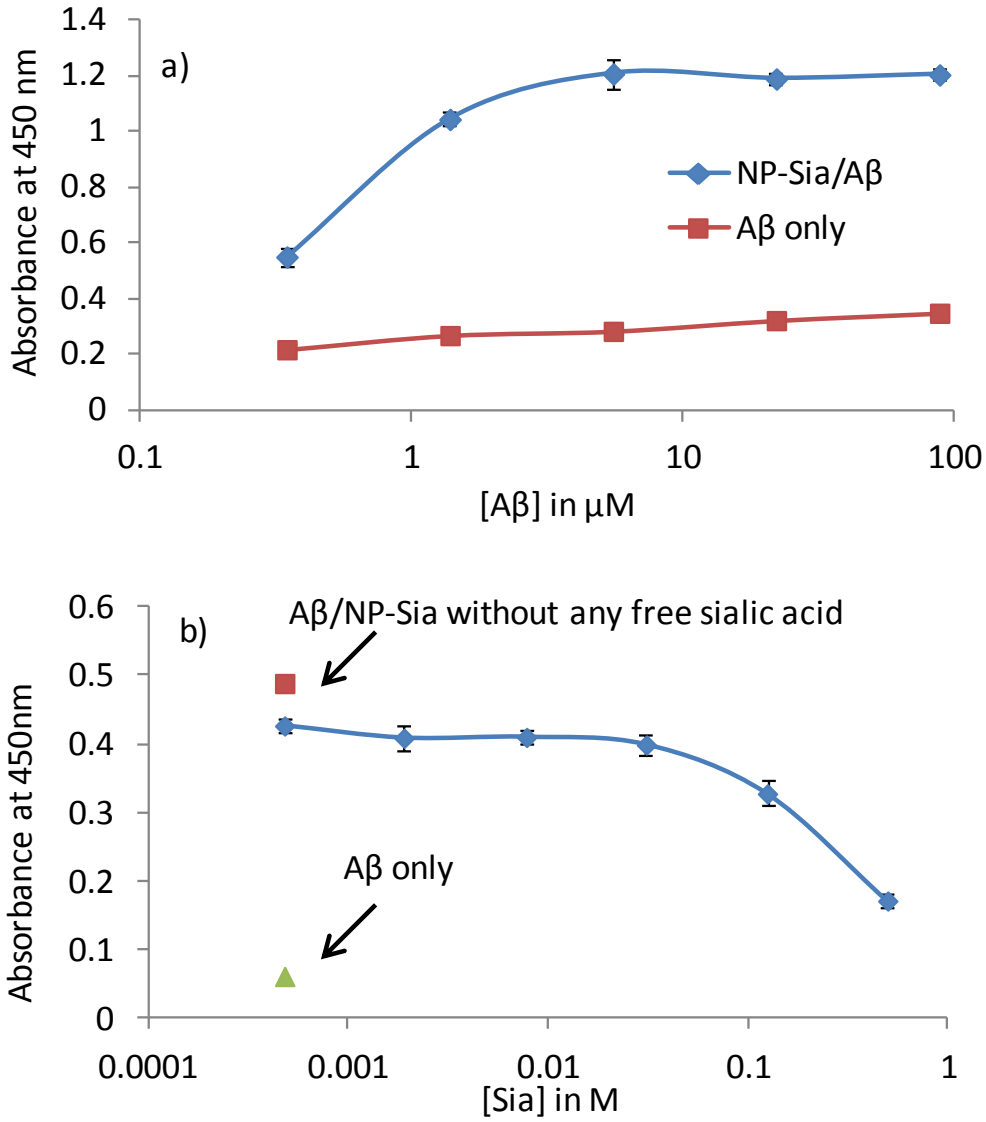

Figure 2.4: (a) ELISA curve for Aβ binding to immobilized NP-Sia); (b) ELISA curve of Aβ (0.5 µM) binding to immobilized NP Sia in the presence of increasing concentration of free sialic acid (blue circle).

In ELISA, blocking agents such as bovine serum albumin (BSA) is commonly employed to reduce the non-specific adsorption of proteins on the microtiter plate, including some for Aβ binding studies.[28b, 77] However, in our assays, we observed a considerable difference between the BSA-blocked and unblocked wells, where the wells incubated with BSA showed

significantly higher Aβ binding even without any NP present compared to those not containing BSA **(Figure 2.5b)**. Varying the amount of BSA (0.1% - 5%) as well as using milk as the blocking agent did not resolve this problem. We attributed this to the adsorption of Aβ by BSA or milk proteins. This outcome was in agreement with a report showing the strong affinities of plasma proteins such as albumin with Aβ,[78] suggesting the importance of protein free blocking in ELISA for Aβ detection.

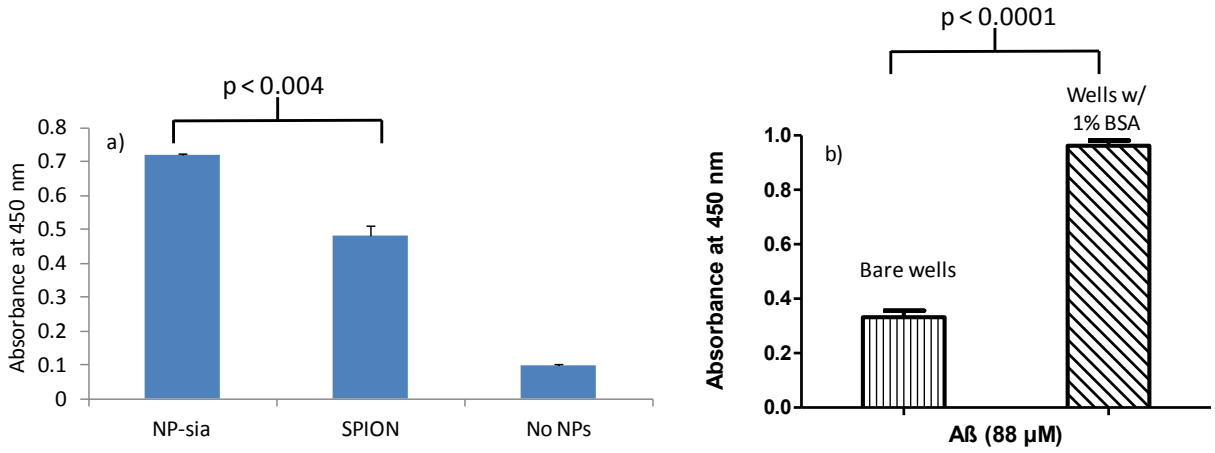

Figure 2.5: a) Absorbance of Aβ binding to wells containing NP-Sia, SPION and bare wells suggesting the importance of sialic acid in Aβ recognition; b) Bare ELISA wells showed significantly less Aβ binding compared to wells incubated with 1% BSA

To further prove the binding between Aβ and NP-Sia, we performed Prussian blue staining, which is a staining method specific for iron. NP-Sia by itself could bind to the 24 well cell culture plate, which was evident from the bright blue color when Prussian blue reagent was added to wells incubated with NP-Sia **(Figure 2.6a)**. If Aβ binds with free NP-Sia, the Aβ/NP-Sia complex should have reduced adhesion to the microtiter plate due to shielding of NP-Sia by

Aβ. Indeed, when NP-Sia was pre-incubated with Aβ fibril (25 μM) and then added to the plate followed by washing, much reduced blue color was observed with Prussian blue staining **(Figure 2.6b)**. Higher concentration of Aβ (100 μM) further decreased the level of Prussian blue **(Figure 2.6c)**. Aβ by itself did not bind much with the wells under the experimental condition. These observations support the conclusion that NP-Sia can bind with Aβ.

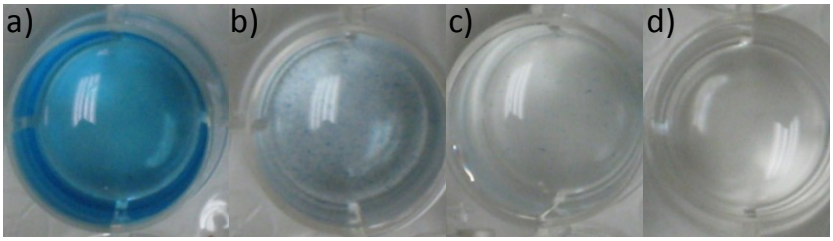

Figure 2.6: Pictures of 24 well cell culture plates after incubation with a) NP-Sia (200 μg/mL); b) NP-Sia (200 μg/mL) with Aβ (25 μM); c) NP-Sia (200 μg/mL) with Aβ (100 μM); and d) Aβ (100 μM). After washing, the wells were treated with Prussian blue

2.4 Confirmation of Aβ and NP-Sia Binding by Tyrosine Fluorescence Measurement and TEM

Aβ contains a tyrosine residue (Tyr10), the intrinsic fluorescence of which can be used to monitor binding.[28b] Aβ monomer (30 μM) was incubated with various concentrations of NP-Sia (0.02, 0.2, and 2 mg/mL) at room temperature. After 24 hours, the solution was centrifuged and the tyrosine fluorescence of the supernatant was recorded **(Figure 2.7a)**. Centrifugation of Aβ or NP-Sia alone at 10,000 g did not produce any pellets or fluorescence changes. However,

incubation of Aβ with NP-Sia followed by centrifugation showed a dose dependent decrease of supernatant fluorescence. The fluorescence intensity dropped to baseline levels with 2 mg/mL NP-Sia suggesting complete removal of Aβ from the solution. A pellet was observed at the bottom in tubes where NP-Sia was incubated with Aβ, indicating that NP-Sia formed aggregates with Aβ. The binding between NP-Sia and Aβ was confirmed by TEM of the pellets (**Figure 2.7b-d)**. Unlike free Aβ, it was not necessary to add uranyl acetate to stain Aβ since the NP bound provided sufficient contrast in TEM. Extensive aggregates were evident from TEM images with higher concentrations of NP-Sia **(Figure 2.7b-d)**.

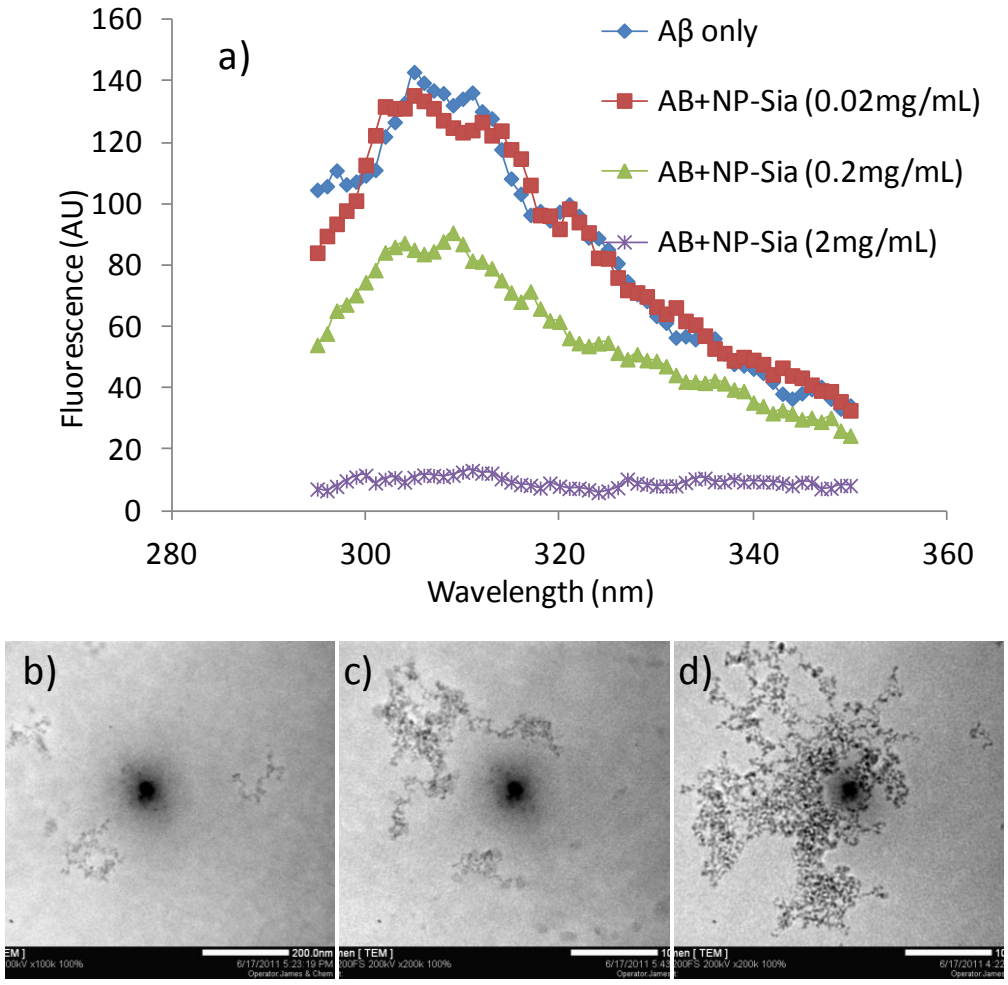

Figure 2.7: a) Emission spectra of supernatants upon incubation of Aβ with NP-Sia followed by centrifugation (excitation λ=280 nm). TEM images of the pellets obtained by incubating Aβ with b) 0.02 mg/mL, c) 0.2 mg/mL, and d) 2 mg/mL of NP-Sia after centrifugation

2.5 NP-Aβ binding Detected by MRI

Due to their high magnetic relaxivities, the superparamagnetic nanoparticles are useful contrast agents for T2/T2* based MR imaging.[79] Another interesting property of the magnetic nanoparticles is that their transverse relaxivities can be significantly enhanced when they form

larger clusters due to target binding.[71a, 80] This magnetic relaxation switching phenomenon has been utilized for biological detections.[71a, 80] As supported by our tyrosine fluorescence and TEM studies discussed above, we envision the multivalent binding of NP-Sia with Aβ should lead to the formation of NP clusters. These clusters can create larger local magnetic field inhomogeneities thus are more efficient in dephasing the spins of surrounding water protons and lowering T2* relaxation time.

The binding of Aβ fibril with NP-Sia was examined by MRI. After incubation of Aβ with NP-Sia (0.1 mg/mL) overnight at room temperature, T2* weighted MR images were acquired. The presence of Aβ led to many more darkened spots compared to NP-Sia alone enabling the detection of Aβ **(Figure 2.8a vs Figure 2.8c)**. Quantification of the images demonstrated that the T2* relaxation time of NP-Sia (0.1 mg/mL) was 23 ms, which was reduced to 16 ms in the presence of Aβ **(Figure 2.8e)**. Addition of 0.1 M free sialic acid during incubation significantly reduced the number of dark spots in T2* weighted images presumably due to the competitive binding of free sialic acid to Aβ **(Figure 2.8b,e)**. This was corroborated by the increase in T2* relaxation time (20 ms). Similar phenomena were observed when Aβ monomer was incubated with NP-Sia **(Figure 2.9)**.

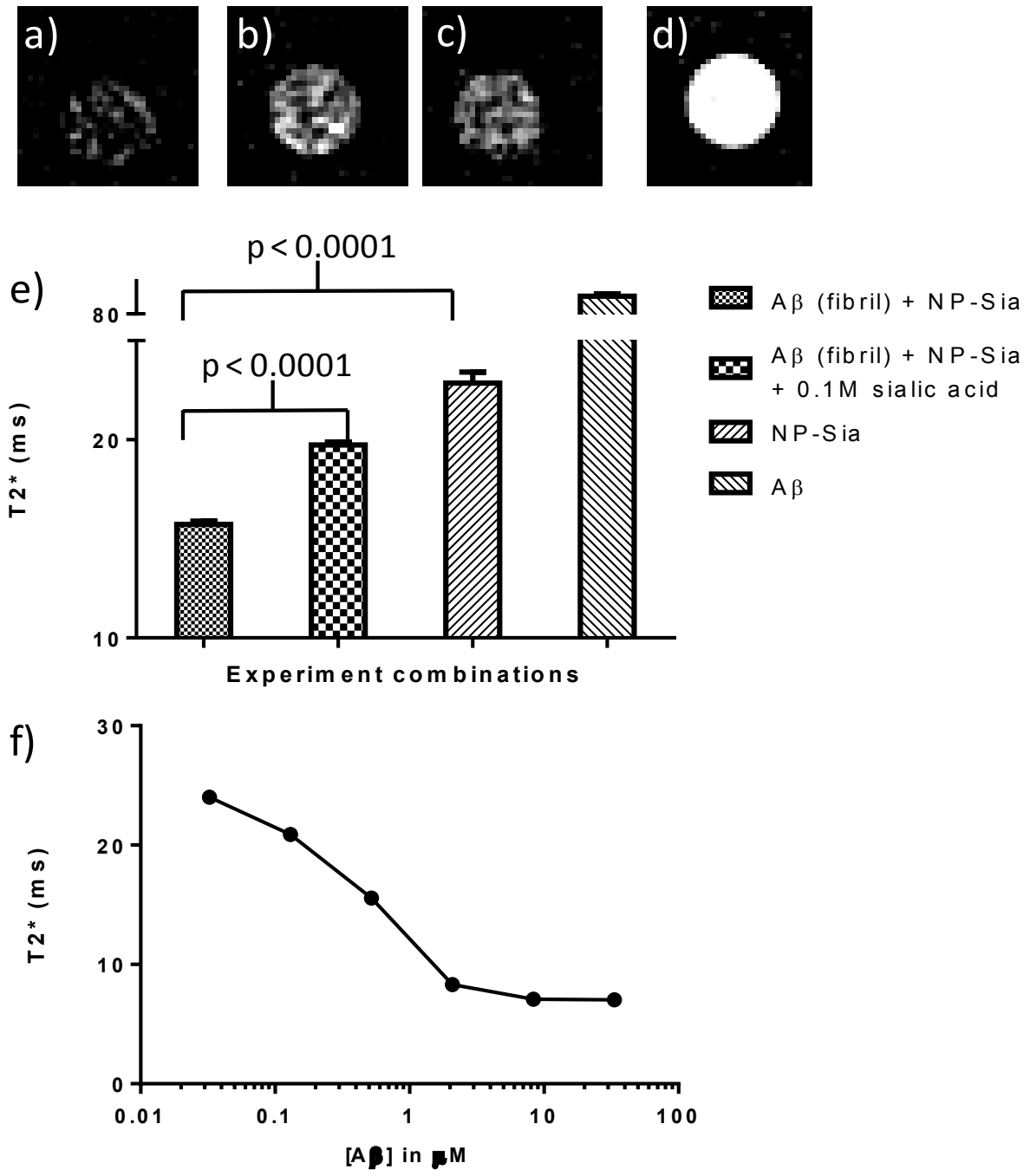

Figure 2.8: T2* weighted MR images of (a)-(d) incubation of NP-Sia with Aβ fibrils and their controls. (e) Quantification of T2* (ms) of images in (a)−(d). (f) Changes of T2* relaxation time (ms) in the presence of increasing concentrations of Aβ.

In another experiment, increasing concentrations of Aβ were incubated with fixed amount of NP-Sia (0.1 mg/mL). Higher Aβ concentration should lead to more extensive NP-Sia aggregation and reduction of T2* relaxation time, which was observed experimentally **(Figure 2.8f)**. The limit of detection was 0.05 μM Aβ in this experiment.

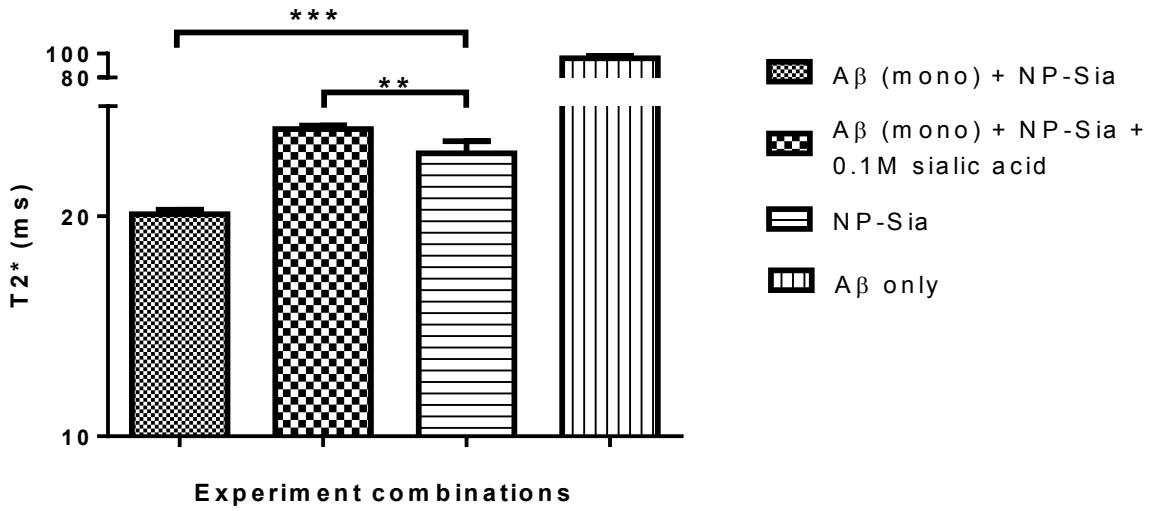

Figure 2.9: MRI generated T2* values of NP-Sia/Aβ binding. NP-Sia (0.1 mg/mL) incubated with Aβ monomers (30 μM) and also in the presence of free sialic acid (0.1 M). The error bars represent the standard deviation of three measurements

2.6 *Ex vivo* Detection of Aβ by NP-Sia Aided MRI

To test the selectivity of NP-Sia in tissue binding and lay the foundation for future *in vivo* applications, we examined *ex vivo* detection of Aβ by NP-Sia in a mouse brain. Brains were

harvested from C57BL6 mice and incubated in a solution of Aβ fibril for 48 hours. Aβ was absorbed on the surface of the brains and the unbound Aβ was removed by thorough washing. The Aβ containing brains were then treated with NP-Sia followed by removal of unbound particles. T2* weighted MR images were acquired, and dark spots were observed on the surface of Aβ brains incubated with NP-Sia **(Figure 2.10a)**. The dark spots on the surface disappeared when free sialic acid was added during incubation to compete with NP-Sia binding **(Figure 2.10b)**. As a control, normal mouse brain was incubated with NP and Aβ brains were imaged using the same MRI protocol. No darkening of brain surface was observed in these cases **(Figure 2.10c, d)**. Furthermore, Prussian blue staining showed that only Aβ brains incubated with NP-Sia exhibited the characteristic blue color due to the presence of iron **(Figure 2.10e)**, whereas the other brains (Aβ brain + NP-Sia + free sialic acid, normal brain + NP-Sia, Aβ brain) showed little blue coloration **(Figure 2.10f,g,h)**, thus supporting MRI results. These observations suggest that NP-Sia did not non-specifically bind with brain components and Aβ could be detected by NP-Sia aided MRI in this *ex vivo* model.

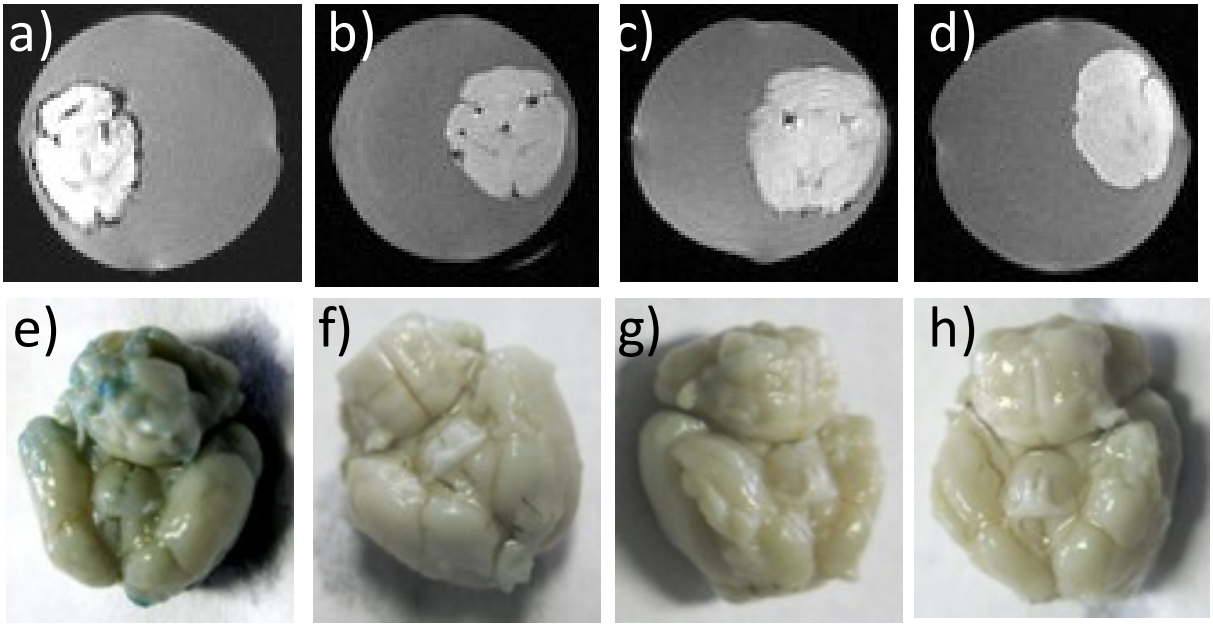

Figure 2.10: T2* weighted MR images of (a) Aβ mouse brain incubated with NP-Sia; (b) Aβ brain incubated with NP-Sia in the presence of free sialic acid; (c) brain incubated with NP-Sia; and (d) Aβ brain; Prussian blue staining of the previous mouse brains

2.7 Effect of NP-Sia on Aβ Aggregation

After demonstrating Aβ can bind with NP-Sia, we assessed the effects of NP on Aβ aggregation and fibril growth via native gel electrophoresis. Native PAGE gels can preserve the fibrillar and protofibrillar integrity of Aβ and prevent the potential fibril deaggregation in the presence of detergent such as sodium dodecyl sulfate.[28c] Aβ monomers were incubated with NP-Sia at 25 °C followed by native-PAGE gel electrophoresis. At room temperature, Aβ aggregation was slower with significant amounts of oligomers observed after 24 hours **(Figure 2.11**, Lane 1**)**. With increasing concentrations of NP-Sia (0.02 to 2 mg/mL), the oligomers of Aβ disappeared with concomitant increase in fibrils formed **(**Lanes 2-4 of **Figure 2.11**, and

Figure 2.12**)**. This indicates that NP-Sia can reduce the amount of the Aβ oligomers in solution presumably by expediting the formation of Aβ fibrils.

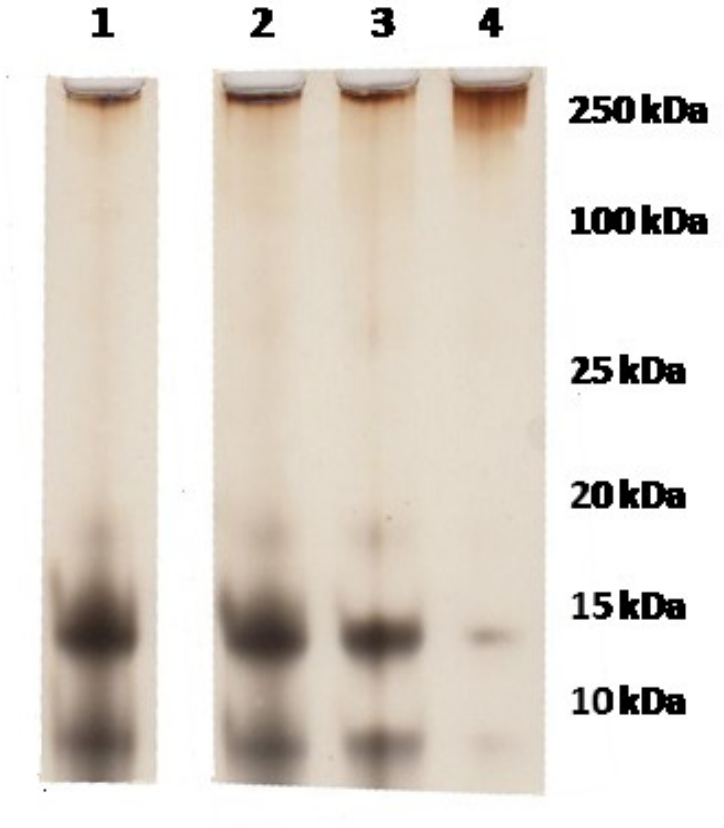

Figure 2.11: PAGE gel of Aβ. Aβ only (Lane 1); Aβ incubated with 0.02 mg/mL (Lane 2); 0.2 mg/mL (Lane 3); and 2 mg/mL (Lane 4) of NP-Sia

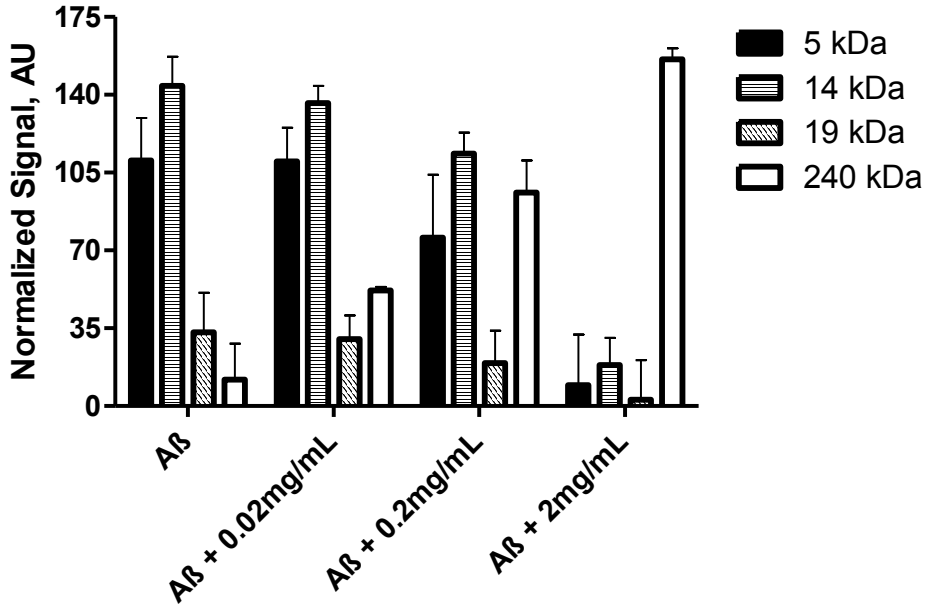

Figure 2.12: Quantification of the intensities of various bands of the PAGE gel. Aβ only (Lane 1); Aβ incubated with 0.02mg/mL (Lane 2); 0.2mg/mL (Lane 3); and 2mg/mL (Lane 4) of NP-Sia. 5 kDa are the Aβ monomer. 14 kDa and 19 kDa are oligomers. 250 kDa are fibrils

2.8 NP-Sia Effect on Aβ-Induced Cytotoxicity

For potential applications in Aβ detection and AD diagnosis, it is crucial that the contrast agents do not cause toxicities to the neuronal cells. To evaluate this, cell viability MTS assays were performed using SH-SY5Y neuroblastoma cells. The MTS assay is a colorimetric assay measuring the metabolic activities of mitochondria. Aβ exhibited significant cytotoxicities **(**Figure 2.13**a)** with IC_{50} value about 2 μM. NP-Sia (250 μg/mL) was found to be non-toxic to the cells, suggesting the high bio-compatibility of the NPs. To confirm the MTS assay results, another cell viability assay, i.e., LIVE/DEAD assay, was utilized. The LIVE/DEAD assay

determines cell viability based on plasma membrane integrity and esterase activity, which is complementary to MTS. Consistent with the MTS assay results, the LIVE/DEAD assay gave similar IC_{50} values for Aβ induced cytotoxicity **(Figure 2.14)**.

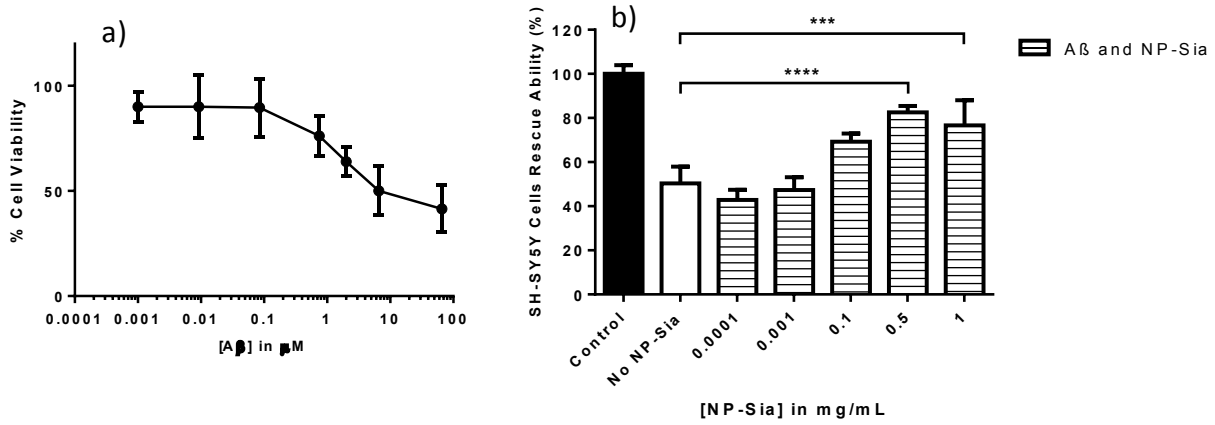

Figure 2.13: a) Viability of SH-SY5Y neuroblastoma cells decreased with increasing concentration of Aβ as determined by a MTS cell viability assay. b) Addition of NP-Sia to SH-SY5Y neuroblastoma cells incubated with Aβ (2 μM) reduced Aβ induced cytotoxicity

Although there is ongoing debate regarding the cause of AD, it is generally accepted that the aggregation state of Aβ is crucial in determining its degree of neurotoxicity and the soluble Aβ oligomeric form may be the key effectors of cytotoxicity in AD.[13-14, 81] As NP-Sia can sequester Aβ and reduce the amounts of oligomers in solution, we envision that NP-Sia can potentially protect cells from Aβ induced cytotoxicities. To test this possibility, SH-SY5Y cells were treated with fixed concentration of Aβ (2 μM) in the presence of variable amounts of NP-Sia (0.0001, 0.001, 0.1, and 0.5 mg/mL). Without NP-Sia, approximately 50% of the cells

remained viable after 24 hour incubation. A dose dependent increase in cell viability was observed with increasing concentrations of NP-Sia in both MTS and LIVE/DEAD assays, where 0.5 mg/mL of NP-Sia was able to increase the viability of the cell cells to 80% **(Figure 2.13b)**. This suggests that NP-Sia can mitigate the toxicity of Aβ, presumably by segregating Aβ in the fibril form on the NP. The full impact of NP-Sia and NP-Sia/Aβ complex on brain as well as the clearance of NP-Sia/Aβ complex *in vivo* will need to be established through further studies.

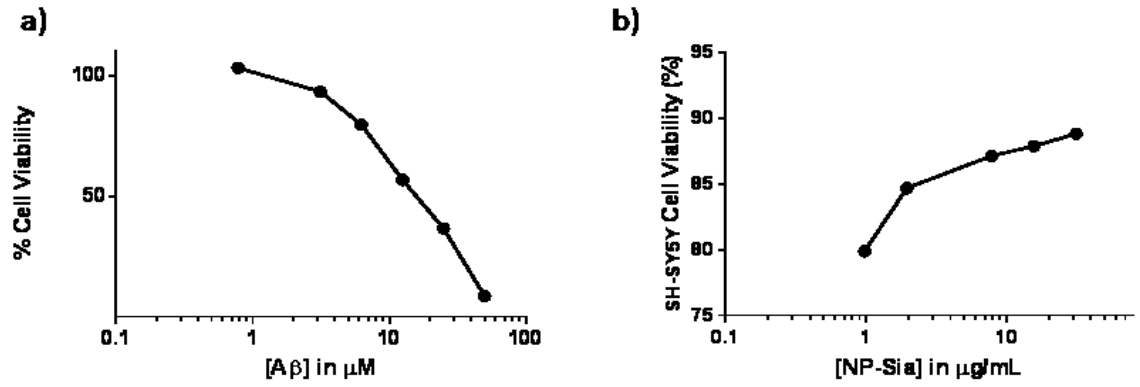

Figure 2.14: a) Viability of SH-SY5Y neuroblastoma cells decreased with increasing concentration of Aβ as determined by a LIVE/DEAD cell viability assay. b) Addition of NP-Sia to SH-SY5Y cells incubated with Aβ protected cells from Aβ induced cytotoxicity

Compared to literature reports of Aβ molecular imaging,[63] our approach is unique in that we take advantage of the interactions between Aβ and carbohydrates. While the results are promising, further studies are necessary to demonstrate the sensitivity and the selectivity of NP-Sia in transgenic mice and humans and compare with those of other probes.

For future Aβ plaque imaging *in vivo*, it will be crucial that the contrast agent can access the plaques in the brain. To bypass the BBB, contrast agents can be injected directly into the

brain.[63d] A less invasive method is to administer the contrast agent in combination with agents such as mannitol to temporarily open up the tight junctions in the BBB.[63c] Alternatively, cell-penetrating peptides[82] can be immobilized onto the nanoparticles to facilitate crossing of the BBB.[83] With its large surface area, NP-Sia is amenable to further modification to enhance its ability to cross the BBB. The implications of these suggested modifications will be further discussed and tested in the next chapter.

2.9 Conclusion

We demonstrated that glyconanoparticles could selectively bind Aβ. The protein free blocking was important in ELISA assays to avoid the non-specific absorption Aβ to plates. The superparamagnetic nature of the glyconanoparticles enabled the detection of Aβ by MRI both *in vitro* and *ex vivo* on mouse brains. NP-Sia expedited the formation of Aβ fibril, thus converting Aβ to its less toxic form and protecting the cells from Aβ induced cytotoxicities. Other carbohydrates such as full structure of GM1 and glycosaminoglycans can be utilized to further enhance Aβ binding selectivity and specificity. These attributes coupled with the high biocompatibility, magnetic relaxivity and large surface area bode well for potential *in vivo* application of glyconanoparticles for Aβ detection and imaging.

2.10 Experimental Section

Materials and Instrumentation

Unless otherwise indicated, all starting materials, reagents and solvents were obtained from commercial suppliers and used as supplied without further purifications. Iron(III) chloride hexahydrate ($FeCl_3 \cdot 6H_2O$) was purchased from Honeywell Riedel-de Haen, Iron(II) chloride tetrahydrate ($FeCl_2 \cdot 4H_2O$), dextran (9−11 kDa), epichlorohydrin, bovine serum albumin (BSA), dimethylsulfoxide (DMSO), ethyl-(3,3-dimethylaminopropyl) carbodiimide hydrochloride (EDC), bovine serum albumin (BSA), and sodium chloride were purchased from Sigma-Aldrich. Ammonium hydroxide (NH_4OH, 28−30%) and hydrogen peroxide (30%) were purchased from CCI. Amberlite IR 120 hydrogen form (Amberlite H+) was purchased from Fluka. 1,1,1,3,3,3-Hexafluoro-2-propanol 99.9% was purchased from Acros. Buffered 10% formalin solution was purchased from Azer Scientific. Potassium ferrocyanide $K_4Fe(CN)_6$ trihydrate was purchased from Mallinckrodt. 3,3′,5,5′-tetramethylbenzidine (TMB) was purchased from Acros Organics. Thioflavin T (ThT), UltraPure Grade was purchased from AnaSpec. Beta amyloid (1-42) was purchased from GL Biochem. (Shanghai) Ltd. (No. 52487). SH-SY5Y cells were purchased from American Type Culture Collection (ATCC). Phosphate buffered saline (PBS), Dulbecco's modified Eagle medium (DMEM), sodium pyruvate (100 mM), glutamine, penicillin−streptomycin (Pen Strep) mixture, the Aβ 1-16 (6E10) monoclonal antibody, SIG-39320 was purchased from Covance, and goat anti-mouse HRP-conjugated secondary antibody, was purchased from BioRad. Tween 20 was purchased from BioRad. CellTiter 96 Aqueous One

solution containing 3-(4,5-dimethylthiazol-2-yl)-5-(3-carboxy-methoxyphenyl)-2-(4-sulfophenyl)-2H-tetrazolium (MTS) was purchased from Promega. Ultrathin-carbon type A, 400 mesh copper grids for TEM were purchased form Ted Pella, Inc. Ultrafiltration membranes and centrifugal filters were purchased from Millipore, while dialysis tubings were obtained from BioDesign Inc. SH-SY5Y cells were cultured in DMEM. All cell culture media was supplemented with 10% inactivated FBS, 1% Pen-Strep mixture, glutamine (2 mM), and sodium pyruvate (1 mM). Dynamic light scattering (DLS) and zeta potential measurements were performed on a Zetasizer Nano zs apparatus (Malvern, U.K.). Transmission electron microscopy (TEM) images were collected on a JEM-2200FS operating at 200 kV using Gatan multiscan CCD camera with Digital Micrograph imaging software. Thermogravimetric analysis (TGA) was carried on a Thermal Advantage (TA-Instruments-Waters LLC) TGA-Q500 series and the samples were burned under nitrogen. Fluorescence emission spectra were recorded on a HITACHI F-4500 Fluorescence. Native-PAGE gel analysis was performed via ImageJ 1.42q (NIH). Spectrometer provided with a continuous (CW) high power Xe lamp as the excitation source. FACS experiments were conducted on a BD Vantage SE flow cytometer. HRMAS NMR experiments were carried out on a Varian Inova-500 NMR spectrometer equipped with a 4 mm gHXNanoprobe.

Synthesis of SPION

To a solution of dextran (10 g) in 0.22 μm filter filtered deionized water (23 mL), an aqueous solution of (0.7g, 2.6 mmol) $FeCl_3.6H_2O$ (1 mL) was added, and the mixture was cooled

in an ice bath (ice/water). To improve the magnetic properties of the iron oxide nanoparticles, the mixture was stirred under Argon gas for 2 hours to eliminate oxygen from the reaction flask. A freshly prepared 0.22 μm filtered aqueous solution containing $FeCl_2.4H_2O$ (0.28 g, 1.4 mmol) in water (1 mL) was added to the cooled solution. Chilled 30% NH_4OH (1 mL) was added dropwise while stirring rapidly. The black suspension was brought to 70-80 ºC over a 1 hour period, and maintained at this temperature for additional 90 min. After being cooled to room temperature, the suspension was dialyzed (MWCO 14,000) against distilled water (20 L bucket, 4 changes). The excess ammonium hydroxide, ammonium chloride, and dextran were further removed by ultrafiltration (MWCO 100,000). After 4 washes, the suspension was concentrated to ~ 75 mL, collected and centrifuged to remove any large particulates. Cross-linking the dextran coating on the surface of DSPION was achieved by adding an aqueous sodium hydroxide solution (5 M, 20 mL) and epichlorohydrin (10 mL). The mixture was stirred rapidly for 24 hr at room temperature. The excess epichlorohydrin was removed by dialysis against distilled water (MWCO 14,000) in a 20 L bucket (6 changes). The solution was concentrated to ~ 100 mL by ultrafiltration. The introduction of primary amino groups to the surface of the cross-linked dextran coated DSPION was achieved by adding 30% NH_4OH (20 mL) and stirring the mixture at 37 ºC for 36 hours. The colloidal solution was dialyzed (MWCO 14,000) against distilled water (20 L bucket, 4 changes), and then concentrated to 50 mL by ultrafiltration (MWCO 100,000) to yield DSPION-NH2.

Synthesis of NP-Sia

An aqueous solution of sialic acid 2[71b] (100 mg, 0.208 mmol) and EDC (150 mg, 0.78 mmol) in water (10 mL) was stirred for 30 minutes at room temperature. NP-NH_2 (100 mg in 15 mL of pH 8.5 carbonate buffer) was added and stirred for 12 hours at room temperature. The reaction mixture was centrifuged through 100,000 MWCO Amicon centrifugal filters. The supernatant was collected and an aqueous solution of 0.01 M sodium hydroxide was added till the pH value reached 12. The reaction mixture was stirred at room temperature for 15 minutes and the solution was neutralized by careful addition of 0.01 M hydrochloric acid. The reaction mixture was centrifuged through 100,000 MWCO Amicon centrifugal filters. The supernatant was diluted with water and centrifuged again. This process was repeated three times.

High-Resolution Magic Angle Spinning NMR

HRMAS NMR experiments were carried out on a Varian Inova- 500 NMR spectrometer equipped with a 4 mm gHXNanoprobe (Variannmr Inc., Palo Alto, CA) available at the University of Tennessee Health Science Center (Memphis, TN). The HR-MAS probe with internal lock is capable of performing either direct or indirect (inverse) detection experiments. Magic angle spinning (MAS) experiments were performed at spinning rates of up to 2.5 kHz using a 40 μL glass rotor. NP-Sia was dissolved in D_2O solvent and was further diluted at different concentrations with D_2O to find out the concentration limit to the NMR signal broadening. HRMAS 1H-NMR spectra were obtained using 100-600 scans for each experiment.

The sample temperature was regulated with an accuracy of ± 0.1 °C.

Thiobarbituric Acid Assay

NP-Sia was treated with 0.2% sodium dodecylsulfate (SDS) in 0.1 N H_2SO_4 to the final concentration of 2.86 mg/mL at 85°C for 60 minutes to hydrolyze the sialic acid from the nanoparticle. It was then incubated at 37 °C for 30 minutes, and then treated with 50 µL periodic acid (25mM H_5IO_6 in 125mM HCl) for 30 min at 37 °C. The excess periodic acid was inactivated with 40 µL sodium meta-arsenite (2% $NaAsO_2$ in 500mM HCl). When the resulting yellow-brownish color (color of the liberated iodine) disappeared, 200 µL of thiobarbituric acid (0.1M 4,6- dihydroxypyrimidine-2-thiol, pH 9) (pH adjusted with 0.1 mol/L NaOH) was added. The reaction tubes were incubated in a boiling water bath for 10 min. The tubes were transferred to an ice-water bath for 2 min followed by 2-min incubation at 37 °C. (The latter incubation improves the extent and increases the rate of chromophore extraction.) The colored complex was extracted by adding 500 µL butanol/HCl solution (n-butanol containing 5.7% of 10.5M HCl) with vigorous agitation. The two phases were separated by centrifugation for 5 minutes. 250 µL of the upper phase was placed into a 96-well flat-bottomed microtiter plate and the absorbance was determined at 550nm using a microplate spectrophotometer.1, 2

Deaggregation and Preparation of Aβ

Synthetic Aβ (1-42) peptide (1 mg) was dissolved in spectroscopy grade 99.9% 1,1,1,3,3,3-hexafluoro-2-propanol (3 mL), sonicated for 15 minutes and lyophilized for 72 hours. The thin peptide film was dissolved in 0.22 μm filtered solution of 10 mM NaOH solution (0.25 mL) followed by dilution with deionized water (0.625 mL) and PBS buffer (0.625 mL) to the desired final volume of 1.5 mL (The stock Aβ solution concentration is 147.7 μM). For experiments requiring fibril formation, the previous solution was incubated for 48 hours at 37 °C.

ThT Assay

ThT fluorescence measurements were performed in a clear bottom black 96-well fluorescence plate (COSTAR 3695-96) on a FLUOstar OPTIMA (BMG Labtechnologies). The control solutions were 250 μL of tris buffer, 250 μL of 20 μM Aβ (Aβ (20 μM)), and 250 μL of 20 μM ThT. 50 μL of Aβ (20 μM) solutions were added to 200 μL of different concentrations of (10, 20, and 50 μM) ThT solutions. ThT fluorescence measurements were performed with λex = 440 nm (10 nm bandpass) and λem = 489 nm (10 nm bandpass).

ELISA assay

To a well in a Nunc MaxiSorp 96-well ELISA plate was added 50 μL of NP-Sia solution (0.5 mg/mL), which was incubated at 37 °C overnight. After washing the wells with 3 x 300 mL PBST, 50 μL of Aβ solutions with various concentrations were added to the wells (0.34, 1.38, 5.53, 22.1, 88.5 μM) and incubated at 22 °C for 12 hours. The plates were washed with 3 x 300 mL PBST and the anti-Aβ (1-16) IgG (6E10) monoclonal antibody, SIG-39320 (50 μL per well, 0.137nM, 1:24000 in 1% (w/v) BSA containing PBS) was added, which in turn was incubated at 22 °C for 1 hour. After washing with 3 x 300 μL PBST, the solution was discarded and the wells were washed three times with 300 μL PBST and incubated for 1 hour with 50 μL of the goat anti-mouse HRP-conjugated secondary antibody (1.7 nM, 1:18000 in 1% (w/v) BSA in PBS). The solution was discarded, and the wells were washed three times with 300 μL PBST. To a freshly prepared 3,3',5,5'-tetramethylbenzidine (TMB) solution (5 mg of TMB was dissolved in 2 mL of DMSO and then diluted to 20 mL with citrate phosphate buffer), 20 μL of H_2O_2 was added. This mixture (150 μL) was immediately added to the ELISA wells. Blue color was allowed to develop for 10-20 minutes. The reaction was quenched (yellow color) by addition of 0.5 M H_2SO_4 (50 μL/well) and the absorbance was measured at 450 nm on an iMark™ Microplate Reader.

For sialic acid inhibition assay, a solution of NP-Sia (0.5 mg/mL, 50 μL) was incubated in a 96-well plate at 37 °C overnight. After washing the wells with PBST (3 x 300 μL), Aβ (0.5 μM, 50 μL) was added to the wells immediately followed addition 50 μL of different dilutions of pH 7.4 sialic acid solution (0.00048, 0.0019, 0.0078, 0.031, 0.125, 0.5 M). The plate was incubated at 22 °C for 12 hours. The previous protocols were then followed for antibody incubation and color development.

Intrinsic Tyrosine Fluorescence Assay

An Aβ solution in 10 mM NaOH (443 μM, 13.5 μL) was added to a solution of NP-Sia with different concentrations 0.02, 0.2, and 2 mg/mL NP-Sia to a final volume of 200 μL in eppendorf® tubes. The tubes were gently mixed and incubated at room temperature for 24 hours. After incubation, the samples were centrifuged for 20 minutes at 10,000 x *g* to sediment fibrils and aggregates. The tyrosine fluorescence of the supernatant was measured via HITACHI F-4500 Fluorometer (excitation wavelength at 280 nm).

Aβ/NP-Sia Binding MRI Experiments

Six eppendorf tubes containing nanoparticles and Aβ were incubated in PBS buffer (total volume 750 μL) for 24 hours at room temperature. The final concentration of NP-Sia was 0.33 mg/mL and final concentration for Aβ was 10 μM. For sialic acid competition experiments, free sialic acid (0.1 M) was added. The composition of the tubes was as follows: only Aβ, only NP-Sia, fibrillar Aβ+NP-Sia, fibrillar Aβ+NP-Sia+0.1 M free sialic acid, monomeric Aβ+NP-Sia, and monomeric Aβ+NP-Sia+0.1 M free sialic acid (each tube had a total volume of 750 μL in PBS buffer). Following incubation, 2% agarose gel (1.75 mL) was added to the incubated samples to make the final volume of 2.5 mL in 5 mL-polystyrene round-bottom FACS tubes (BD Falcon). The tubes were placed at room temperature for 5 min and then at 4 °C till the time of

MRI. To evaluate the T2* characteristics of the nanoparticles in phantoms, the following parameters were used: head coil, 3D fast spoiled gradient recalled echo sequence, flip angle = 15°, 16 echo times (TEs) = 2.1 ms, 4.6 ms, 7.0 ms, 9.4 ms, 11.8 ms, 14.3 ms, 16.7 ms, 19.1 ms, 21.5 ms, 24.0 ms, 26.4 ms, 28.8 ms, 31.2 ms, 33.7 ms, 36.1 ms, and 38.5 ms, time of repetition = 41.9 ms, receiver bandwidth = ± 62.5 kHz, field of view = 16 cm, slice thickness = 1.5 mm, number of slices = 16, acquisition matrix = 256 × 256, and number of excitation = 1.

Binding Assessment via TEM

Similar sample preparation protocol to intrinsic tyrosine fluorescence was used for TEM imaging. 10 μL of the samples were deposited on ultrathin-carbon type A, 400 mesh copper grids (Ted Pella, Inc.) and let to evaporate under the hood. Once dry, 1% solution of uranyl acetate was added for 10 seconds and the solution was wicked away with filter paper. The grids were then washed with water, and dried for 15 min at room temperature.

Aβ and NP-Sia Binding Using Prussian Blue Staining

Aβ solutions (0.5 mL, 25 and 100 μM) were added to two eppendorf tubes containing solutions of NP-Sia (0.5 mL, 200 μg/mL) respectively. Control solutions were prepared by addition of PBS buffer (0.25 mL) into two eppendorf tubes containing NP-Sia (0.25 mL, 200 μg/mL) or Aβ (0.25 mL, 100 μM). All samples were rotated on a tube rotator overnight at room

temperature then incubated for 1 hour at 37 °C. NP-Sia/Aβ mixtures and control solutions (0.5 mL each) were pipetted to 24-well Costar cell culture, flat-bottomed plate and then incubated for 4 hours at 37 °C. After thoroughly washing the wells with PBS (5 x 0.5 mL), the Gomori's modified Prussian blue solution (0.5 mL) was added to each well and incubated for 10-15 minutes. Blue color was developed in wells containing NP-Sia. (Gomori's modified Prussian blue preparation: 2 mL of 10% $K_4Fe[CN]_6$ solution mixed with 2 mL of 20 % v/v HCl solution.)

Native-PAGE

Samples preparation was conducted exactly as described for the intrinsic tyrosine fluorescence experimenta1 procedure. 13.5 μL of Aβ in 10 mM NaOH (443 μM) was added to 200 μL pf NP-Sia (0.02, 0.2, and 2 mg/mL) in eppendorf® tubes. The tubes were gently mixed and incubated at room temperature for 24 hours. After incubation, 20 μL of the mixture was added to 5 mL of non-SDS sample buffer and was subjected to electrophoresis (200 V) on an 18% native-PAGE gel. The gels were then stained with Coomassie (for Aβ characterization) and silver staining (for Aβ/NP-Sia binding).

MRI Experiments

All MRI experiments were carried out on a GE 3T Signa® HDx MR scanner (GE Healthcare, Waukesha, WI).

NP-Sia Relaxivity Measurements

Seven different dilutions of the NP-Sia (0.00001, 0.0001, 0.001, 0.0125, 0.05, 0.1 mg/mL) were prepared to a final volume of 5 mL in 15 mL-centrifuge tubes (Corning). The tubes were placed on a polystyrene tube holder. To evaluate the R2 characteristics of the nanoparticles in phantoms, the following parameters were used: Head coil, 2D fast spin echo, flip angle = 90°, eight echo times (TEs) = 8.0 ms, 16.0 ms, 23.9 ms, 31.9 ms, 39.9 ms, 47.9 ms, 55.8 ms and 63.8 ms, time of repetition (TR) = 500 ms, receiver bandwidth (rBW) = ± 31.2 kHz, field of view (FOV) = 16 cm, slice thickness = 3 mm, number of slices = 2, acquisition matrix = 256 × 256 and number of excitation (NEX) = 1. To evaluate the R1 characteristics of the nanoparticles in phantoms, the following parameters were used: Head coil, 2D inversion recovery spin echo, flip angle = 90°, echo time = 15 ms, time of repetition = 2500 ms, inversion time = 50 ms, 100 ms, 400 ms, 700 ms and 1000 ms, receiver bandwidth = ± 15.6 kHz, field of view = 16 cm, slice thickness = 3 mm, number of slices = 1, acquisition matrix = 256 × 128 and number of excitation = 1. The R1 was estimated based on the spin recovery curve after inversion.

Determination of Detection Limit of Aβ

Eight 15 mL centrifuge tubes of constant concentration of nanoparticles and variable concentration of Aβ were incubated in PBS buffer (total volume of 3 mL/each) for 24 hours at room temperature. The final concentration of NP-Sia was 0.083 mg/mL and final concentration for series of Aβ solutions were 0.033, 0.130, 0.521, 2.083, 8.333, 33.333 μM. The remaining two tubes were considered blanks (contained 3 mL of NP-Sia with a final concentration of 0.083 mg/mL only). To evaluate the T2* characteristics of the nanoparticles in phantoms, the following parameters were used: head coil, 3D fast spoiled gradient recalled echo sequence, flip angle = 15°, 16 echo times (TEs) = 2.1 ms, 4.6 ms, 7.0 ms, 9.4 ms, 11.8 ms, 14.3 ms, 16.7 ms, 19.1 ms, 21.5 ms, 24.0 ms, 26.4 ms, 28.8 ms, 31.2 ms, 33.7 ms, 36.1 ms, and 38.5 ms, time of repetition = 41.9 ms, receiver bandwidth = ± 62.5 kHz, field of view = 16 cm, slice thickness = 1.5 mm, number of slices = 16, acquisition matrix = 256 × 256, and number of excitation = 1.

***Ex-vivo* Brain Aβ/NP-Sia Binding MRI Experiments**

The brains of C57BL6 mice were harvested and fixed in buffered 10% formalin solution for 48 hours. After washing with deionized water, brains were incubated with 22 μM Aβ (4 mL) for 48 hours at 4 ºC. The Aβ treated brains were incubated with NP-Sia (0.6 mg/mL, 4 mL) for 24 hours at 37 ºC after washing with deionized water. After incubation, the brains were washed thoroughly and placed in a 6-well plate (Costar 3516, Corning) in water. For the sialic acid competition experiment, 0.1 M free sialic acid was added with NP-Sia (4 mL). The brains were imaged with the following parameters (T2* weighted sequence): Wrist coil, 3D fast spoiled

gradient recalled echo sequence, flip angle = 15°, echo times = 9.8 ms, time of repetition = 20 ms, receiver bandwidth = ± 7.8 kHz, field of view = 8 cm, slice thickness = 0.5 mm, number of slices = 48, acquisition matrix = 256 × 256, and number of excitation = 3.

Prussian Blue Staining of Mice Brains

The same brains used in *ex-vivo* Aβ/NP-Sia MRI binding experiment were stained directly after imaging. Brains were soaked in 10% $K_4Fe[CN]_6$ solution and incubated for 10 min, then transferred to a vial containing a mixture of 10 wt % $K_4Fe[CN]_6$ /20 wt % HCl with a volume ratio of 1:1 for 10 min (Gomori's modified Prussian blue). The tissues were washed with water for four times. A blue color was observed on the areas bearing iron oxide nanoparticles.

MTS Cytotoxicity Assay:

SH-SY5Y cells were plated into 96-well plates at a density of 4 x 10^4 cells per well in 10% DMEM cell culture media for 24 hours at 37 °C and 5% CO_2. The culture medium was replaced with 2% serum solution of different concentrations of Aβ (0.001. 0.0092, 0.085, 0.75, 2, 5.5, 66 μM, 100 μL/well). After 24 hour incubation at 37 °C, the medium was replaced with MTS solution (20 μL in 200 μL) in culture medium and incubated for 6 hours at 37 °C. The developed brown color in the wells was an indication of live cells. The absorption of the plate was measured at 490 nm on iMark™ Microplate Reader (BioRad). Wells without cells (blanks)

were subtracted as background from each sample. To test the effect of NP-Sia on Aβ induced cytotoxicity, cells were incubated with Aβ (2 μM). Various concentrations of NP-Sia (0.0001, 0.001, 0.1, and 0.5 mg/mL) were added. The cell viabilities were evaluated in a similar manner as described above.

LIVE/DEAD® Cytotoxicity Assay

SH-SY5Y cells were plated into 24-well plates at a density of 1 x 10^4 cells per well in cell culture medium for 24 hours at 37 °C and 5% CO_2. Then the culture medium was replaced with non-serum DMEM media of 0.78, 3.125, 6.25, 12.5, 25, and 50 μM Aβ solution (100 μL/well). After 24 hour incubation at 37 °C and 5% CO_2, the supernatant was carefully collected (but not discarded due to the fact that it might contain dead cells). To detach cells 200 μL trypsin was added to each well. Then 500 μL of serum containing DMEM media was added. Cells from each well were collected and added to the corresponding supernatant, and after gentle swirling the tubes were centrifuged for 5 minutes at 2500 rpm at 4°C. Supernatants were discarded and the cells were washed with serum-free DMEM media. This process was repeated twice. After the final wash the cells were resuspended in 500 μL LIVE/DEAD® solution and transferred to FACS tubes on ice. Tubes were removed from the ice container and incubated at room temperature for 10 minutes and they were analyzed with the flow cytometry. Flow cytometry was set to measure the green fluorescence emission of calcein at 530 nm, 30 nm bandpass (emission 488 nm) and red fluorescence emission of ethidium homodimer-1 (EthD-1) at 660 nm, 20 bandpass. Standard compensation was performed using single color stain cells. Preparation of

the LIVE/DEAD solution was done by adding 10 μL of supplied 2 mM EthD-1 stock solution (component B) and 2 μL of the supplied 4mM calcein AM stock solution (component A) to 5 mL of DMEM. The controls used for this assay were unstained cells, Aβ untreated cells, and dead cells (50% ethanol fixed).

Rescue of SH-SY5Y Cells by NP-Sia as Determined by the LIVE/DEAD® Assay

SH-SY5Y cells were plated into 24-well plates at a density of 1 x 10^4 cells per well in cell culture medium for 24 hours at 37 °C and 5% CO_2. The culture medium was replaced with non-serum DMEM media of 2 μM Aβ (250 μL/well) in addition to 250 μL/well of different concentration of NP-Sia (0.97, 1.95, 7.81, 15.62, and 31.25 μg/mL). After 24 hour incubation at 37 °C and 5% CO_2, the supernatant was carefully collected (but not discarded due to the fact that it might contain dead cells). To detach cells 200 μL trypsin was added to each well. 500 μL of serum containing DMEM media was added. Cells from each well were collected and added to the corresponding supernatant, and after gentle swirling the tubes were centrifuged for 5 minutes at 2500 rpm at 4°C. Supernatants were discarded and the cells were washed with serum-free DMEM media. This process was repeated twice. After the final wash the cells were resuspended in 500 μL LIVE/DEAD® solution and transferred to FACS tubes on ice. Tubes were removed from the ice container and incubated at room temperature for 10 minutes and they were analyzed with the flow cytometry. Flow cytometry was used to measure the green fluorescence emission of calcein at 530 nm, 30 nm bandpass (emission 488 nm) and red fluorescence emission of ethidium homodimer-1 (EthD-1) at 660 nm, 20 nm bandpass. Standard compensation was

performed using single color stain cells. Preparation of the LIVE/DEAD solution was done by adding 10 μL of supplied 2 mM EthD-1 stock solution (component B) and 2 μL of the supplied 4mM calcein AM stock solution (component A) to 5 mL of DMEM.

The controls used for this assay were unstained cells, Aβ untreated cells, dead cells (50% ethanol fixed), 2 μM Aβ treated cells, and only-NP-Sia treated cells.

Chapter 3 Bovine Serum Albumin Functionalized Glyconanoparticles for Beta Amyloid Detection and Blood-Brain Barrier Crossing Assessment

3.1 Introduction

The unique function of the BBB makes it the brain's first line of defense against influx of various toxins and harmful organisms. This important physical and physiological barrier is constituted by the brain capillary endothelial cells connected by tight junctions and supported by pericytes and astrocytes. The BBB is very selective to molecules that can pass to the brain. For instance, it permits the passage of essential nutrients while preventing the molecules that cannot pass through the tight junctions but can possibly diffuse transcellularly. Molecules which are small, lipid-soluble and unionized, can diffuse via the transcellular lipophilic pathway. Larger molecules like transferrin can only pass through receptor mediated transcytosis and, however cationic peptides can pass through adsorptive mediated transcytosis (Scheme 3.1). On the other hand, some molecules such as glucose is taken up by receptor mediated, from the lumen to the brain interstitium.[84]

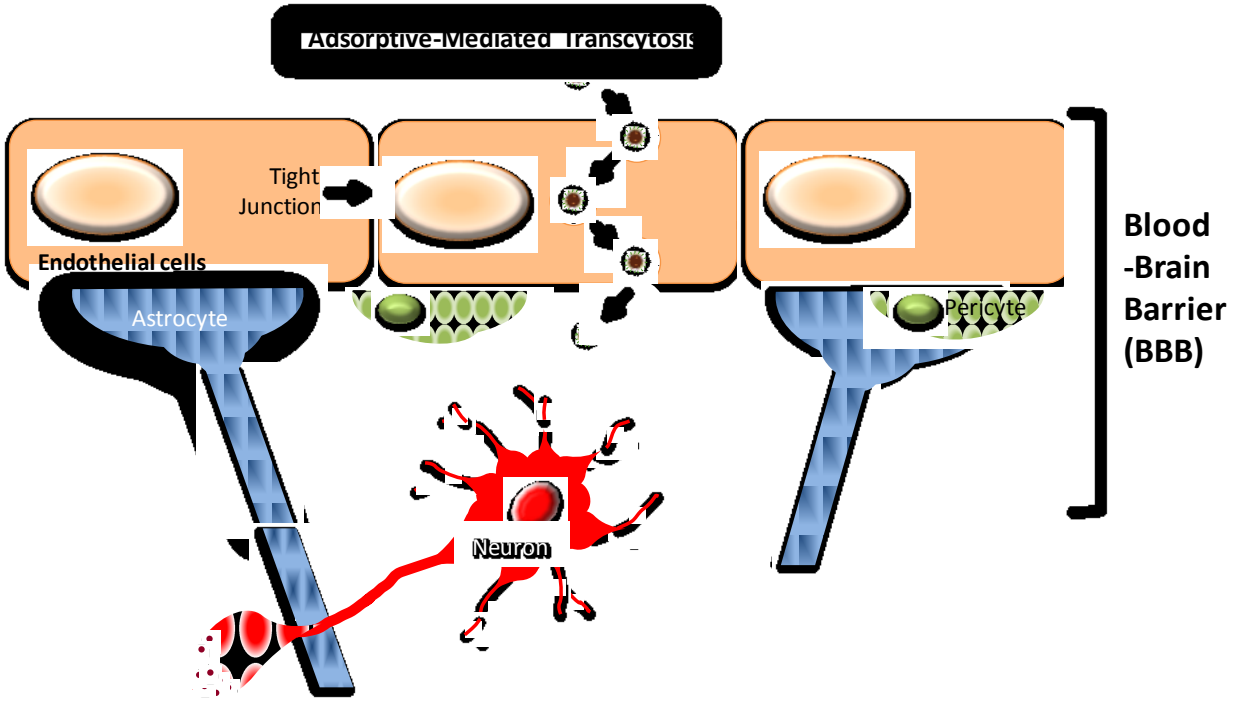

Scheme 3.1: A schematic diagram illustrating the different components of the Blood-Brain Barrier and adsorptive-mediate transcytosis

These characteristics make the targeted delivery through the BBB one of the most challenging fields in delivering diagnostic and therapeutic agents to the brain. Remarkably, almost 100% of large and 98% of small molecules cannot penetrate the BBB,[85] which highlights the importance of BBB "crossability" of the developed drugs, especially for neurological disorders.

A noticeable emphasis has been put on developing diagnostic and therapeutic carriers to deliver drugs to the brain. Due to their broad functionalization capabilities in addition to their versatile nature, nanomaterials are considered important candidates to play the role of drug carriers.[86] Nevertheless, the issue of BBB permeability still poses a challenge in the field of

nanotechnology. Many studies explored the role of nanomaterials, such as, liposomes, nanoparticles, dendrimers, polymersomes and micelles hold, as potential agents to deliver drugs to the brain.[87 88]

This permeability problem is considered an obstacle for diagnosing different neurological disorders such as Parkinson's and Alzheimer's disease (AD). The nature of those diseases requires effective penetration of diagnostics and therapeutic drugs across the BBB. For instance, in AD, it had been shown that beta amyloids (Aβ) constitute the hallmark protein of the disease.[5] And they can be detected by designing vehicles that pass the BBB.

Many targeting ligands, such as apolipoprotein,[89] transferrin,[90] angiopeptide,[91] and cationic-proteins[92] have been utilized to modify the nanomaterials' surfaces in order to increase BBB permeability. It is noteworthy that magnetic nanoparticles were found to be promising carriers, due to their non-invasive detection via magnetic resonance imaging (MRI). Nevertheless, the poor brain uptake and targeting constitute the main challenge of the field.[93]

In our previous investigation[44a] we demonstrated that sialic acid functionalized iron-oxide nanoparticles can bind to Aβ peptides *in vitro* and ex-vivo. The functionalization with sialic acid is crucial due to its biomimetic Aβ binding. For instance, GM1 (a ganglioside abundant in neuronal plasma),[25] which has a terminal sialic acid moiety,[26b, 66b, 94] was found to form GM1-Aβ complexes in the brains of AD patients[26b] with GM1 shown to serve as nucleation site on neuronal cells surfaces for aggregation of Aβ[66b] Moreover, we demonstrated that incubation of those nanoparticles reduced Aβ cytotoxicity to neuroblastoma cells.[44a]

However, in our ELISA assays, we observed a considerable difference between the BSA-blocked and unblocked wells, where the wells incubated with BSA showed significantly higher

Aβ binding even without any NP present compared to those not containing. In our previous work, we established that Aβ/protein-blocking agent adsorption, can lead to false ELISA readings. This outcome was in agreement with a report showing the strong affinities of plasma proteins such as albumin with Aβ

We have also established that a common blocking agent in enzyme ELISA namely, BSA showed a considerable binding with Aβ. That outcome was in agreement with a report that shows a strong interaction between albumin and Aβ.[78] These findings inspired us to design a sialic acid-decorated and BSA-coated iron-oxide nanoparticles. By replacing dextran coating with bovine serum albumin (BSA) we hypothesized that the NP-Aβ binding would be improved. The other improvement was the crosslinking or cationization of BSA with diamines. This was designed to direct BBB permeability via adsorptive-mediates transcytosis,[95] while carefully noting that the zeta potential values of within 10 mV are optimal for *in vivo* delivery of nanoparticles to the brain.[96] Additionally, the optimization of the particles size to less than 100 nm was also suggested to improve the pharmacokinetics of those nanoparticles[97] and their endocytosis by the brain capillary endothelial cells.[98] In this work we test the binding affinity of those NP-BSA_x-Sia to Aβ, while exploring the means to transport those nanoparticles through the BBB by performing endothelial cells transcytosis assays and animal MRI scans.

3.2 Preparation and Characterization of NP-BSA_x-Sia

The magnetic glyconanoparticles were synthesized by conjugating the sialic acid moieties with the Fe_3O_4 core magnetic nanoparticles (Scheme 3.2). The superparamagnetic nanocrystals

were prepared via the thermal decomposition of iron (III) acetylacetonate, with three different surfactants, namely 1,2-hexadecanediol, oleic acid, and oleyl amine, under high temperature and inert conditions. After several steps of washings and purification, the surface ligands of nanoparticles were exchanged with tetramethylammonium hydroxide (TMAOH). The reaction completion was determined when the organic layer-soluble nanoparticles moved into the aqueous layer. The secondary exchange of TMAOH with BSA was achieved overnight at room temperature stirring. It is noteworthy that the stirring should be done in a medium speed and in room temperature to prevent protein denaturing, usually observed as bubble formation. To assure the adsorptive-mediated transcytosis, the cationization of NP-BSA was performed.[99] NP-BSA (zeta potential (ζ) = − 6.56 mV) were cross-linked with 2,2′-(ethylenedioxy)bis(ethylamine) using a carbodiimide mediated chemistry (EDC), to yield positively charge NP-BSA_x (ζ = + 11.2 mV). The extent of cationization was greatly dependent on the pH of the reaction where pH = 6 was found to be optimal.[100] Conjugation of sialic acid achieved by EDCI-coupling of Sia-OMe to the NP-BSA_x. The resulting nanoparticles NP-BSA_x-Sia-OMe were subject to saponification to remove the methyl ester in the sugar moiety to yield NP-BSA_x-Sia (ζ = + 5.16 mV). For transcytosis and confocal microscopy experiments, nanoparticles NP-BSA_x-Sia were labeled with fluorescein isothiocyanate (FITC) to yield NP-BSA_x-Sia-FITC (ζ = + 3.01 mV).

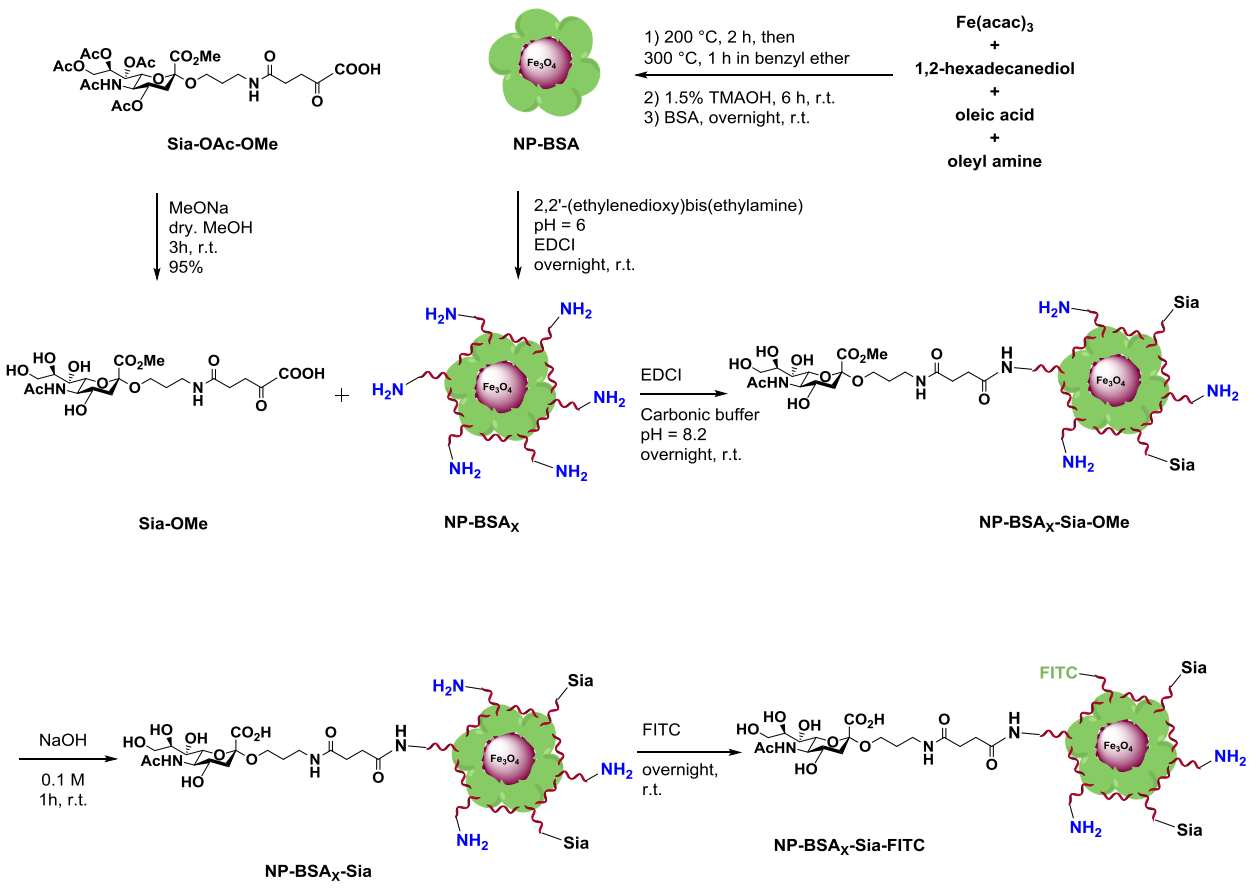

Scheme 3.2: Synthesis of NP-BSAx-Sia and NP-BSAx-Sia-FITC

Characterization of nanoparticles was achieved by multiple methods. The core diameters of the nanoparticles were shown to be ~5 nm where they were observed under transmission electron microscopy (TEM). **(Figure 3.1a-b)** The hydrodynamic diameter of NP-BSA$_x$-Sia (size = 87 nm) were determined by dynamic light scattering technique (DLS). As indicated above, the positive surface charge of the nanoparticles was a crucial characteristic in our nanoparticle choice, hence zeta potential (ζ) surface charge measurements (in PBS buffer) showed a systematic increase in ζ value upon crosslinking with the diamine moiety (− 6.56 to + 11.2 mV). That zeta potential was reduced to + 5.16 mV upon conjugating some of the positively charged

amine moieties with Sia. The total organic content was determined by thermogravimetric analysis (TGA). The BSA_x-Sia represented 73.7% of the weight of the NP-BSA_x-Sia **(Figure 3.1c)**. The extent of sialic acid conjugation was calculated by performing the thiobarbituric acid Assay (TBA), where sialic acid was selectively cleaved under mild acid conditions. And the amount of sialic acid accounted for 7% of the weight of the nanoparticles **(Figure 3.1d)**.

The NP-BSA_x-Sia contrast agents were determined to have high magnetic relaxivity. (The R2* magnetic relaxation rate (R2* = 1/T2*) of NP-BSA_x-Sia was measured to be 135.9 mM^{-1} s^{-1} at 3T) **(Figure 3.1e)**.

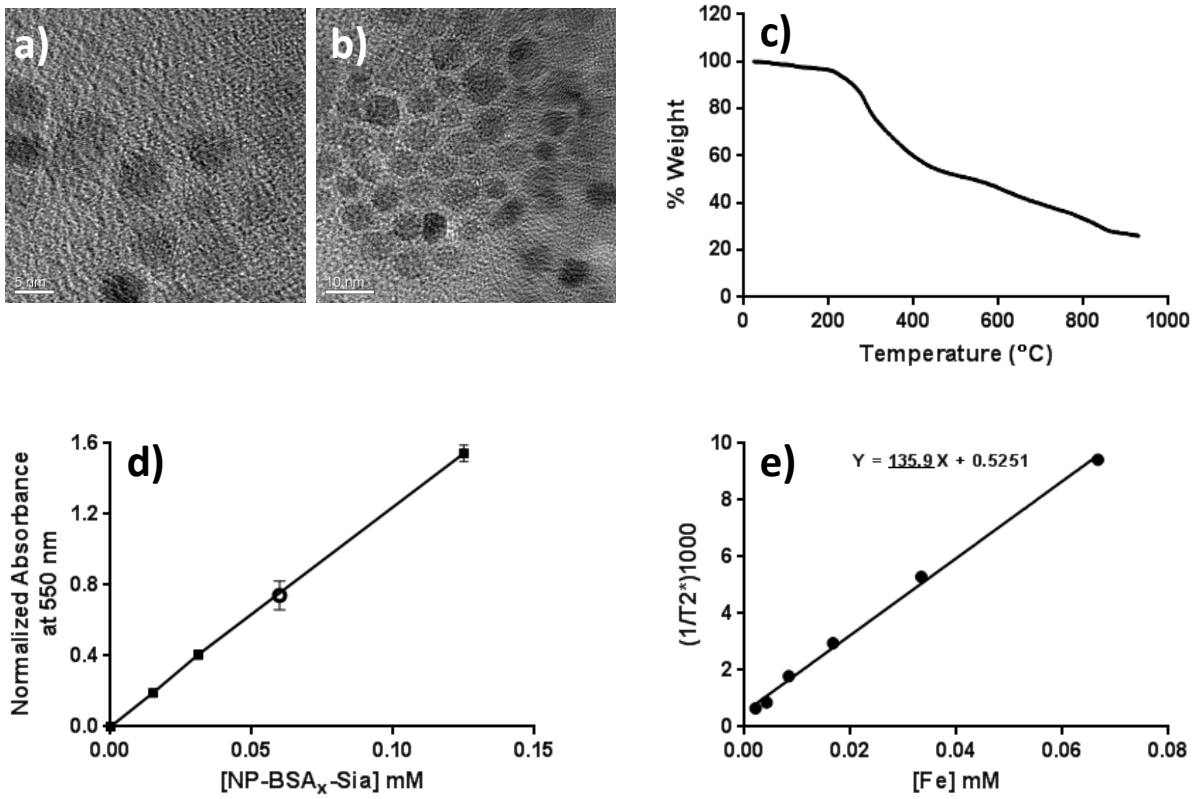

Figure 3.1: TEM images of NPs (a) scale 10 nm and (b) 5 nm. (c) thermogravimetric analysis (TGA) of the NP-BSAx-Sia; (d) TBA assay showed the amount of sialic acid was 0.06 mM; (e) T2* relaxivity characterization of NP-BSAx-Sia. The R2* value is 135.9 mM -1 s-1

3.3 Assessment of NP-BSA$_x$-Sia and NP- BSA$_x$ Binding with Aβ via ELISA

The nanoparticle-Aβ binding was verified by enzyme-linked immunosorbent assay (ELISA) **(Scheme 3.3)**. Two different types were used to study the binding, namely NP-BSA$_x$-Sia and NP-BSA$_x$. These specific nanoparticles were used to establish the importance of sialic acid in the binding.[44a]. The choice of Aβ (1−42) peptide was also adopted for two reasons. First, it is a major component of amyloid peptides in the senile plaques in AD brains[72] and it is

considered the most toxic Aβ forms.[73] Second, it is used to compare the binding to our previous results. Aβ fibrils were prepared by dissolving the peptides in 10 mM NaOH solution. After 10 minutes of sonication, the peptides were neutralized with diluted HCl solution to pH = 6, and then diluted in PBS buffer to the desired final concentration. The Aβ fibrils were obtained after incubation the monomers at 37 °C for 48 h without stirring. The obtained fibrils along with the two types of nanoparticles were used for the ELISA. A solution of NP-BSA_x-Sia and NP-BSA_x were added to separate wells in a 96-well Nunc MaxiSorp flat-bottom microtiter plate. After overnight incubation, the nanoparticles adhered to the bottom of the wells. Aβ solutions were added to the NP-BSA_x-Sia and NP-BSA_x coated wells followed by thorough PBST washing and addition of an anti-Aβ IgG primary antibody. The amount of Aβ bound was quantified by the absorbance change of each well upon incubation with an anti-IgG secondary antibody linked with horseradish peroxidase (HRP).

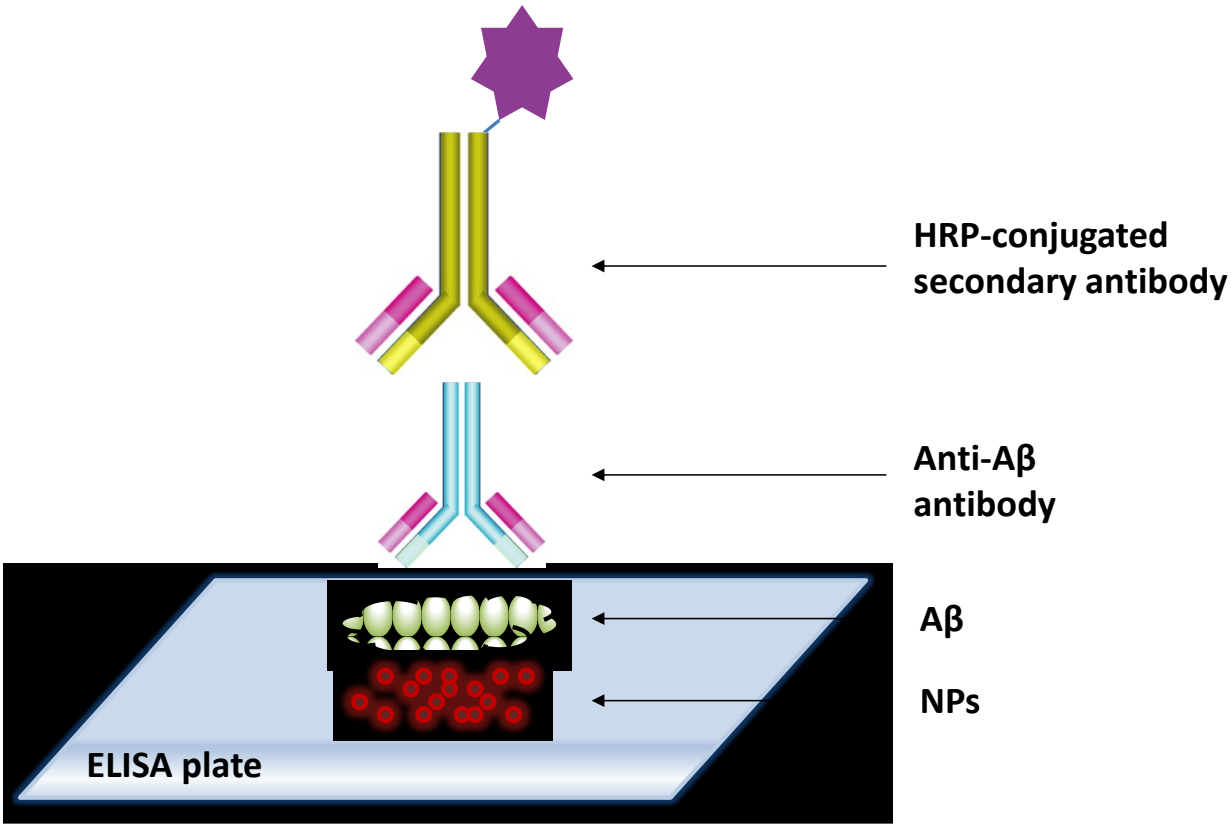

Scheme 3.3: Schematic diagram of the ELISA design

The problem of non-specific adsorption of protein to the microtiter plates in ELISA is a common one. Blocking agents such as bovine serum albumin (BSA) is typically employed to reduce this non-specific adsorption. These blocking agents are also used in some for Aβ binding studies.[28b, 77] However, in our assays, we observed a considerable difference between the BSA-blocked and unblocked wells, where the wells incubated with BSA showed significantly higher Aβ binding even without any NP present compared to those not containing. In our previous work, we established that Aβ/protein-blocking agent adsorption, can lead to false ELISA readings. This outcome was in agreement with a report showing the strong affinities of plasma proteins such as albumin with Aβ.[78]

The increasing Aβ concentration showed a concentration dependent increase in absorbance. The apparent K_d was found to be 0.6 μM **(Figure 3.2)**. The NP-BSA_x-Sia and NP-BSA_x showed similar binding patterns. However sialic acid conjugation, enhanced the binding by 21% as compared to the BSA_x nanoparticles. The Aβ showed low absorbance when it was incubated on naked plates after washing **(Figure 3.2)**.

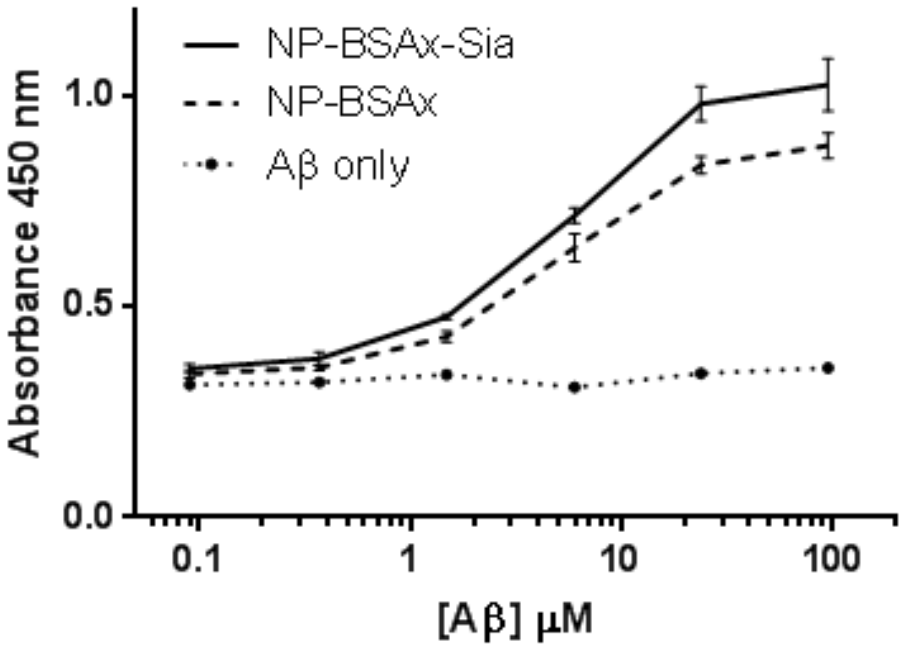

Figure 3.2: ELISA curve for Aβ binding to immobilized NP-BSAx-Sia (solid line), NP-BSAx (dashed line) and Aβ only (dotted line). The error bars in all graphs represent the standard deviation of four wells

To further establish the role of sialic acid in Aβ binding, a competitive ELISA was performed when fixed amount of Aβ was added to NP-BSA_x-Sia coated plates together with free

sialic acid. Our findings were consistent with our previous results where free sialic acid competed with the nanoparticle-conjugated sialic acid for binding with Aβ. After introducing a constant concentration of Aβ to the NP-BSA_x-Sia-coated plate, an increasing concentration free sialic acid was introduced as well. The increased concentration of free sialic acid would lead to a less bound Aβ on the plate, due to competition with the nanoparticle-conjugated ones. As shown in Figure 3.3 the competition ELISA results confirmed the role of sialic acid in Aβ binding.[28h]

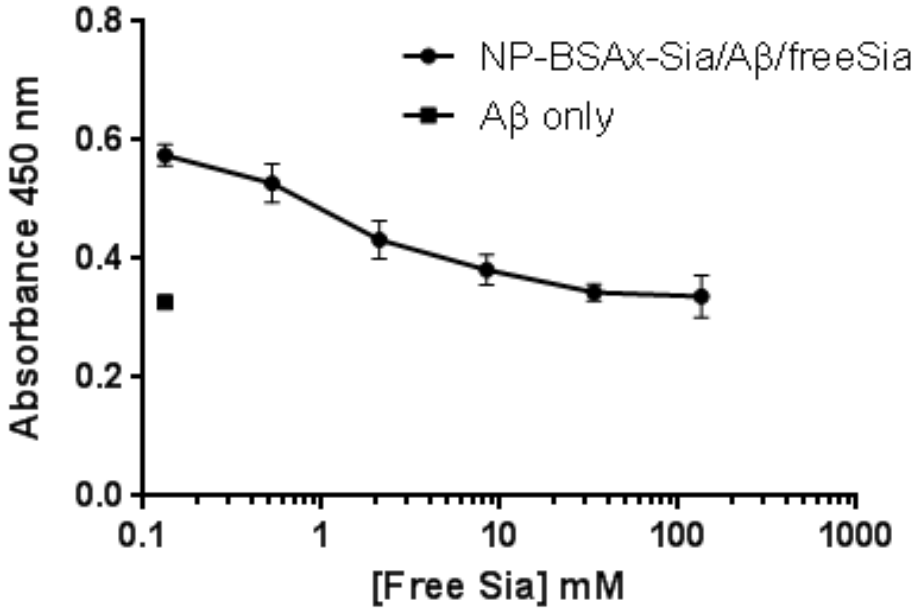

Figure 3.3: ELISA curve of Aβ binding to immobilized NP in the presence of increasing concentration of free sialic acid. Wells containing Aβ (0.5 μM) binding to NP-BSAx-Sia without any free sialic acid (circle) and Aβ (0.5 μM) binding to bare wells (square)

3.4 Evidence for NP-BSA$_x$-Sia uptake by bEnd.3 endothelial cells

After establishing the NP-Aβ binding, we wanted to lay the foundation to test that binding *in vivo*. To establish that, we had to, first, test the BBB crossing capability of our nanoparticles via *in vitro* transcytosis model (uptake and consequent release by endothelial cells). The kinetics of the uptake of nanoparticles by the bEnd.3 endothelial cells was examined by flow cytometry using FITC-labeled NP-BSA$_x$-Sia. bEnd.3 cells were incubated by NP-BSA$_x$-Sia-FITC 1, 3, and 7 hours, followed by washing with PBS to remove unbound and adsorbed nanoparticles. **Figure 3.4** shows the time dependent uptake of NP-BSA$_x$-Sia-FITC. It was observed that labeled nanoparticles needed around three hours to get internalized by the cells, and the incubation for extended hours did not show a significant increase in the extent of endocytosis.

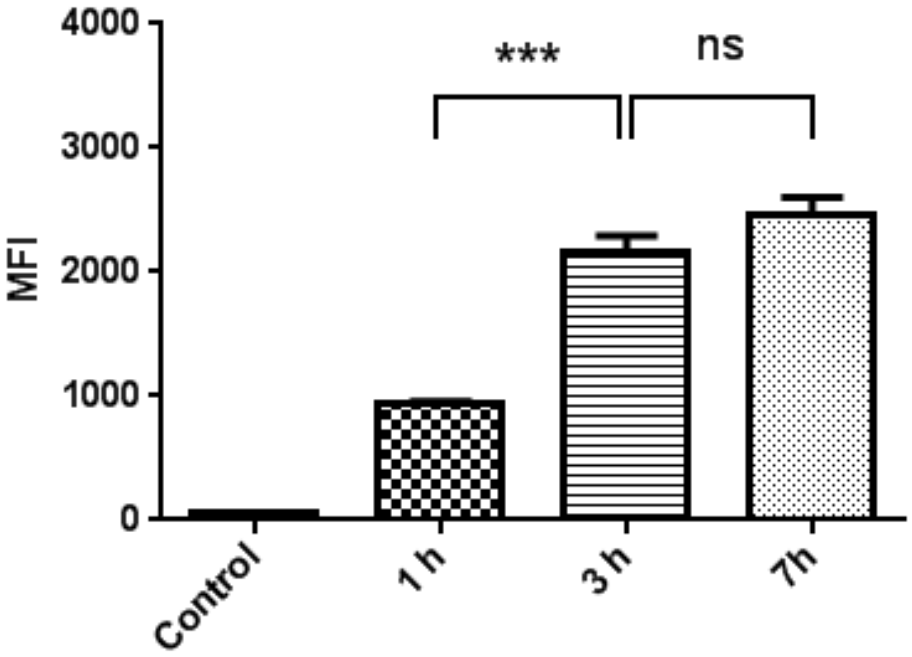

Figure 3.4: Time dependent uptake of NP-BSAx-Sia by bEnd.3 endothelial cells as determined by flow cytometry

To confirm the uptake of the nanoparticles, confocal microscopy imaging experiment was performed. **Figure 3.5** shows that NP-BSA_x-Sia-FITC were internalized to the cells' interior without crossing into the nucleus. The FITC-signal of nanoparticles co-localized with lysotracker red signal, which is an indication that they were internalized by lysosomes. This was clearly observed in the photomicrograph/overly image **(Figure 3.5e)**. It was noteworthy that the use of phenol red DMEM media showed a slight coloration of the cell (data not shown), hence the use of phenol red-free media is highly recommended (all assays were done with phenol red-free DMEM media).

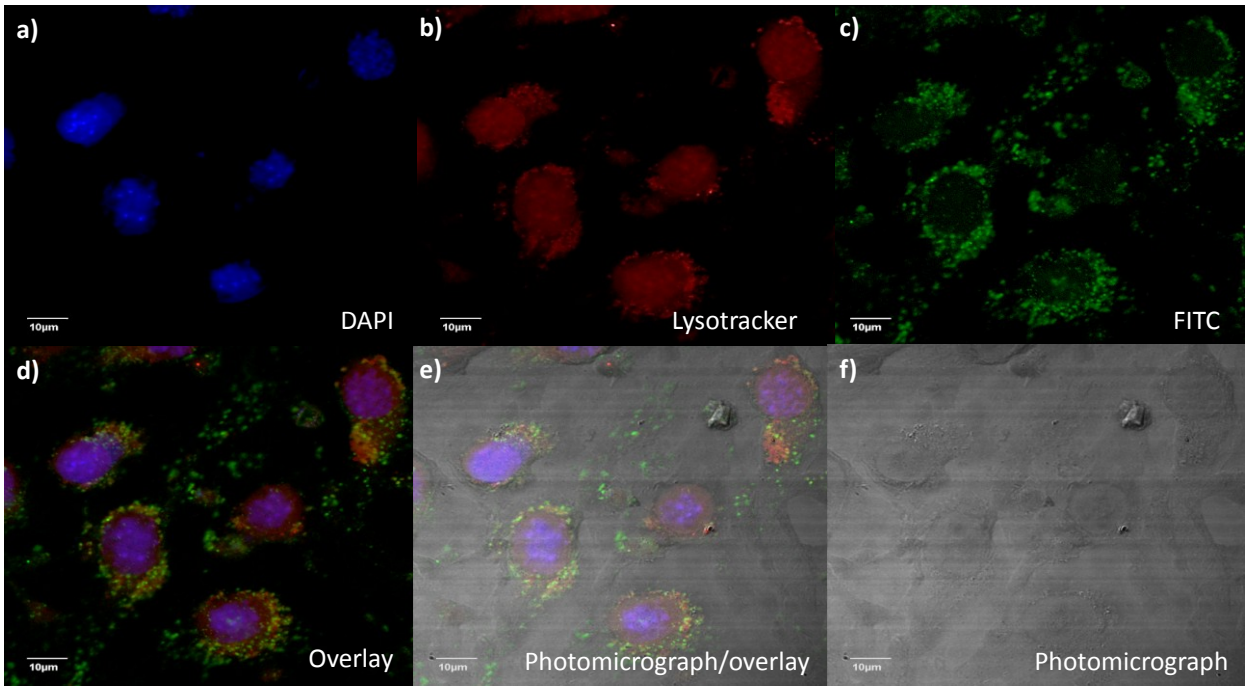

Figure 3.5: Confocal microscopy images showing the uptake of NP-BSAx-Sia by the bEnd.3 endothelial cells. DAPI (a); Texas red (b); FITC channels (c); overlay (d) and the photomicrograph/overlay and photomicrograph were shown in (e) and (f), respectively

Finally to examine any possible role of sialic acid in the uptake of those nanoparticles, two kinds of nanoparticles namely, NP-BSA_x-Sia-FITC and NP-BSA_x-FITC were studied by flow cytometry. The two types of nanoparticles with same fluorescence intensity were incubated with bEnd.3 cells for three hours, and then washed thoroughly to remove any unbound or adsorbed nanoparticles. The flow cytometry data showed that NP-BSA_x-FITC showed a stronger signal than NP-BSA_x-Sia-FITC, indicating an enhanced internalization of sialic acid nanoparticles **(Figure 3.6)**. This can be explained by the increased adsorptive mediates

transcytosis of cationic proteins, especially that NP-BSA$_x$-Sia showed lower zeta potential values than the NP-BSA$_x$.

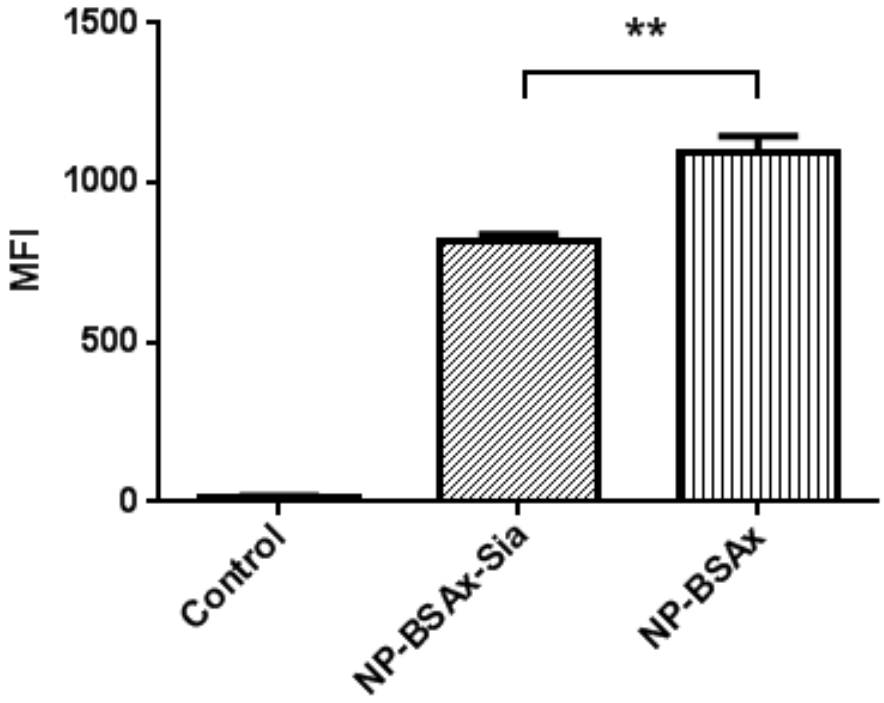

Figure 3.6: Flow cytometry analysis showed that binding and uptake of NP-BSAx were higher than NP-BSAx-Sia

3.5 Evidence for Exocytosis of the NP-BSA$_x$-Sia-FITC from bEnd.3 Endothelial Cells

In order to demonstrate that our nanoparticles can be used as BBB crossing particles, we monitored their release by endothelial cells, by performing the exocytosis assay. This assay would enable us to trace the release of uptaken fluorescently-labled nanoparticles, by measuring

their fluorescence intensity. As opposed to nanoparticle endocytosis,[101] exocytosis is a far less studied phenomenon.[102] The assay started by an overnight incubation of bEnd.3 endothelial cells. Then the cells were washed thoroughly to get rid of unattached cells. FITC-labeled NP-BSA_x-Sia nanoparticles in a serum free DMEM media were added to the attached cells and incubated for 5 hours, to ensure the endocytosis of the nanoparticles. After incubation, the un-endocytosed nanoparticles were washed thoroughly (more than 5 time) to remove any adsorbed nanoparticles on the cell surface. The fluorescence of the FITC-labeled nanoparticles were measured after adding a known volume of serum free DMEM media. The fluorescence was measured by withdrawing 100 μL of the supernatant, and dispensing it into a black-bottomed 96-well plate. It is important to maintain the total volume the same throughout the assay by returning the withdrawn sample and also to replenish any evaporated serum free DMEM. **Figure 3.7** shows a steep increase in the fluorescence signal indicating a prompt release of the FITC-labeled nanoparticles, where almost half of the exocytosed nanoparticles were released in the first five hours, and reached a maximum after 24 hours. This is an indication that nanoparticles can be released from endothelial cells after being taken up.

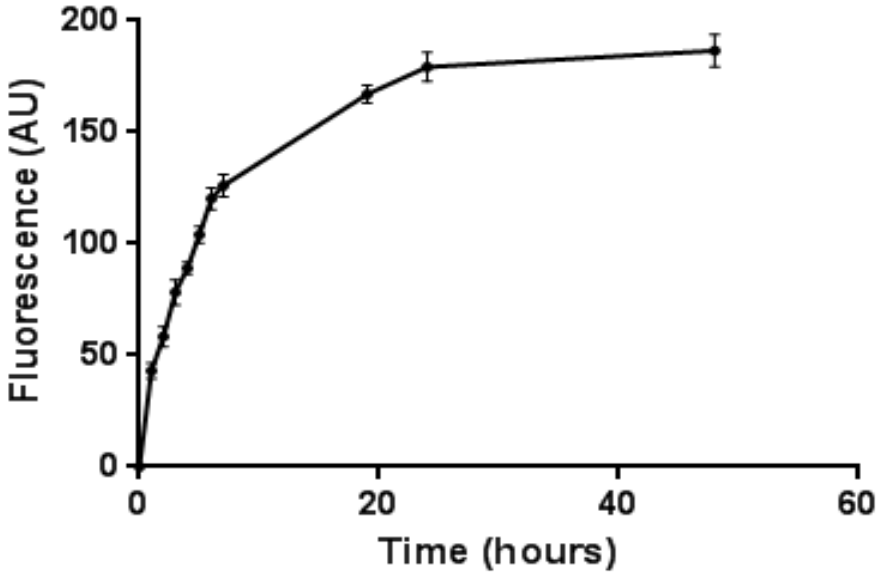

Figure 3.7: Time dependent release of NP-BSAx-Sia from bEnd.3 endothelial cells showing that the internalized nanoparticles can be exported

3.6 Assessment of NP-BSA$_x$-Sia transcytosis through bEnd.3 endothelial cells

Having demonstrated that NP-BSA$_x$-Sia can be uptaken by endocytosis and released by exocytosis in separate assays, we studied the two consecutive processes by conducting the transcytosis assay. The transcytosis assays are typically done *in vitro* using primary brain capillary endothelial cells, which resemble the BBB. These approach was found to be an effective one especially at early passages.[103] However, several disadvantages can be noted using this method. For instance, handling primary brain capillary endothelial cell-based *in vitro* models require high skilled scientists and are extremely time consuming. They are also prone to potential contaminations from other brain cells which affect the permeability.[104] To minimize those

drawbacks we adopted an *in vitro* model that uses immortalized mouse brain endothelial cell line namely, bEnd.3. Besides reducing the risks of contamination these cells maintain the BBB characteristics over multiple passages, as indicated in several studies.[104-105] To distinguish the direction of NP transport, layers of bEnd.3 endothelial cells were grown on a permeable transwell filter. The NP solution was added to the upper chamber and the ability of nanoparticles to penetrate through the monolayer was assessed by monitoring the fluorescence of the lower chamber as a function of time. Trans-Endothelial Electrical Resistance (TEER) values (average after two weeks = 133 Ω/cm^2) were in agreement with the bEnd.3 endothelial cell monolayer resistance **(Figure 3.8)**.[106]

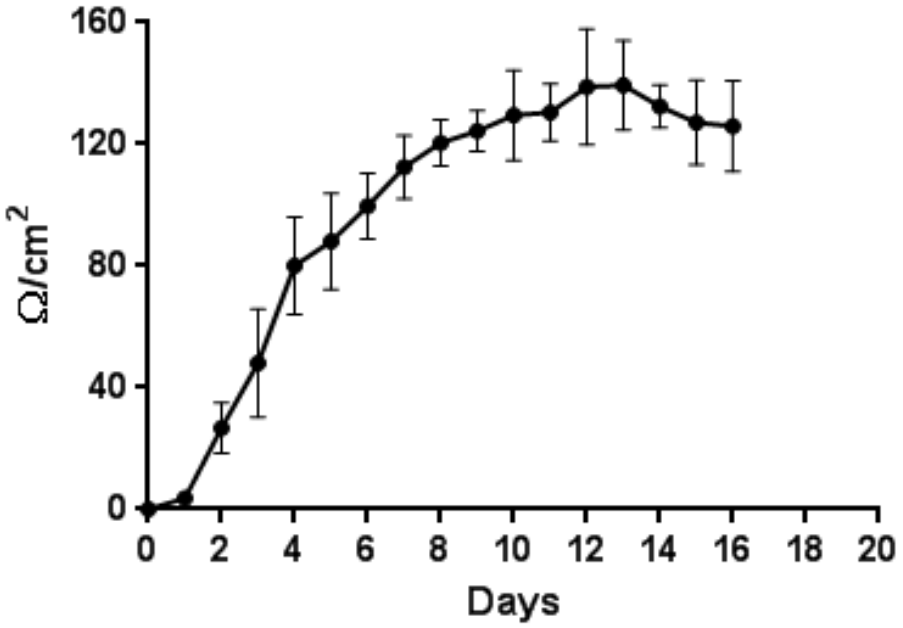

Figure 3.8: Time dependant variation of the trans-endothelial electrical resistance (TEER) values of bEnd.3 endothelial cells

Moreover, TEER measurements showed that addition of NP-BSA_x-Sia-FITC or NP-BSA_x-FITC did not change the electrical resistance through of the cell layers through the entire assay **(Figure 3.9)** suggesting that the nanoparticles did not affect the tight junctions of the cells. To demonstrate the permeability of our vehicles, we decided to use NP-BSA_x-FITC and NP-BSA_x-Sia-FITC. As shown in **Figure 3.10**, NP-BSA_x-FITC exhibited higher fluorescence than the NP-BSA_x-FITC in the bottom well, as detected after 32 hours of incubation, indicating an enhanced penetration through the monolayer. This finding is in agreement with the endocytosis data where NP-BSA_x-FITC were uptaken faster than NP-BSA_x-Sia-FITC. These results highlight the impact of surface charge of nanoparticles on the penetration of endothelial cells.

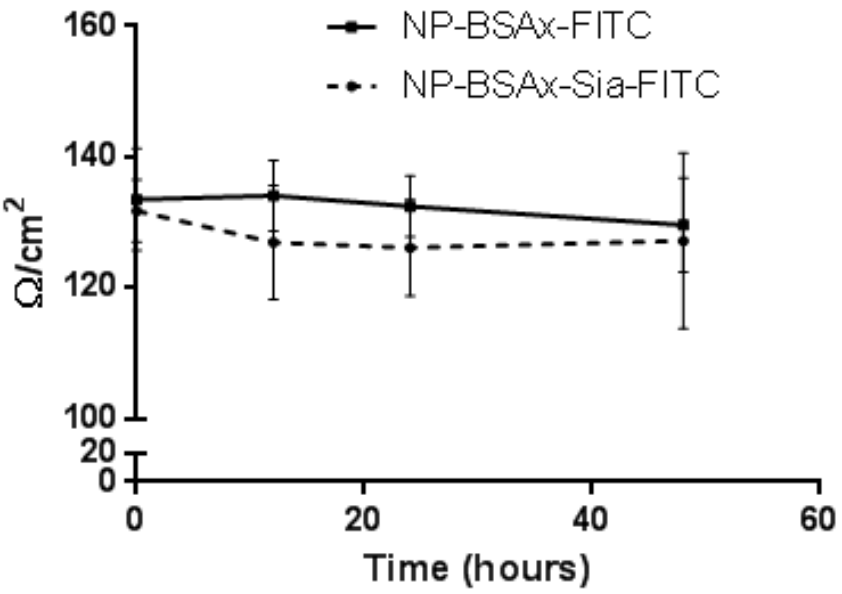

Figure 3.9: The effect of NP-BSAx-FITC and NP-BSAx-Sia-FITC on the trans-endothelial electrical resistance (TEER) values of bEnd.3 endothelial cells. Nanoparticles did not show any disruption of the tight junctions

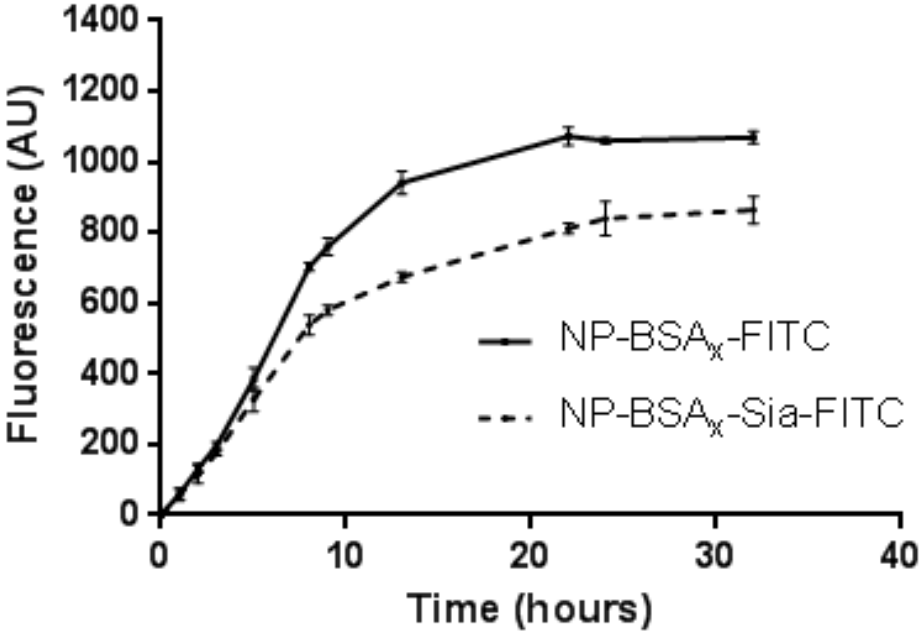

Figure 3.10: Penetration of nanoparticles through bEnd.3 monolayers. NP-BSAx-FITC show increased penetration compared to the NP-BSAx-Sia-FITC

3.7 Cytotoxicity of NP-BSA$_x$-Sia to bEnd.3 endothelial cells

To demonstrate that those nanoparticles can be safely used in *in vitro* and *in vivo* experiments an MTS cytotoxicity assay was done. bEnd.3 endothelial cells were incubated for 24 hours and after washing with PBS, sialic acid functionalized BSA nanoparticles were incubated for 4 hours. Subsequently 10% MTS reagent was introduced after a thorough PBS wash and the cells were incubated for an hour in 37 °C incubator. The brown coloration was an indication of cell viability. As demonstrated in **Figure 3.11** nanoparticles showed excellent cell viability until

0.1 mg/mL concentration. The viability was observed to decrease for the higher concentration such as the 1 mg/mL one.

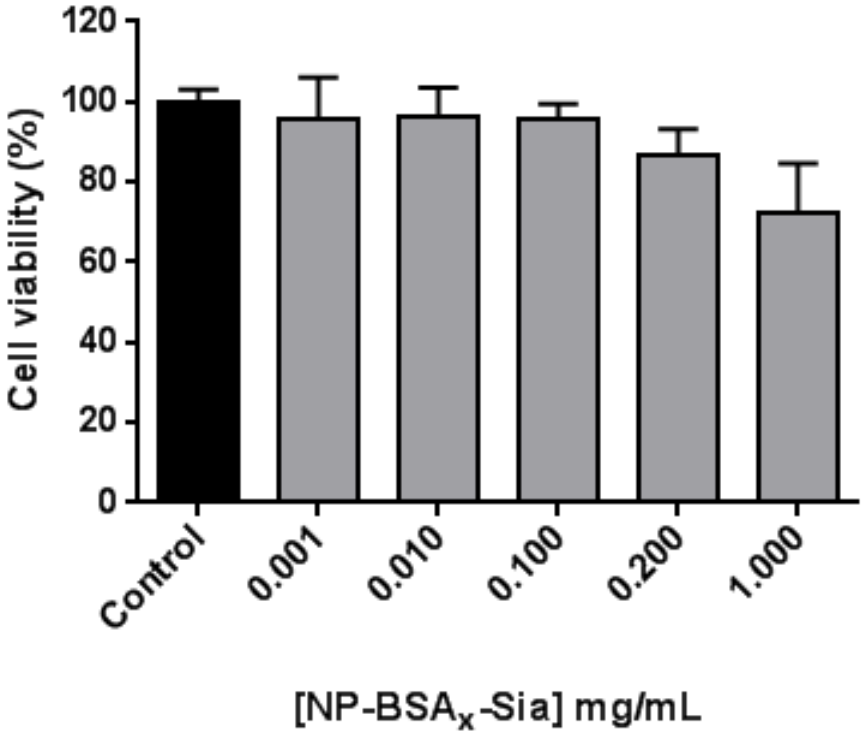

Figure 3.11: Cytotoxicity of NP-BSAx-Sia to bEnd.3 endothelial cells

3.8 *Ex Vivo* Detection of Aβ by NP-BSA$_x$-Sia via MRI

To reaffirm the binding selectivity of our nanoparticles to Aβ and to further improve our *ex vivo* Aβ –detection model, we tested both NP-BSA$_x$-Sia and NP-BSA$_x$ capabilities to detect Aβ on mouse brains. Mice brains were harvested and incubated in a solution of Aβ fibrils for 24

h. After Aβ being absorbed on the surface of the brains, the unbound Aβ was removed by thorough deionized water washing. The Aβ-adsorbed brains were then incubated with both NP-BSA_x-Sia and NP-BSA_x in separate wells at 37 °C for 12 hours. This was followed by another thorough wash to remove unbound nanoparticles. T2* weighted MR images were acquired and dark spots were observed on the surface of Aβ brains incubated with NP-BSA_x-Sia. However the dark spots' intensity was lower for the NP-BSA_x which supported the ELISA results **(Figure 3.12a-b)**. **Figure 3.12c** shows the effect of free-sialic acid competition with NP-BSA_x-Sia as reduced dark spots on the brain's surface. Two mouse brain controls were used to test the binding of NP-BSA_x-Sia without Aβ incubation and Aβ without NP incubation using the same MRI protocol. Insignificant darkening of the brain surface was observed in the case of NP-BSA_x-Sia and no darkening for the Aβ only case **(Figure 3.12d-e)**. Additionally, Prussian blue staining was used to detect iron though the blue coloration of the nanoparticles. Aβ/NP-BSA_x-Sia incubated brains showed a distinctive darker blue color where Aβ/NP-BSA_x incubated brains showed fewer blue spots upon treating them with Prussian blue **(Figure 3.12f-g)**. For free sialic acid-inhibition, only-Aβ and only-NP-BSA_x-Sia brains showed a coloration that was consistent with the MRI results **(Figure 3.12h-j)**. These observations suggest that NP-BSA_x-Sia did not nonspecifically bind with brain components and Aβ could be detected by NP-BSA_x-Sia aided MRI in this *ex vivo* model.

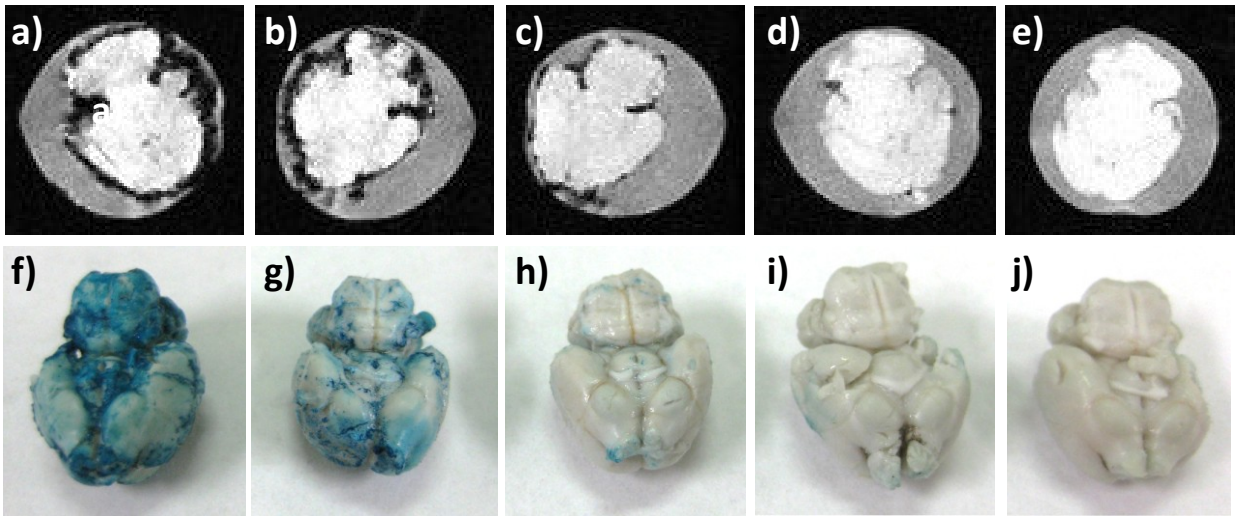

Figure 3.12: T2* weighted MR and Prussian blue staining images of the *ex vivo* experiment

T2* weighted MR images of (a) Aβ mouse brain incubated with NP-BSA_x-Sia; (b) Aβ mouse brain incubated with NP-BSA_x;(c) Aβ mouse brain incubated with NP-BSA_x-Sia in the presence of free sialic acid; (d) normal mouse brain incubated with NP-BSA_x-Sia; and (e) Aβ mouse brain; Prussian blue staining of (f) Aβ mouse brain incubated with NP-BSA_x-Sia; (g) Aβ mouse brain incubated with NP-BSA_x; (h) Aβ mouse brain incubated with NP-BSA_x-Sia in the presence of free sialic acid; (i) normal mouse brain incubated with NP-BSA_x-Sia; and (j) Aβ mouse brain

3.9 *In vivo* evaluation of the NP-BSA_x-Sia via BBB crossing

All previous endothelial cells transcytosis experiments results pointed toward promising *in vivo* assessments of those BSA-nanoparticles. The BBB crossing of NP-BSA_x-Sia was investigated by measuring the changes in the MRI signals. The *in vivo* imaging was done on female mice. The mice were anesthetized with 2% isoflurane oxygen flow through a hose extended into the MRI coil. The mouse was placed still in a supine position using medical tapes in an MRI wrist coil. After a pre-injection scan, mice were injected retro-orbitally and MRI-

scanned. Several scans were run to detect the change in the post-injection signals, namely at 16, 27, 38, 49, and 60 minutes. **Figure 3.13a** shows the MRI image of the mouse brain before injection, and **Figure 3.13b-c** show the images of the scanned mouse after 16 and 60 minutes, respectively. To quantify the changes observed in **Figure 3.13**, we constructed the time vs normalized T2* change graph **(Figure 3.14). Figure 3.14** demonstrated that after the first scan (16 min) the T2* weighted image signal was reduced significantly which is indicative of the presence of the NP-BSA_x-Sia in the brain area. Expectedly, the consequent scans show apparent gradual clearance of nanoparticles from the brain to a certain point where it plateaued after the 4^{th} scan. The statistical analysis of the normalized T2* weighted image signal showed that the amount of nanoparticles that did not clear from the brain were significant, as indicated by the *p*-value (0.0204) of pre-injection and 4^{th} scans.

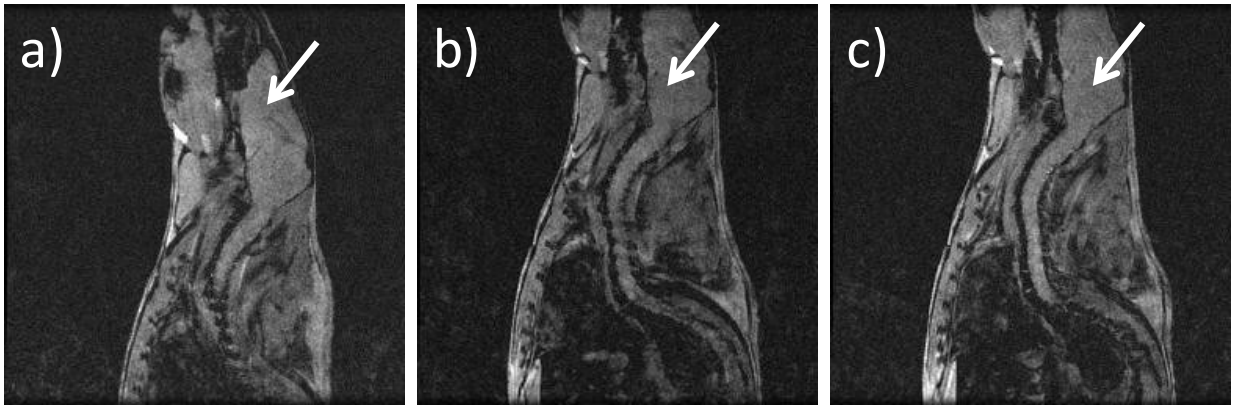

Figure 3.13: MRI images of scanned mouse brain. (a) Pre-injection; (b) 16 minutes after NP-BSA_x-Sia injection; and (c) 49 minutes after NP-BSA_x-Sia injection

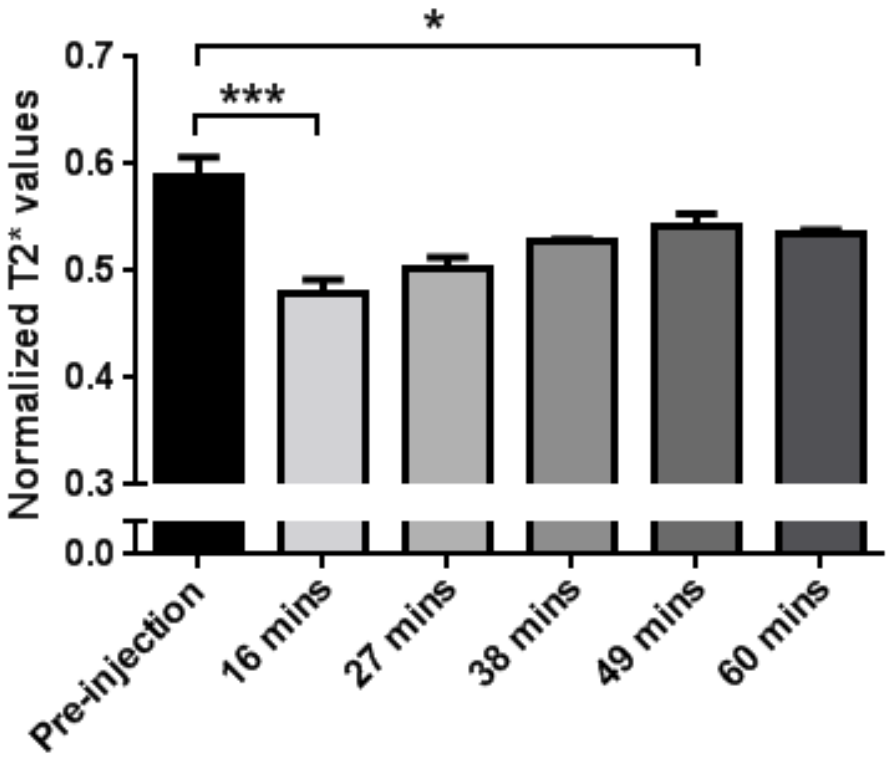

Figure 3.14: Normalized T2* weighted image signal of mouse brain. Pre-injection normalized T2* value dropped after injecting with NP-BSA_x-Sia and started to increase upon clearing from the brain. The values showed a plateau after the 4th post injection scan

To further verify these results, the same mice were sacrificed and their blood was drawn via a heart puncture (left ventricle). Immediately, 2 mL of cold PBS was injected to the left ventricle and, the intensity dark red color of the liver was noticeably reduced. This procedure was performed to ensure the clearance of blood and nanoparticles from the blood vessels. After fixing the harvested brains in 10% formaline solution for 24 hours, they were bisected and subjected to Prussian blue staining. The two controls used in this experiment were one mouse that was injected with PBS and was sacrificed and PBS perfused (negative control) and a second

mouse was injected with NP-BSA_x-Sia and sacrificed but not perfused with PBS (positive control).

The Prussian blue staining results were consistent with the *in vivo* imaging data where the NP-BSA_x-Sia injected and perfused mouse showed a blue coloration in the hippocampus and other areas of the brain **(Figure 3.15a)**. Alternatively, the negative control mouse's brain showed a very pale blue coloration of the brain due to residual blood **(Figure 3.15b)**. Finally, the positive control mouse's brain showed darker blue coloration on the entire brain **(Figure 3.15c)**. MRI mouse scans and *ex vivo* Prussian blue experiments demonstrated the apparent capability of NP-BSA_x-Sia to cross the BBB.

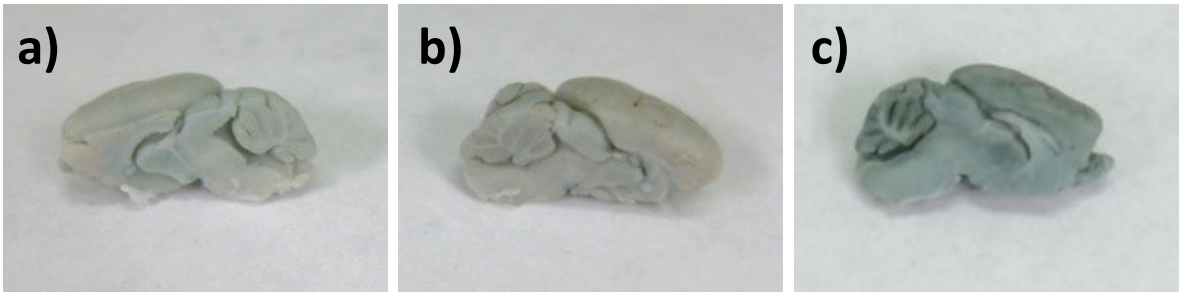

Figure 3.15: Prussian blue staining of mice half brains. (a) NP-BSA_x-Sia injected and PBS perfused; (b) PBS injected and PBS perfused; and (c) NP-BSA_x-Sia injected and unperfused mice brains

3.10 Conclusion

In this work we demonstrated that sialic acid conjugated BSA-nanoparticles could selectively bind Aβ. Moreover, the *ex vivo* binding of NP-BSA_x-Sia to the exogenous Aβ were demonstrated via MRI, due to the superparamagnetic nature of the nanoparticles. The BBB crossing was first demonstrated via studying the NP uptake, then the release from bEend.3 endothelial cells and, finally via a BBB-transcytosis model. Lastly, the *in vivo* BBB crossing was confirmed by injection-followed MRI analysis which was followed by staining of the harvested brains. Both methods highlight the promising role of such vehicles for potential *in vivo* application of sialic acid functionalized BSA-nanoparticles for Aβ detection and imaging.

3.11 Future Directions

Although the preliminary *in vivo* experiments indicated that NP-BSA_x-Sia have crossed the BBB, the extent of this crossing can be confirmed by using higher concentration of nanoparticles on multiple mice. Furthermore, the affirmation of the BBB crossing characteristic would pave the road to the *in vivo* Aβ binding experiments, which is considered one of the ultimate goals of this approach. The *in vivo* Aβ binding experiments are envisioned to be performed on AD transgenic (Tg) mice where the presumed binding of nanoparticles to Aβ would be detected via MRI, in addition to other techniques like Thioflavin T or Congo Red for the detection of Aβ fibrils, or Prussian Blue and histological staining for nanoparticle detection.

There are other possible approaches that can be adopted to detect the *in vivo* binding of nanoparticles to Aβ in the brain, and also the tracking of nanoparticles in the other organs. One

of these methods is the use of radio-labeled isotope functionalized nanoparticles, where they can be tracked and quantified in the organ of interest by the liquid scintillation counting (LSC).

The whole point of using sialic acid in our work was to mimic the sialic acid-containing gangliosides on the neuronal cells, however once the *in vivo* experiments show a promising outcome, the GM1 functionalized nanoparticles would be a logical continuation of our current work, where this biomimetic approach would structurally resemble the neuronal cell surface and might demonstrate an arguably improved binding to Aβ.

In addition to these future directions and guidelines, we should be initiating a thorough investigation aimed at understanding the NP/Aβ binding on a molecular level. For instance, when we hypothesize that the nanoparticles bind to fibrilar form of Aβ, the only way to test that hypothesis is by running the ThT assay. It is crucial that we investigate this by successfully separating different population of these aggregates and test the binging with our nanoparticles, after thoroughly characterizing them.

The path for the successful *in vivo* detection of Aβ using our approach is still lined with hurdles, however this work paves the road and lays the foundation to a comprehensive research aimed at noninvasively detecting *in vivo* Aβ, and constitutes a modest step towards the early detection of Alzheimer's disease.

3.12 Experimental Section

Materials and Instrumentation

Unless otherwise indicated, all starting materials, reagents and solvents were obtained from commercial suppliers and used as supplied without further purifications. Iron (III) acetylacetonate [$Fe(acac)_3$], oleyl amine, 1,2-hexadecanediol, oleic acid (OA), benzyl ether, bovine serum albumin (BSA), ethyl-(3,3-dimethylaminopropyl) carbodiimide hydrochloride (EDC), 2,2′-(Ethylenedioxy)bis(ethylamine), tetramethylammonium hydroxide were purchased from Sigma-Aldrich and hydrogen peroxide (30%) was purchased from CCI. Amberlite IR 120 hydrogen form (Amberlite H+) was purchased from Fluka. Buffered 10% formalin solution was purchased from Azer Scientific. Potassium ferrocyanide $K_4Fe(CN)_6$ trihydrate was purchased from Mallinckrodt. 3,3′,5,5′-tetramethylbenzidine (TMB) and 1,1,1,3,3,3-Hexafluoro-2-propanol 99.9% were purchased from Acros Organics. Thioflavin T (ThT), UltraPure Grade was purchased from AnaSpec. Beta amyloid (1-42) was purchased from GL Biochem. (Shanghai) Ltd. bEnd.3 endothelial cells were purchased from American Type Culture Collection (ATCC). Phosphate buffered saline (PBS), Dulbecco's modified Eagle medium (DMEM), sodium pyruvate (100 mM), glutamine, penicillin−streptomycin (Pen Strep) mixture were purchased from Gibco. The Aβ 1-16 (6E10) monoclonal antibody, SIG-39320 was purchased from Covance, and goat anti-mouse HRP-conjugated secondary antibody, was purchased from BioRad. Tween 20 was purchased from BioRad. CellTiter 96 Aqueous One solution containing 3-(4,5-dimethylthiazol-2-yl)-5-(3-carboxy-methoxyphenyl)-2-(4-sulfophenyl)-2H-tetrazolium (MTS) was purchased from Promega. Ultrathin-carbon type A, 400 mesh copper grids for TEM

were purchased form Ted Pella, Inc. Ultrafiltration membranes and centrifugal filters were purchased from Millipore, while dialysis tubings were obtained from BioDesign Inc. bEnd.3 cells were cultured in DMEM. All cell culture media was supplemented with 10% inactivated FBS, 1% Pen-Strep mixture, and L-glutamine (2 mM). Dynamic light scattering (DLS) and zeta potential measurements were performed on a Zetasizer Nano zs apparatus (Malvern, U.K.). Transmission electron microscopy (TEM) images were collected on a JEM-2200FS operating at 200 kV using Gatan multiscan CCD camera with Digital Micrograph imaging software. Thermogravimetric analysis (TGA) was carried on a Thermal Advantage (TA-Instruments-Waters LLC) TGA-Q500 series and the samples were burned under nitrogen. FACS experiments were conducted on a BD Vantage SE flow cytometer.

Synthesis of NP-OA

Iron (III) acetylacetonate [$Fe(acac)_3$] (0.71 g; 2 mmol), 1,2-hexadecanediol (2.58 g; 10 mmol), oleic acid (1.69 g; 6 mmol), oleyl amine (1.61 g; 6 mmol), and benzyl ether (40 ml) were mixed together and stirred under a flow of nitrogen. The mixture was heated to 200 °C for 2 hours followed by refluxing (>300 °C) for 1 hour. The black mixture was cooled to room temperature and ethanol (50 ml) was added. The iron oxide nanoparticles were separated by an external magnet, and washed three times with ethanol to remove excess starting material. The iron oxide nanoparticles were dispersed in hexane (50 ml) and the dispersion was placed on an external magnet to remove undispersed magnetic material. The supernatant containing the nanoparticles was centrifuged at 6000 rpm to remove the non magnetic large particulates. 300

mg of OA-coated iron oxide nanoparticles (NP-OA) dispersed in 50 ml chloroform were collected (6 mg/ml). The nanoparticles had a core size of 7 nm as determined by TEM.

Synthesis of NP-BSA

BSA-coated nanoparticles were obtained when 15 ml of 2 mg/ml of (NP-OA) in chloroform was added to 1.5% tetramethylammonium hydroxide (TMAOH) in 30 ml of water and was stirred vigorously for 6 hours at room temperature. The reaction completion can be monitored by observing the nanoparticles move from the heavier chloroform (organic) layer to the lighter water (aqueous) layer due to the ligand exchange between oleic acid and TMAOH. The reaction mixture was centrifuged and then we separated via separatory funnel. 30 mg of bovine serum albumin (BSA) was dissolved in 50 ml of water and then added to the aqueous nanoparticles layer separated above. The reaction was stirred overnight at medium stirring speed at the room temperature. The reaction mixture was then purified by ultrafiltration (MWCO 100,000) to remove the excess BSA and TMAOH. The purified NP-BSA were diluted with water to a final volume of 50 ml, and placed on an external magnet to remove large particulates.

Synthesis of NP-BSA$_x$

BSA-crosslinking was achieved by reacting NP-BSA with 2,2′-(Ethylenedioxy)bis(ethylamine). 13.2 mg in 20 ml of NP-BSA (0.66 mg/ml) was sonicated for

15 minutes, and was added to pH = 6 neutralized 16.5 ml of 2,2′-(Ethylenedioxy)bis(ethylamine) and stirred for 5 minutes at room temperature. 300mg of EDCI was added and the reaction mixture was stirred at room temperature overnight. The reaction mixture was dialyzed for 24 hours and then further purified by ultrafiltration (MWCO 100,000) to remove the excess 2,2′-(Ethylenedioxy)bis(ethylamine), EDCI and other byproducts.

Synthesis of NP-BSA$_x$-Sia

Sialic acid-linker monomers were prepared following previously reported methods.[107] Sialic acid-linker (60 mg, 0.125 mmol) and EDCI (72 mg, 0.375 mmol) in water (5 mL) were stirred for 30 min at room temperature. NP-BSA$_x$ (50 mg in 15 mL in pH 8.5 carbonate buffer) was added and stirred for 12 h at room temperature. The reaction mixture was centrifuged through 100 000 MWCO Amicon centrifugal filters. The supernatant was collected and adequate amount of aqueous solution of 0.01 M sodium hydroxide was added until the pH value reached 9. The reaction mixture was stirred at room temperature for 15 min, and the solution was neutralized by careful addition of 0.01 M hydrochloric acid. The reaction mixture was centrifuged through 100 000 MWCO Amicon centrifugal filters. The supernatant was diluted with water and centrifuged again. This process was repeated three times.

Synthesis of NP-BSA$_x$-Sia-FITC.

Fluorescein isothiocyanate (FITC) functionalization was achieved by reacting NP-BSA$_x$-Sia with FITC. 5 mg of FITC were added to 30 mg of 1 mg/ml NP-BSA$_x$-Sia and the reaction mixture was stirred overnight at room temperature. The reaction mixture was dialyzed for 24 hours and then further purified by ultrafiltration (MWCO 100,000) to remove the excess FITC.

TEM Sample Preparation

10 μL of the samples were deposited on ultrathin-carbon type A, 400 mesh copper grids (Ted Pella, Inc.) and let to evaporate under the hood. The grids were then washed with water, and dried for 15 min at room temperature.

DLS Sample Preparation

All nanoparticles samples were sonicated for half an hour and then transferred to a Malvern folded capillary cell for size and zeta-potential measurements. All measurements were performed in PBS buffer.

Quantification of Sia via TBA

NP-Sia was treated with 0.2% sodium dodecylsulfate (SDS) in 0.1 N H_2SO4 to the final concentration of 2.86 mg/mL at 85°C for 60 minutes to hydrolyze the sialic acid from the nanoparticle. It was then incubated at 37 °C for 30 minutes, and then treated with 50 μL periodic acid (25mM H5IO6 in 125mM HCl) for 30 min at 37 °C. The excess periodic acid was inactivated with 40 μL sodium meta-arsenite (2% $NaAsO_2$ in 500mM HCl). When the resulting yellow-brownish color (color of the liberated iodine) disappeared, 200 μL of thiobarbituric acid (0.1M 4,6- dihydroxypyrimidine-2-thiol, pH 9) (pH adjusted with 0.1 mol/L NaOH) was added. The reaction tubes were incubated in a boiling water bath for 10 min. The tubes were transferred to an ice-water bath for 2 min followed by 2-min incubation at 37 °C. (The latter incubation improves the extent and increases the rate of chromophore extraction.) The colored complex was extracted by adding 500 μL butanol/HCl solution (n-butanol containing 5.7% of 10.5M HCl) with vigorous agitation. The two phases were separated by centrifugation for 5 minutes. 250 μL of the upper phase was placed into a 96-well flat-bottomed microtiter plate and the absorbance was determined at 550nm using a microplate spectrophotometer.[108]

Deaggregation and Preparation of Aβ

Synthetic Aβ(1−42) peptide (1 mg) was dissolved in spectroscopy grade 99.9% 1,1,1,3,3,3- hexafluoro-2-propanol (3 mL), sonicated for 15 min, and lyophilized for 72 h. The thin peptide film was dissolved in 0.22 μm filtered solution of 10 mM NaOH solution (0.25 mL), after 10 minute sonication, the solution was carefully neutralized with diluted HCl solution to pH

= 6. The neutralized solution was diluted with PBS buffer to the desired final volume of 1.5 mL (the stock Aβ solution concentration is 147.7 μM). For experiments requiring fibril formation, the previous solution was incubated for 48 h at 37 °C.

ELISA Assay of NP-BSA$_x$-Sia Binding with Aβ

To a well in a Nunc MaxiSorp 96-well ELISA plate was added 50 μL of NP-BSA$_x$-Sia solution (0.5 mg/mL), which was incubated at 37 °C for 12 hours. After washing the wells with 3 × 300 mL PBST, 50 μL of Aβ solutions with various concentrations were added to the wells (0.09, 0.37, 1.48, 6.0, 23.75, and 95.0 μM) and incubated at 22 °C for 12 h. The plates were washed with 3 × 300 mL PBST and the anti- Aβ(1−16) IgG (6E10) monoclonal antibody, SIG-39320 (50 μL per well, 0.137nM, 1:24 000 in 1% (w/v) BSA containing PBS) was added, which in turn was incubated at 22 °C for 1 h. After washing with 3 × 300 μL PBST, the solution was discarded and the wells were washed three times with 300 μL of PBST and incubated for 1 h with 50 μL of the goat anti-mouse HRP-conjugated secondary antibody (1.7 nM, 1:18 000 in 1% (w/v) BSA in PBS). The solution was discarded, and the wells were washed three times with 300 μL of PBST. To a freshly prepared 3,3′,5,5′-tetramethylbenzidine (TMB) solution (5 mg of TMB was dissolved in 2 mL of DMSO and then diluted to 20 mL with citrate phosphate buffer), 20 μL of H_2O_2 was added. This mixture (150 μL) was immediately added to the ELISA wells. Blue color was allowed to develop for 10−20 min. The reaction was quenched (yellow color) by addition of 0.5 M H_2SO4 (50 μL/well) and the absorbance was measured at 450 nm on an iMark microplate reader. For sialic acid inhibition assay, a solution of NP-Sia (0.5 mg/mL, 50 μL) was incubated in a 96-well plate at 37 °C overnight. After washing the wells with PBST (3 × 300

μL), Aβ (0.5 μM, 50 μL) was added to the wells immediately followed addition 50 μL of different dilutions of pH 7.4 sialic acid solution (0.00013, 0.00052, 0.0021, 0.0084, 0.033, 0.135 M). The plate was incubated at 22 °C for 12 h. The previous protocols were then followed for antibody incubation and color development.

Kinetics of NP-BSAx-Sia Uptake by bEnd.3 Endothelial Cells via Flow Cytometry

bEnd.3 cells (1 x 10^5 cells/well, 3mL) were allowed to attach in a 6-well plate overnight at 37 °C and 5% CO_2. The cells were washed twice with PBS, and 3mL of NP-BSA_x-Sia-FITC (83 μg/ml) in serum-free DMEM were added. The plate was incubated for 1, 3 and 7 hours at 37 °C and 5% CO_2. The cells were then washed with PBS (3 times) and trypsinized with 0.25% trypsin-EDTA (1 ml). Trypsin was neutralized with serum-containing DMEM, and the cells were collected by centrifugation (2500 rpm; 4 °C). The cells were resuspended in PBS (300 μl) and transferred to FACS tubes. The cells were stored on ice till the time of FACS analysis. The endocytosis of NP-BSA_x-Sia-FITC vs NP-BSA_x-FITC was also studied by repeating the same procedure but with 3 hour nanoparticle incubation.

NP-BSA_x-Sia Uptake by bEnd.3 Endothelial Cells via Confocal Microscopy

bEnd.3 cells (3 x 10^5 cells per well, 2 mL) were cultured in a 4- well chambered plate at 37 °C and 5% CO_2 for 24 h. The culture medium was removed and the cells were washed with PBS (3 times). NP-BSA_x-Sia-FITC in serum-free DMEM was added. The cells were incubated

with the NPs for 5 h. Lysotracker red (1 mM, 50 mL per well) was added 1 h before completion of incubation. The supernatant was removed. The cells were washed trice with PBS, and mixed with 10% formalin (0.5 mL per well) for 15 min. Formalin was removed and the cells were washed trice with PBS. 4′,6-diamidino-2-phenylindole (DAPI, 300 nM, 300 mL per well) was added, and the cells were incubated for 4–5 min. The supernatant was removed, and the cells were washed with PBS and water. The plate was covered by an aluminum foil and stored at 4 °C until imaging time.

Time Dependent Exocytosis of NP-BSA$_x$-Sia from bEnd.3 Endothelial Cells

bEnd.3 cells ($3x10^5$ cells/well) were cultured in a 35 mm cell culture plate overnight at 37 °C and 5% CO_2. The supernatant was removed and the cells were washed with PBS trice. NP-BSA$_x$-Sia-FITC (0.1 mg/mL, 2 ml) in serum free DMEM media was added and the cells were incubated for 5 h at 37 °C and 5% CO_2 after which the supernatant was removed and the cells were washed with PBS six times to ensure the complete removal of NPs from the surface of the cells. Fresh serum-free DMEM (2 ml) was added to the plate, which was incubated at 37 °C and 5% CO_2. 100 µl of the supernatant were transferred at specific time points to a black, bottom-clear 96-well plate, and fluorescence was measured on a plate reader (excitation wavelength 488 nm; emission wavelength 520 nm). The drawn samples were returned to the plate to maintain a constant volume through the experiment.

Uptake and Release of NP-BSA$_x$-Sia Through bEnd.3 Endothelial Cells via Transcytosis Assay

bEnd.3 cells were cultured in a 100 mm cell culture plate at 37 °C and 5% CO_2 till it reached 80% confluency. Cells were trypsinized, collected by centrifugation, and resuspended in 10% FBS–DMEM to a final concentration of 13.44 x 10^4 cells per ml. Serum containing DMEM (1.5 ml) was added to the wells of a 12-well plate, above which the transwell inserts were placed. 500 ml of the cell suspension was added to each transwell (6.72 x 10^4 cells per transwell). The plate was incubated at 37 °C and 5% CO_2 for 2 weeks. The growth media was changed every day. The integrity of the multilayered cell culture was assessed by transendothelial electrical resistance (TEER) measurements using a Millicell-ERS Volt-Ohm Meter (Millipore). Transendothelial electrical resistance after the period of two weeks was founds to be 133 Ω.cm^2. After 2 weeks, the growth media was removed and the cell layer was washed with PBS. 1.5 ml of serum free DMEM was added to the bottom of the 12-well plate wells. Two transwells received NP-BSA$_x$-Sia-FITC in serum-free DMEM (0.5 ml, 0.32 mg/ml), and a fluorescently equivalent amount of NP-BSA$_x$-FITC in serum-free DMEM (0.5 ml, 0.23 mg/ml). 100 ml aliquots were drawn at different time points from the lower compartment and the fluorescence was assessed on a plate reader (excitation wavelength 488 nm; emission wavelength 520 nm). After measurement, the aliquots were returned to their respective wells. The volume in the bottom wells was maintained at 1.5 ml.

MRI Experiments

All MRI experiments were carried out on a GE 3T Signa® HDx MR scanner (GE Healthcare, Waukesha, WI).

NP-BSA$_x$-NP Relaxivity

Seven different dilutions of the NP-BSA$_x$-Sia (0.488, 0.976, 1.953, 3.906, 7.812, 15.625, 31.25, 62.5, 125, 250 μg/mL) were prepared to a final volume of 3 mL in FACS tubes. The tubes were placed on a polystyrene tube holder. To evaluate the R2 characteristics of the nanoparticles in phantoms, the following parameters were used: Head coil, 2D fast spin echo, flip angle = 90°, eight echo times (TEs) = 8.0 ms, 16.0 ms, 23.9 ms, 31.9 ms, 39.9 ms, 47.9 ms, 55.8 ms and 63.8 ms, time of repetition (TR) = 500 ms, receiver bandwidth (rBW) = ± 31.2 kHz, field of view (FOV) = 16 cm, slice thickness = 3 mm, number of slices = 2, acquisition matrix = 256 × 256 and number of excitation (NEX) = 1. To evaluate the R1 characteristics of the nanoparticles in phantoms, the following parameters were used: Head coil, 2D inversion recovery spin echo, flip angle = 90°, echo time = 15 ms, time of repetition = 2500 ms, inversion time = 50 ms, 100 ms, 400 ms, 700 ms and 1000 ms, receiver bandwidth = ± 15.6 kHz, field of view = 16 cm, slice thickness = 3 mm, number of slices = 1, acquisition matrix = 256 × 128 and number of excitation = 1.

Ex Vivo Brain Aβ/NP Binding Experiments (MRI)

The brains of C57BL6 mice were harvested and fixed in buffered 10% formalin solution for 24 h. After washing with deionized water, brains were incubated with 27 μM Aβ (4 mL) for 12 h at 4 °C. The Aβ treated brains were incubated with 0.6 mg/mL, 4 mL of NP-BSA_x-Sia and NP-BSA_x for 12 h at 37 °C after washing with deionized water. After incubation, the brains were washed thoroughly and placed in a 24-well plate in PBS. For the sialic acid competition experiment, 0.1 M free sialic acid was added with NP-BSA_x-Sia (4 mL). Two control brains were treated in a similar manner (concentrations, temperatures and duration), however one was first incubated with Aβ only then PBS after DI water washing, and the other was incubated with PBS and then with NP-BSA_x-Sia after DI water washing.

The brains were imaged with the following parameters (T2* weighted sequence): wrist coil, 3D fast spoiled gradient recalled echo sequence, flip angle = 15°, echo times = 9.93 ms, time of repetition = 20.4 ms, receiver bandwidth = ±7.8 kHz, field of view = 6 cm, slice thickness = 0.5 mm, number of slices = 40, acquisition matrix = 256 × 256, and number of excitation = 3.

Prussian Blue Staining of Mice Brains

The same brains used in the *ex vivo* Aβ/NP-Sia MRI binding experiment were stained directly after imaging. Brains were soaked in 10% $K_4Fe[CN]_6$ solution, incubated for 10 min, and then transferred to a vial containing a mixture of 10 wt % $K_4Fe[CN]_6$/20 wt % HCl with a

volume ratio of 1:1 for 10 min (Gomori's modified Prussian blue). The tissues were washed with water four times. A blue color was observed on the areas bearing iron oxide nanoparticles.

Procedures for *in vivo* Mice Brain MRI Experiment

All animal experiments were in accordance with the guidelines and the approval of Institutional Animal Care and Use Committee, Michigan State University. CD-1 Mice (n=4, female, 6-8 months old, ~ 0.3 kg body weight).

For MRI, Mice were anesthetized with 2% isoflurane/ oxygen flow, the mice were held in a supine position on plastic boards with medical tape to minimize motion artifact and placed inside an wrist coil for MRI. MRI was carried out on a GE 3 T Signa® HDx MR scanner (GE Healthcare, Waukesha, WI). After a pre injection scan, the mice were injected with NP-BSA_x-Sia in the retro-orbital of the mice with a 100 μL, 20 mg/kg dose). Five post-injection scans were taken, specifically at the 16, 27, 38, 49, and 60 minutes. To compare the T2* effect due to the uptake of the nanoparticles in the *in vivo* mouse brain, the following parameters were used: Wrist coil, 3D fast spoiled gradient recalled echo sequence, flip angle = 15°, echo time (TE) = 10.6 ms, time of repetition (TR) = 21.8 ms, receiver bandwidth (rBW) = ± 7.8 kHz, field of view (FOV) = 4 cm, slice thickness = 0.5 mm, number of slices = 32, acquisition matrix = 256 × 256, and number of excitation (NEX) = 3. To quantify the MR signal changes over time from NP injection, the signal intensities from the brain images acquired before injection and after injections were normalized by the mean signal intensity of the muscle at the anterior neck using ImageJ software. Muscle signals provided good calibration of the slight variation of background in images acquired at different time points.

Prussian Blue Staining of CD-1 Mice Brains

The animals were sacrificed and their abdominal cavity was cut and the heart was reached after cutting the diaphragm. The blood was drawn from the left ventricle in the apex of the heart. A 2 mL of cold PBS was injected to the left ventricle via a syringe. Each brain was removed quickly, fixed with 10% formalin solution for 24 hours, and subjected to Prussian blue staining (see *ex vivo* brain staining procedure). As a negative control, a mouse was injected with 100 μL PBS (instead of nanoparticles) and sacrificed then PBS perfused. And the other mouse, which was injected with 100 μL, 20 mg/kg dose of NP-BSA_x-Sia and sacrificed but not perfused with PBS was the positive control.

Assessing NP-BSA_x-NP Cytotoxicity via MTS Assay

bEnd.3 cells were plated into 96-well plates at a density of $4x10^4$ cells per well in 10% DMEM cell culture media for 24 h at 37 °C and 5% CO_2. The culture medium was replaced with non-serum solution of different concentrations of NP-BSA_x-Sia (0.001, 0.01, 0.1, 0.2, 1 mg/mL/well). After 4 h incubation at 37 °C, the medium was replaced with MTS solution (20 μL in 200 μL) in culture medium and incubated for 1 h at 37 °C. The developed brown color in the wells was an indication of live cells. The absorption of the plate was measured at 490 nm in an

iMark microplate reader (BioRad). Wells without cells (blanks) were subtracted as background from each sample.

REFERENCES

REFERENCES

1. Alzheimer's Association *Alzheimer's disease facts and figures*; Alzheimer Foundation: Washington, DC, 2014.

2. (a) Hebert, L. E.; Weuve, J.; Scherr, P. A.; Evans, D. A., Alzheimer disease in the united states (2010-2050) estimated using the 2010 census. *Neurology* **2013,** *80* (19), 1778-1783; (b) Wimo, A.; Winblad, B., Economic aspects on drug therapy of dementia. *Curr. Pharm. Design* **2004,** *10* (3), 295-301.

3. Selkoe, D. J., The molecular pathology of Alzheimer's disease. *Neuron* **1991,** *6*, 487-498.

4. Selkoe, D. J., Amyloid β-protein deposition as a seminal pathogenetic event in AD: An hypothesis. *Neurobiol. Aging* **1990,** *11* (3), 299.

5. (a) Hardy, J. A.; Higgins, G. A., Alzheimers-disease - the amyloid cascade hypothesis. *Science* **1992,** *256* (5054), 184-185; (b) Selkoe, D. J., Alzheimers-disease - a central role for amyloid. *J. Neuropath. Exp. Neur.* **1994,** *53* (5), 438-447.

6. (a) Mattson, M. P., Pathways towards and away from Alzheimer's disease (vol 430, pg 631, 2004). *Nature* **2004,** *431* (7004), 107-107; (b) Selkoe, D. J., Alzheimer disease: Mechanistic understanding predicts novel therapies. *Annal. Int. Med.* **2004,** *140* (8), 627-638; (c) Selkoe, D. J., Cell biology of protein misfolding: The examples of Alzheimer's and Parkinson's diseases. *Nat. Cell Biol.* **2004,** *6* (11), 1054-1061.

7. (a) Hartmann, T.; Bieger, S. C.; Bruhl, B.; Tienari, P. J.; Ida, N.; Allsop, D.; Roberts, G. W.; Masters, C. L.; Dotti, C. G.; Unsicker, K.; Beyreuther, K., Distinct sites of intracellular production for Alzheimer's disease A-beta 40/42 amyloid peptides. *Nat. Med.* **1997,** *3* (9), 1016-1020; (b) Bitan, G.; Kirkitadze, M. D.; Lomakin, A.; Vollers, S. S.; Benedek, G. B.; Teplow, D. B., Amyloid beta-protein (A beta) assembly: A beta 40 and A beta 42 oligomerize through distinct pathways. *Proc. Natl. Acad. Sci. U.S.A.* **2003,** *100* (1), 330-335.

8. Masters, C. L.; Cappai, R.; Barnham, K. J.; Villemagne, V. L., Molecular mechanisms for Alzheimer's disease: Implications for neuroimaging and therapeutics. *J. Neurochem.* **2006,** *97* (6), 1700-1725.

9. Terry, R. D.; Masliah, E.; Salmon, D. P.; Butters, N.; DeTeresa, R.; Hill, R.; Hansen, L. A.; Katzman, R., Physical basis of cognitive alterations in Alzheimer's disease: Synapse loss is the major correlate of cognitive impairment. *Annal. Neurol.* **1991,** *30*, 572-580.

10. Lesne, S.; Kotilinek, L.; Ashe, K. H., Plaque-bearing mice with reduced levels of oligomeric amyloid-beta assemblies have intact memory function. *Neuroscience* **2008,** *151* (3), 745-749.

11. (a) Nordberg, A., Amyloid plaque imaging in vivo: Current achievement and future prospects. *Eur. J. Nucl. Med. Mol. Imag.* **2008,** *35(Suppl. 1)*, S46-S50; (b) Villemagne, V. L.; Fodero-Tavoletti, M. T.; Pike, K. E.; Cappai, R.; Masters, C. L.; Rowe, C. C. T., The art of loss: Abeta imaging in the evaluation of Alzheimer's disease and other dementias. *Mol. Neurobiol.* **2008,** *38*, 1-15.

12. Walsh, D. M.; Klyubin, I.; Shankar, G. M.; Townsend, M.; Fadeeva, J. V.; Betts, V.; Podlisny, M. B.; Cleary, J. P.; Ashe, K. H.; Rowan, M. J.; Selkoe, D. J., The role of cell-derived oligomers of A beta in Alzheimer's disease and avenues for therapeutic intervention. *Biochem. Soc. Trans.* **2005,** *33*, 1087-1090.

13. Lesne, S.; Koh, M. T.; Kotilinek, L.; Kayed, R.; Glabe, C. G.; Yang, A.; Gallagher, M.; Ashe, K. H., A specific amyloid-beta protein assembly in the brain impairs memory. *Nature* **2006,** *440* (7082), 352-357.

14. Shankar, G. M.; Li, S.; Mehta, T. H.; Garcia-Munoz, A.; Shepardson, N. E.; Smith, I.; Brett, F. M.; Farrell, M. A.; Rowan, M. J.; Lemere, C. A.; Regan, C. M.; Walsh, D. M.; Sabatini, B. L.; Selkoe, D. J., Amyloid-beta protein dimers isolated directly from Alzheimer's brains impair synaptic plasticity and memory. *Nat. Med.* **2008,** *14* (8), 837-842.

15. Puzzo, D.; Privitera, L.; Leznik, E.; Fa, M.; Staniszewski, A.; Palmeri, A.; Arancio, O., Picomolar amyloid-beta positively modulates synaptic plasticity and memory in hippocampus. *J. Neurosci.* **2008,** *28* (53), 14537-14545.

16. Meyer-Luehmann, M.; Spires-Jones, T. L.; Prada, C.; Garcia-Alloza, M.; de Calignon, A.; Rozkalne, A.; Koenigsknecht-Talboo, J.; Holtzman, D. M.; Bacskai, B. J.; Hyman, B. T., Rapid appearance and local toxicity of amyloid-beta plaques in a mouse model of Alzheimer's disease. *Nature* **2008,** *451* (7179), 720-U5.

17. Pimplikar, S. W., Reassessing the amyloid cascade hypothesis of Alzheimer's disease. *Int. J. Biochem. Cell Biol.* **2009,** *41* (6), 1261-1268.

18. Kirkitadze, M. D.; Condron, M. M.; Teplow, D. B., Identification and characterization of key kinetic intermediates in amyloid β-protein fibrillogenesis. *J. Mol. Biol.* **2001,** *312*, 1103-1119.

19. (a) Schauer, R., Achievements and challenges of sialic acid research. *Glycoconjugate J.* **2000,** *17* (7-9), 485-499; (b) Angata, T.; Varki, A., Chemical diversity in the sialic acids and related alpha-keto acids: An evolutionary perspective. *Chem. Rev.* **2002,** *102* (2), 439-469; (c) Ilver, D.; Johansson, P.; Miller-Podraza, H.; Nyholm, P. G.; Teneberg, S.; Karlsson, K. A., Bacterium-host protein-carbohydrate interactions. In *Recognition of Carbohydrates in Biological Systems, Part B: Specific Applications,* 2003**;** Vol. (363), pp 134-157; (d) Lehmann, F.; Tiralongo, E.; Tiralongo, J., Sialic acid-specific lectins: Occurrence, specificity and function. *Cell. Mol. Life Sci.* **2006,** *63* (12), 1331-1354.

20. Varki, A., Sialic acids in human health and disease. *Trends Mol. Med.* **2008,** *14* (8), 351-360.

21. (a) Weinhold, B.; Seidenfaden, R.; Rockle, I.; Muhlenhoff, M.; Schertzinger, F.; Conzelmann, S.; Marth, J. D.; Gerardy-Schahn, R.; Hildebrandt, H., Genetic ablation of polysialic acid causes severe neurodevelopmental defects rescued by deletion of the neural cell adhesion molecule. *J. Biol. Chem.* **2005,** *280* (52), 42971-42977; (b) Johnson, C. P.; Fujimoto, I.; Rutishauser, U.; Leckband, D. E., Direct evidence that neural cell adhesion molecule (NCAM) polysialylation increases intermembrane repulsion and abrogates adhesion. *J. Biol. Chem.* **2005,** *280* (1), 137-145; (c) El Maarouf, A.; Petridis, A. K.; Rutishauser, U., Use of polysialic acid in repair of the central nervous system. *Proc. Natl. Acad. Sci. U.S.A.* **2006,** *103* (45), 16989-16994; (d) Rutishauser, U., Polysialic acid in the plasticity of the developing and adult vertebrate nervous system. *Nat. Rev. Neurosci.* **2008,** *9* (1), 26-35.

22. (a) Dekan, G.; Gabel, C.; Farquhar, M. G., Sulfate contributes to the negative charge of podocalyxin, the major sialoglycoprotein of the glomerular-filtration slits. *Proceedings of the National Academy of Sciences of the United States of America* **1991,** *88* (12), 5398-5402; (b) Gelberg, H.; Healy, L.; Whiteley, H.; Miller, L. A.; Vimr, E., In vivo enzymatic removal of alpha 2->6-linked sialic acid from the glomerular filtration barrier results in podocyte charge alteration and glomerular injury. *Lab. Invest.* **1996,** *74* (5), 907-920.

23. (a) Varki, A., Glycan-based interactions involving vertebrate sialic-acid-recognizing proteins. *Nature* **2007,** *446* (7139), 1023-1029; (b) Crocker, P. R.; Paulson, J. C.; Varki, A., Siglecs and their roles in the immune system. *Nat. Rev. Immunol.* **2007,** *7* (4), 255-266.

24. Kracun, I.; R¨osner, H.; Cosovic, C.; Stavljenic, A., Topographical atlas of the gangliosides of the adult human brain. *J. Neurochem.* **1984,** *43*, 979-989.

25. Nagai, Y., Functional roles of gangliosides in bio-signaling. *Behav. Brain Res.* **1995,** *66*, 99-104.

26. (a) Pitto, M.; Raimondo, F.; Zoia, C.; Brighina, L.; Ferrarese, C.; Masserini, M., Enhanced GM1 ganglioside catabolism in cultured fibroblasts from Alzheimer patients. *Neurobiol. Aging* **2005,** *26* (6), 833-838; (b) Yanagisawa, K.; Odaka, A.; Suzuki, N.; Ihara, Y., GM1 ganglioside-bound amyloid beta-protein (Abeta): A possible form of preamyloid in alzheimer's disease. *Nat. Med.* **1995,** *1*, 1062-1066.

27. Hardy, J.; Selkoe, D. J., Medicine - the amyloid hypothesis of Alzheimer's disease: Progress and problems on the road to therapeutics. In *Science*, 2002; Vol. 297, pp 353-356.

28. (a) Ariga, T.; Kobayashi, K.; Hasegawa, A.; Kiso, M.; Ishida, H.; Miyatake, T., Characterization of high-affinity binding between gangliosides and amyloid beta-protein. *Arch. Biochem. Biophys.* **2001,** *388* (2), 225-230; (b) Fraser, P. E.; Darabie, A. A.; McLaurin, J., Amyloid-beta interactions with chondroitin sulfate-derived monosaccharides and disaccharides - implications for drug development. *J. Biol. Chem.* **2001,** *276* (9), 6412-6419; (c) Walsh, D.; Lomakin, A.; Benedek, G.; Condron, M.; Teplow, D., Amyloid β-protein fibrillogenesis: Detection of a protofibrillar intermediate. *J. Biol. Chem.* **1997,** *272*, 22364-22372; (d) Kakio, A.; Nishimoto, S.; Yanagisawa, K.; Kozutsumi, Y.; Matsuzaki, K., Cholesterol-dependent formation of GM1 ganglioside-bound amyloid beta-protein, an endogenous seed for Alzheimer amyloid. In *J. Biol. Chem.*, 2001; Vol. 276, pp 24985-24990; (e) Kakio, A.; Yano, Y.; Takai, D.; Kuroda, Y.; Matsumoto, O.; Kozutsumi, Y.; Matsuzaki, K., Interaction between amyloid beta-protein aggregates and membranes. *J. Pept. Sci.* **2004,** *10* (10), 612-621; (f) Matsuzaki, K.; Horikiri, C., Interactions of amyloid beta-peptide (1-40) with ganglioside-containing membranes. *Biochemistry* **1999,** *38* (13), 4137-4142; (g) Fung, J.; Darabie, A. A.; McLaurin, J., Contribution of simple saccharides to the stabilization of amyloid structure. *Biochem. Biophys. Res. Commun.* **2005,** *328* (4), 1067-1072; (h) Williamson, M. P.; Suzuki, Y.; Bourne, N. T.; Asakura, T., Binding of amyloid beta-peptide to ganglioside micelles is dependent on histidine-13. *Biochem. J* **2006,** *397*, 483-490; (i) Yanagisawa, K.; Odaka, A.; Suzuki, N.; Ihara, Y., GM1ganglioside-bound amyloidbeta-protein(Abeta):Apossibleformofpreamyloidinalzheimer's disease. *Nat. Med.* **1995,** *1*, 1062-1066; (j) Ariga, T.; Yu, R. K., GM1inhibitsamyloidbeta-protein-inducedcytokine release. *Neurochem.Res.* **1999,** *24*, 219-226; (k) Wakabayashi, M.; Okada, T.; Kozutsumi, Y.; Matsuzaki, K., GM1 ganglioside-mediated accumulation of amyloid beta-protein on cell membranes. *Biochem. Biophys. Res. Commun.* **2005,** *328*, 1019-1023; (l) McLaurin, J.; Chakrabartty, A., Membrane disruption by Alzheimer beta-amyloid peptides mediated through specific finding to either phospholipids or gangliosides - implications for neurotoxicity. *J. Biol. Chem.* **1996,** *271* (43), 26482-26489; (m) ChooSmith, L. P.; Surewicz, W. K., The interaction between alzheimer amyloid beta(1-40) peptide and ganglioside GM1-containing membranes. *FEBS Lett.* **1997,** *402* (2-3), 95-98; (n) McLaurin, J.; Franklin, T.; Fraser, P. E.; Chakrabartty, A., Structural transitions associated with the interaction of Alzheimer beta-amyloid peptides with gangliosides. *J. Biol. Chem.* **1998,** *273* (8), 4506-4515; (o) Choo-Smith, L.-P. I.; Garzon-Rodriguez, W.; Glabe, C. G.; Surewicz, W. K., Acceleration of amyloid fibril formation by

specific binding of A-beta-(1-40) peptide to ganglioside-containing membrane vesicles. *J. Biol. Chem.* **1997,** *272* (37), 22987-22990.

29. (a) Yanagisawa, K., Role of gangliosides in Alzheimer's disease. *Biochim. Biophys. Acta-Biomembr.* **2007,** *1768* (8), 1943-1951; (b) Ariga, T.; McDonald, M. P.; Yu, R. K., Role of ganglioside metabolism in the pathogenesis of Alzheimer's disease - a review. *J. Lipid Res.* **2008,** *49* (6), 1157-1175; (c) Yanagisawa, K., Pathological significance of ganglioside clusters in alzheimer's disease. *J. Neurochem.* **2011,** *116* (5), 806-812; (d) Matsuzaki, K.; Kato, K.; Yanagisawa, K., A beta polymerization through interaction with membrane gangliosides. *Biochim. Biophys. Acta-Mol. Cell Biol. Lipids* **2010,** *1801* (8), 868-877.

30. Yanagisawa, K.; Ihara, Y., GM1 ganglioside-bound amyloid beta-protein in alzheimer's disease brain. *Neurobiol. Aging* **1998,** *19* (1), S65-S67.

31. Yamamoto, N.; Hasegawa, K.; Matsuzaki, K.; Naiki, H.; Yanagisawa, K., Environment- and mutation-dependent aggregation behavior of Alzheimer amyloid β-protein. . *J. Neurochem.* **2004,** *90*, 62-69.

32. Wakabayashi, M.; Okada, T.; Kozutsumi, Y.; Matsuzaki, K., GM1 gangliosidemediated accumulation of amyloid β-protein on cell membranes. . *Biochem. Biophys. Res. Commun.* **2005,** *328*, 1019-1023.

33. (a) Kakio, A.; Nishimoto, S. I.; Yanagisawa, K.; Kozutsumi, Y.; Matsuzaki, K., Cholesterol-dependent formation of GM1 ganglioside-bound amyloid beta-protein,an endogenous seed for Alzheimer amyloid. *J.Biol.Chem.* **2001,** *276*, 24985-24990; (b) Kakio, A.; Yano, Y.; Takai, D.; Kuroda, Y.; Matsumoto, O.; Kozutsumi, Y.; Matsuzaki, K., Interaction between amyloid beta-protein aggregates and membranes. *J. Pept. Sci.* **2004,** *10*, 612-621; (c) Yamamoto, N.; Matsubara, T.; Sato, T.; Yanagisawa, K., Age-dependent high-density clustering of GM1 ganglioside at presynaptic neuritic terminals promotes amyloid β-protein fibrillogenesis. *Biochim. Biophys. Acta* **2009,** *1778*, 2717-2726; (d) Patel, D.; Henry, J.; Good, T., Attenuation of beta-amyloid induced toxicity by sialic acid-conjugated dendrimeric polymers. *Biochim. Biophys. Acta-Gen. Subj.* **2006,** *1760* (12), 1802-1809; (e) Patel, D. A.; Henry, J. E.; Good, T. A., Attenuation of beta-amyloid-induced toxicity by sialic-acid-conjugated dendrimers: Role of sialic acid attachment. *Brain Res.* **2007,** *1161*, 95-105; (f) McLaurin, J.; Chakrabartty, A., Characterization of the interactions of Alzheimer beta-amyloid peptides with phospholipid membranes. *Eur. J. Biochem.* **1997,** *245* (2), 355-363; (g) Dhavale, D.; Henry, J. E., Evaluation of sialic acid-analogs for the attenuation of amyloid-beta toxicity. *Biochim. Biophys. Acta-Gen. Subj.* **2012,** *1820* (10), 1475-1480.

34. (a) Ariga, T.; Kobayashi, K.; Hasegawa, A.; Kiso, M.; Ishida, H.; Miyatake, T., Characterization of high-affinity binding between gangliosides and amyloid betaprotein. . *Arch. Biochem. Biophys.* **2001,** *388* (2), 225-230; (b) Ariga, T.; Yu, R. K., GM1 inhibits amyloid beta-

protein-induced cytokine release. *Neurochem. Res.* **1999,** *24* (2), 219-226; (c) Matsuzaki, K.; Horikiri, C., Interactions of amyloid beta-peptide (1-40) with ganglioside-containing membranes. *Biochemistry* **1999,** *38* (13), 4137-4142; (d) Wakabayashi, M.; Okada, T.; Kozutsumi, Y.; Matsuzaki, K., GM1 ganglioside mediated accumulation of amyloid beta-protein on cell membranes. *Biochem. Biophys. Res. Commun.* **2005,** *328* (4), 1019-1023; (e) Yanagisawa, K.; Odaka, A.; Suzuki, N.; Ihara, Y., GM1 ganglioside-bound amyloid beta-protein (A beta): A possible form of preamyloid in Alzheimer's disease. *Nat. Med.* **1995,** *1* (10), 1062–1066; (f) Zha, Q.; Ruan, Y.; Hartmann, T.; Beyreuther, K.; Zhang, D., GM1 ganglioside regulates the proteolysis of amyloid precursor protein. *Mol. Psychiatry* **2004,** *9* (10), 946-952.

35. Weis, W. I.; Drickamer, K., Structural basis of lectin-carbohydrate recognition. *Annu. Rev. Biochem.* **1996,** *65*, 441-473.

36. Wade, A.; Robinson, A. E.; Engler, J. R.; Petritsch, C.; James, C. D.; Phillips, J. J., Proteoglycans and their roles in brain cancer. *FEBS Journal* **2013,** *280* (10), 2399-2417.

37. (a) Snow, A. D.; Mar, H.; Nochlin, D.; Kimata, K.; Kato, M.; Suzuki, S.; Hassell, J.; Wight, T. N., The presence of heparan-sulfate proteoglycans in the neuritic plaques and congophilic angiopathy in Alzheimers-disease. *Am. J. Pathol.* **1988,** *133* (3), 456-463; (b) Snow, A. D.; Mar, H.; Nochlin, D.; Sekiguchi, R. T.; Kimata, K.; Koike, Y.; Wight, T. N., Early accumulation of heparan-sulfate in neurons and in the beta-amyloid protein-containing lesions of Alzheimers-disease and downs-syndrome. *Am. J. Pathol.* **1990,** *137* (5), 1253-1270; (c) Perlmutter, L. S.; Chui, H. C.; Saperia, D.; Athanikar, J., Microangiopathy and the colocalization of heparan-sulfate proteoglycan with amyloid in senile plaques of Alzheimers-disease. *Brain Res.* **1990,** *508* (1), 13-19.

38. McLaurin, J.; Franklin, T.; Zhang, X. Q.; Deng, J. P.; Fraser, P. E., Interactions of Alzheimer amyloid-beta peptides with glycosaminoglycans - effects on fibril nucleation and growth. *Eur. J. Biochem.* **1999,** *266* (3), 1101-1110.

39. Snow, A. D.; Sekiguchi, R. T.; Nochlin, D.; Kalaria, R. N.; Kimata, K., Heparan-sulfate proteoglycan in diffuse plaques of hippocampus but not of cerebellum in Alzheimers-disease brain. *Am. J. Pathol.* **1994,** *144* (2), 337-347.

40. (a) Buee, L.; Ding, W.; Delacourte, A.; Fillit, H., Binding of secreted human neuroblastoma proteoglycans to the Alzheimers amyloid A4 peptide. *Brain Res.* **1993,** *601* (1-2), 154-163; (b) Buee, L.; Ding, W. H.; Anderson, J. P.; Narindrasorasak, S.; Kisilevsky, R.; Boyle, N. J.; Robakis, N. K.; Delacourte, A.; Greenberg, B.; Fillit, H. M., Binding of vascular heparan-sulfate proteoglycan to Alzheimers amyloid precursor protein is mediated in part by the N-terminal region of A4 peptide. *Brain Res.* **1993,** *627* (2), 199-204.

41. (a) Fraser, P. E.; Nguyen, J. T.; Chin, D. T.; Kirschner, D. A., Effects of sulfate-ions on Alzheimer-beta/A4 peptide assemblies - implications for amyloid fibril proteoglycan interactions. *J. Neurochem.* **1992,** *59* (4), 1531-1540; (b) McLaurin, J.; Fraser, P. E., Effect of amino-acid substitutions on Alzheimer's amyloid-beta peptide-glycosaminoglycan interactions. *Eur. J. Biochem.* **2000,** *267* (21), 6353-6361.

42. Brunden, K. R.; Richtercook, N. J.; Chaturvedi, N.; Frederickson, R. C. A., pH-dependent binding of synthetic beta-amyloid peptides to glycosaminoglycans. *J. Neurochem.* **1993,** *61* (6), 2147-2154.

43. (a) Shaw, C. P.; Middleton, D. A.; Volk, M.; Levy, R., Amyloid-derived peptide forms self-assembled mono layers on gold nanoparticle with a curvature-dependent beta-sheet structure. *ACS Nano* **2012,** *6* (2), 1416-1426; (b) Chan, H.-M.; Xiao, L.; Yeung, K.-M.; Ho, S.-L.; Zhao, D.; Chan, W.-H.; Li, H.-W., Effect of surface-functionalized nanoparticles on the elongation phase of beta-amyloid (1-40) fibrillogenesis. *Biomaterials* **2012,** *33* (18), 4443-4450; (c) Wang, C.; Liu, D.; Wang, Z., Gold nanoparticle based dot-blot immunoassay for sensitively detecting Alzheimer's disease related beta-amyloid peptide. *Chem. Commun.* **2012,** *48* (67), 8392-8394; (d) Triulzi, R. C.; Dai, Q.; Zou, J.; Leblanc, R. M.; Gu, Q.; Orbulescu, J.; Huo, Q., Photothermal ablation of amyloid aggregates by gold nanoparticles. *Colloids Surf., B* **2008,** *63* (2), 200-208; (e) Bastus, N. G.; Kogan, M. J.; Amigo, R.; Grillo-Bosch, D.; Araya, E.; Turiel, A.; Labarta, A.; Giralt, E.; Puntes, V. F., Gold nanoparticles for selective and remote heating of beta-amyloid protein aggregates. *Mater. Sci. Eng., C* **2007,** *27* (5-8), 1236-1240; (f) Antosova, A.; Gazova, Z.; Fedunova, D.; Valusova, E.; Bystrenova, E.; Valle, F.; Daxnerova, Z.; Biscarini, F.; Antalik, M., Anti-amyloidogenic activity of glutathione-covered gold nanoparticles. *Mater. Sci. Eng., C* **2012,** *32* (8), 2529-2535; (g) Bastus, N. G.; Sanchez-Tillo, E.; Pujals, S.; Farrera, C.; Kogan, M. J.; Giralt, E.; Celada, A.; Lloberas, J.; Puntes, V., Peptides conjugated to gold nanoparticles induce macrophage activation. *Mol. Immunol.* **2009,** *46* (4), 743-748; (h) Zhang, D.; Neumann, O.; Wang, H.; Yuwono, V. M.; Barhoumi, A.; Perham, M.; Hartgerink, J. D.; Wittung-Stafshede, P.; Halas, N. J., Gold nanoparticles can induce the formation of protein-based aggregates at physiological ph. *Nano Lett.* **2009,** *9* (2), 666-671; (i) Araya, E.; Olmedo, I.; Bastus, N. G.; Guerrero, S.; Puntes, V. F.; Giralt, E.; Kogan, M. J., Gold nanoparticles and microwave irradiation inhibit beta-amyloid amyloidogenesis. *Nano. Res. Lett.* **2008,** *3* (11), 435-443; (j) Liao, Y.-H.; Chang, Y.-J.; Yoshiike, Y.; Chang, Y.-C.; Chen, Y.-R., Negatively charged gold nanoparticles inhibit Alzheimer's amyloid-beta fibrillization, induce fibril dissociation, and mitigate neurotoxicity. *Small* **2012,** *8* (23), 3631-3639.

44. (a) Kouyoumdjian, H.; Zhu, D. C.; El-Dakdouki, M. H.; Lorenz, K.; Chen, J.; Li, W.; Huang, X., Glyconanoparticle aided detection of beta-amyloid by magnetic resonance imaging and attenuation of beta-amyloid induced cytotoxicity. *ACS Chem. Neurosci.* **2013,** *4* (4), 575-84; (b) Mahmoudi, M.; Quinlan-Pluck, F.; Monopo, M. P.; Sheibani, S.; Vali, H.; Dawson, K. A.; Lynch, I., Influence of the physiochemical properties of superparamagnetic iron oxide nanoparticles on amyloid beta protein fibrillation in solution. *ACS Chem Neurosci.* **2013,** *4* (3), 475-485; (c) Skaat, H.; Margel, S., Synthesis of fluorescent-maghemite nanoparticles as multimodal imaging agents for amyloid-beta fibrils detection and removal by a magnetic field.

Biochem. Biophys. Res. Commun. **2009,** *386* (4), 645-649; (d) Skaat, H.; Shafir, G.; Margel, S., Acceleration and inhibition of amyloid-beta fibril formation by peptide-conjugated fluorescent-maghemite nanoparticles. *J. Nanopart. Res.* **2011,** *13* (8), 3521-3534; (e) Wadghiri, Y. Z.; Li, J.; Wang, J.; Hoang, D. M.; Sun, Y.; Xu, H.; Tsui, W.; Li, Y.; Boutajangout, A.; Wang, A.; de Leon, M.; Wisniewski, T., Detection of amyloid plaques targeted by bifunctional USPIO in Alzheimer's disease transgenic mice using magnetic resonance microimaging. *Plos One* **2013,** *8* (2).

45. (a) Yoo, S. I.; Yang, M.; Brender, J. R.; Subramanian, V.; Sun, K.; Joo, N. E.; Jeong, S.-H.; Ramamoorthy, A.; Kotov, N. A., Inhibition of amyloid peptide fibrillation by inorganic nanoparticles: Functional similarities with proteins. *Angew. Chem. Int. Ed.* **2011,** *50* (22), 5110-5115; (b) Xiao, L.; Zhao, D.; Chan, W.-H.; Choi, M. M. F.; Li, H.-W., Inhibition of beta 1-40 amyloid fibrillation with N-acetyl-l-cysteine capped quantum dots. *Biomaterials* **2010,** *31*, 91-98.

46. (a) Cowan, C. B.; Cote, G. L.; Good, T. A., Development of photocrosslinked sialic acid containing polymers for use in Abeta toxicity attenuation. *Biomaterials* **2008,** *29* (24-25), 3408-3414; (b) Klajnert, B.; Cortijo-Arellano, M.; Bryszewska, M.; Cladera, J., Influence of heparin and dendrimers on the aggregation of two amyloid peptides related to Alzheimer's and prion diseases. *Biochem. Biophys. Res. Commun.* **2006,** *339* (2), 577-582; (c) Chafekar, S. M.; Malda, H.; Merkx, M.; Meijer, E. W.; Viertl, D.; Lashuel, H. A.; Baas, F.; Scheper, W., Branched klvff tetramers strongly potentiate inhibition of beta-amyloid aggregation. *Chembiochem* **2007,** *8* (15), 1857-1864; (d) Klajnert, B.; Wasiak, T.; Ionov, M.; Fernandez-Villamarin, M.; Sousa-Herves, A.; Correa, J.; Riguera, R.; Fernandez-Megia, E., Dendrimers reduce toxicity of A beta 1-28 peptide during aggregation and accelerate fibril formation. *Nanomed-Nanotechnol* **2012,** *8* (8), 1372-1378.

47. (a) Canovi, M.; Markoutsa, E.; Lazar, A. N.; Pampalakis, G.; Clemente, C.; Re, F.; Sesana, S.; Masserini, M.; Salmona, M.; Duyckaerts, C.; Flores, O.; Gobbi, M.; Antimisiaris, S. G., The binding affinity of anti-A beta 1-42 mAb-decorated nanoliposomes to A beta 1-42 peptides in vitro and to amyloid deposits in post-mortem tissue. *Biomaterials* **2011,** *32* (23), 5489-5497; (b) Gobbi, M.; Re, F.; Canovi, M.; Beeg, M.; Gregori, M.; Sesana, S.; Sonnino, S.; Brogioli, D.; Musicanti, C.; Gasco, P.; Salmona, M.; Masserini, M. E., Lipid-based nanoparticles with high binding affinity for amyloid-beta(1-42) peptide. *Biomaterials* **2010,** *31* (25), 6519-6529; (c) Mourtas, S.; Canovi, M.; Zona, C.; Aurilia, D.; Niarakis, A.; La Ferla, B.; Salmona, M.; Nicotra, F.; Gobbi, M.; Antimisiaris, S. G., Curcumin-decorated nanoliposomes with very high affinity for amyloid-beta 1-42 peptide. *Biomaterials* **2011,** *32* (6), 1635-1645; (d) Ikeda, K.; Okada, T.; Sawada, S.-i.; Akiyoshi, K.; Matsuzaki, K., Inhibition of the formation of amyloid beta-protein fibrils using biocompatible nanogels as artificial chaperones. *FEBS Lett.* **2006,** *580* (28-29), 6587-6595; (e) Pai, A. S.; Rubinstein, I.; Onyuksel, H., Pegylated phospholipid nanomicelles interact with beta-amyloid (1-42) and mitigate its beta-sheet formation, aggregation and neurotoxicity in vitro. *Peptides* **2006,** *27* (11), 2858-2866.

48. (a) Le Droumaguet, B.; Nicolas, J.; Brambilla, D.; Mura, S.; Maksimenko, A.; De Kimpe, L.; Salvati, E.; Zona, C.; Airoldi, C.; Canovi, M.; Gobbi, M.; Noiray, M.; La Ferla, B.; Nicotra,

F.; Scheper, W.; Flores, O.; Masserini, M.; Andrieux, K.; Couvreur, P., Versatile and efficient targeting using a single nanoparticulate platform: Application to cancer and Alzheimer's disease. *ACS Nano* **2012,** *6* (7), 5866-5879; (b) Brambilla, D.; Verpillot, R.; Taverna, M.; De Kimpe, L.; Le Droumaguet, B.; Nicolas, J.; Canovi, M.; Gobbi, M.; Mantegazza, F.; Salmona, M.; Nicolas, V.; Scheper, W.; Couvreur, P.; Andrieux, K., New method based on capillary electrophoresis with laser-induced fluorescence detection (CE-LIF) to monitor interaction between nanoparticles and the amyloid-beta peptide. *Anal. Chem.* **2010,** *82* (24), 10083-10089; (c) Cabaleiro-Lago, C.; Quinlan-Pluck, F.; Lynch, I.; Lindman, S.; Minogue, A. M.; Thulin, E.; Walsh, D. M.; Dawson, K. A.; Linse, S., Inhibition of amyloid beta protein fibrillation by polymeric nanoparticles. *J. Am. Chem. Soc.* **2008,** *130* (46), 15437-15443.

49. (a) Li, M.; Yang, X.; Ren, J.; Qu, K.; Qu, X., Using graphene oxide high near-infrared absorbance for photothermal treatment of Alzheimer's disease. *Adv. Mater.* **2012,** *24* (13), 1722-1728; (b) Mahmoudi, M.; Akhavan, O.; Ghavami, M.; Rezaee, F.; Ghiasi, S. M. A., Graphene oxide strongly inhibits amyloid beta fibrillation. *Nanoscale* **2012,** *4* (23), 7322-7325.

50. (a) Kim, J. E.; Lee, M., Fullerene inhibits beta-amyloid peptide aggregation. *Biochem. Biophys. Res. Commun.* **2003,** *303* (2), 576-579; (b) Huang, H. M.; Ou, H. C.; Hsieh, S. J.; Chiang, L. Y., Blockage of amyloid beta peptide-induced cytosolic free calcium by fullerenol-1, carboxylate C60 in PC12 cells. *Life Sci.* **2000,** *66* (16), 1525-1533; (c) Lee, C.-M.; Huang, S.-T.; Huang, S.-H.; Lin, H.-W.; Tsai, H.-P.; Wu, J.-Y.; Lin, C.-M.; Chen, C.-T., C-60 fullerene-pentoxifylline dyad nanoparticles enhance autophagy to avoid cytotoxic effects caused by the beta-amyloid peptide. *Nanomed-Nanotechnol* **2011,** *7* (1), 107-114; (d) Bobylev, A. G.; Kornev, A. B.; Bobyleva, L. G.; Shpagina, M. D.; Fadeeva, I. S.; Fadeev, R. S.; Deryabin, D. G.; Balzarini, J.; Troshin, P. A.; Podlubnaya, Z. A., Fullerenolates: Metallated polyhydroxylated fullerenes with potent anti-amyloid activity. *Org. Biomol. Chem.* **2011,** *9* (16), 5714-5719.

51. (a) Fu, Z.; Luo, Y.; Derreumaux, P.; Wei, G., Induced beta-barrel formation of the Alzheimer's A beta 25-35 oligomers on carbon nanotube surfaces: Implication for amyloid fibril inhibition. *Biophys. J.* **2009,** *97* (6), 1795-1803; (b) Li, H.; Luo, Y.; Derreumaux, P.; Wei, G., Carbon nanotube inhibits the formation of beta-sheet-rich oligomers of the Alzheimer's amyloid-beta (16-22) peptide. *Biophys. J.* **2011,** *101* (9), 2267-2276; (c) de la Fuente, E.; Adura, C.; Kogan, M. J.; Bollo, S., Carbon nanotubes electrochemistry allows the in situ evaluation of the effect of SS-sheet breakers on the aggregation process of SS-amyloid. *Electroanalysis* **2012,** *24* (4), 938-944.

52. Patel, D. A.; Henry, J. E.; Good, T. A., Attenuation of beta-amyloid-induced toxicity by sialic-acid-conjugated dendrimers: Role of sialic acid attachment. *Brain Res.* **2007** *1161*, 95-105.

53. (a) Shinohara, Y.; Hasegawa, Y.; Kaku, H.; Shibuya, N., Elucidation of the mechanism enhancing the avidity of lectin with oligosaccharides on the solid phase surface. *Glycobiology* **1997,** *7* (8), 1201-1208; (b) Matsubara, T.; Iijima, K.; Nakamura, M.; Taki, T.; Okahata, Y.; Sato, T., Specific binding of GM1-binding peptides to high-density GM1 in lipid membranes.

Langmuir **2006,** *23* (2), 708-714; (c) Kuno, A.; Uchiyama, N.; Koseki-Kuno, S.; Ebe, Y.; Takashima, S.; Yamada, M.; Hirabayashi, J., Evanescent-field fluorescence-assisted lectin microarray: A new strategy for glycan profiling. *Nat. Meth.* **2005,** *2* (11), 851-856.

54. Beier, H. T.; Cowan, C. B.; Chou, I. H.; Pallikal, J.; Henry, J. E.; Benford, M. E.; Jackson, J. B.; Good, T. A.; Cote, G. L., Application of surface-enhanced raman spectroscopy for detection of beta amyloid using nanoshells. *Plasmonics* **2007,** *2* (2), 55-64.

55. (a) Fleischm.M; Hendra, P. J.; McQuilla.Aj, Raman-spectra from electrode surfaces. *J. Chem. Soc., Chem. Commun.* **1973,** (3), 80-81; (b) Baker, G. A.; Moore, D. S., Progress in plasmonic engineering of surface-enhanced Raman-scattering substrates toward ultra-trace analysis. *Anal. Bioanal. Chem.* **2005,** *382* (8), 1751-1770; (c) Kneipp, K.; Kneipp, H.; Itzkan, I.; Dasari, R. R.; Feld, M. S., Surface-enhanced Raman scattering and biophysics. *J. Phys.:Condens. Matter* **2002,** *14* (18), R597-R624.

56. Chikae, M.; Fukuda, T.; Kerman, K.; Idegami, K.; Miura, Y.; Tamiya, E., Amyloid-β detection with saccharide immobilized gold nanoparticle on carbon electrode. *Bioelectrochemistry* **2008,** *74*, 118-123.

57. Kakio, A.; Nishimoto, S.; Yanagisawa, K.; Kozutsumi, Y.; Matsuzaki, K., Interactions of amyloid beta-protein with various gangliosides in raft-like membranes: Importance of GM1 ganglioside-bound form as an endogenous seed for Alzheimer amyloid. *Biochemistry* **2002,** *41* (23), 7385-7390.

58. (a) Upadhyaya, L.; Singh, J.; Agarwal, V.; Tewari, R. P., Biomedical applications of carboxymethyl chitosans. *Carbohydr. Polym.* **2013,** *91* (1), 452-466; (b) Shi, S.-F.; Jia, J.-F.; Guo, X.-K.; Zhao, Y.-P.; Chen, D.-S.; Guo, Y.-Y.; Cheng, T.; Zhang, X.-L., Biocompatibility of chitosan-coated iron oxide nanoparticles with osteoblast cells. *Int. J. Nanomed.* **2012,** *7*, 5593-5602.

59. (a) Minati, L.; Grisoli, M.; Bruzzone, M. G., MR spectroscopy, functional MRI, and diffusion-tensor imaging in the aging brain: A conceptual review. *J. Geriatr. Psych. Neur.* **2007,** *20* (1), 3-21; (b) Lehericy, S.; Marjanska, M.; Mesrob, L.; Sarazin, M.; Kinkingnehun, S., Magnetic resonance imaging of Alzheimer's disease. *Eur. Radiol.* **2007,** *17* (2), 347-362; (c) Sandson, T. A.; Oconnor, M.; Sperling, R. A.; Edelman, R. R.; Warach, S., Noninvasive perfusion MRI in Alzheimer's disease: A preliminary report. *Neurology* **1996,** *47* (5), 1339-1342; (d) Alsop, D. C.; Detre, J. A.; Grossman, M., Assessment of cerebral blood flow in Alzheimer's disease by spin-labeled magnetic resonance imaging. *Ann. Neurol.* **2000,** *47* (1), 93-100.

60. (a) De Santi, S.; de Leon, M. J.; Rusinek, H.; Convit, A.; Tarshish, C. Y.; Roche, A.; Tsui, W. H.; Kandil, E.; Boppana, M.; Daisley, K.; Wang, G. J.; Schlyer, D.; Fowler, J.,

Hippocampal formation glucose metabolism and volume losses in mci and AD. *Neurobiol. Aging* **2001,** *22* (4), 529-539; (b) Colloby, S. J.; Fenwick, J. D.; Williams, E. D.; Paling, S. M.; Lobotesis, K.; Ballard, C.; McKeith, I.; O'Brien, J. T., A comparison of Tc-99m-HAMPAO SPECT changes in dementia with lewy bodies and Alzheimer's disease using statistical parametric mapping. *Eur. J. Nucl. Med. Mol. Imaging* **2002,** *29* (5), 615-622; (c) Bonte, F. J.; Harris, T. S.; Roney, C. A.; Hynan, L. S., Differential diagnosis between Alzheimer's and frontotemporal disease by the posterior cingulate sign. *J. Nucl. Med.* **2004,** *45* (5), 771-774; (d) Caroli, A.; Testa, C.; Geroldi, C.; Nobili, F.; Barnden, L. R.; Guerra, U. P.; Bonetti, M.; Frisoni, G. B., Cerebral perfusion correlates of conversion to Alzheimer's disease in amnestic mild cognitive impairment. *J. Neurol.* **2007,** *254* (12), 1698-1707; (e) Mosconi, L.; Tsui, W. H.; De Santi, S.; Li, J.; Rusinek, H.; Convit, A.; Li, Y.; Boppana, M.; de Leon, M. J., Reduced hippocampal metabolism in mci and AD - automated FDG-PET image analysis. *Neurology* **2005,** *64* (11), 1860-1867.

61. Bitan, G.; Vollers, S. S.; Teplow, D. B., Elucidation of primary structure elements controlling early amyloid beta-protein oligomerization. *J. Biol. Chem.* **2003,** *278* (37), 34882-34889.

62. (a) Klunk, W. E.; Engler, H.; Nordberg, A.; Wang, Y. M.; Blomqvist, G.; Holt, D. P.; Bergstrom, M.; Savitcheva, I.; Huang, G. F.; Estrada, S.; Ausen, B.; Debnath, M. L.; Barletta, J.; Price, J. C.; Sandell, J.; Lopresti, B. J.; Wall, A.; Koivisto, P.; Antoni, G.; Mathis, C. A.; Langstrom, B., Imaging brain amyloid in Alzheimer's disease with pittsburgh compound-B. *Ann. Neurol.* **2004,** *55* (3), 306-319; (b) Vanbroeckhoven, C.; Haan, J.; Bakker, E.; Hardy, J. A.; Vanhul, W.; Wehnert, A.; Vegtervandervlis, M.; Roos, R. A. C., Amyloid-beta protein-precursor gene and hereditary cerebral-hemorrhage with amyloidosis (dutch). *Science* **1990,** *248* (4959), 1120-1122; (c) Shoghi-Jadid, K.; Small, G. W.; Agdeppa, E. D.; Kepe, V.; Ercoli, L. M.; Siddarth, P.; Read, S.; Satyamurthy, N.; Petric, A.; Huang, S. C.; Barrio, J. R., Localization of neurofibrillary tangles and beta-amyloid plaques in the brains of living patients with Alzheimer disease. *Am. J. Geriat. Psychiat.* **2002,** *10* (1), 24-35; (d) Rowe, C. C.; Ackerman, U.; Browne, W.; Mulligan, R.; Pike, K. L.; O'Keefe, G.; Tochon-Danguy, H.; Chan, G.; Berlangieri, S. U.; Jones, G.; Dickinson-Rowe, K. L.; Kung, H. P.; Zhang, W.; Kung, M. P.; Skovronsky, D.; Dyrks, T.; Hall, G.; Krause, S.; Friebe, M.; Lehman, L.; Lindemann, S.; Dinkelborg, L. M.; Masters, C. L.; Villemagne, V. L., Imaging of amyloid beta in Alzheimer's disease with F-18-BAY94-9172, a novel pet tracer: Proof of mechanism. *Lancet Neurol.* **2008,** *7* (2), 129-135; (e) Barthel, H.; Gertz, H.-J.; Dresel, S.; Peters, O.; Bartenstein, P.; Buerger, K.; Hiemeyer, F.; Wittemer-Rump, S. M.; Seibyl, J.; Reininger, C.; Sabri, O.; Florbetaben Study, G., Cerebral amyloid-beta PET with Florbetaben (F-18) in patients with Alzheimer's disease and healthy controls: A multicentre phase 2 diagnostic study. *Lancet Neurol.* **2011,** *10* (5), 424-435; (f) Villemagne, V. L.; Ong, K.; Mulligan, R. S.; Holl, G.; Pejoska, S.; Jones, G.; O'Keefe, G.; Ackerman, U.; Tochon-Danguy, H.; Chan, J. G.; Reininger, C. B.; Fels, L.; Putz, B.; Rohde, B.; Masters, C. L.; Rowe, C. C., Amyloid imaging with F-18-florbetaben in Alzheimer disease and other dementias. *J. Nucl. Med.* **2011,** *52* (8), 1210-1217; (g) Wong, D. F.; Rosenberg, P. B.; Zhou, Y.; Kumar, A.; Raymont, V.; Ravert, H. T.; Dannals, R. F.; Nandi, A.; Brasic, J. R.; Ye, W.; Hilton, J.; Lyketsos, C.; Kung, H. F.; Joshi, A. D.; Skovronsky, D. M.; Pontecorvo, M. J., In vivo imaging of amyloid deposition in Alzheimer disease using the radioligand F-18-AV-45

(Flobetapir F 18). *J. Nucl. Med.* **2010,** *51* (6), 913-920; (h) Clark, C. M.; Schneider, J. A.; Bedell, B. J.; Beach, T. G.; Bilker, W. B.; Mintun, M. A.; Pontecorvo, M. J.; Hefti, F.; Carpenter, A. P.; Flitter, M. L.; Krautkramer, M. J.; Kung, H. F.; Coleman, R. E.; Doraiswamy, P. M.; Fleisher, A. S.; Sabbagh, M. N.; Sadowsky, C. H.; Reiman, P. E. M.; Zehntner, S. P.; Skovronsky, D. M.; Grp, A. A. S., Use of Florbetapir-PET for imaging beta-amyloid pathology. *Jama-J. Am. Med. Assoc.* **2011,** *305* (3), 275-283.

63. (a) Siegemund, T.; Paulke, B. R.; Schmiedel, H.; Bordag, N.; Hoffmann, A.; Harkany, T.; Tanila, H.; Kacza, J.; Hartig, W., Thioflavins released from nanoparticles target fibrillar amyloid beta in the hippocampus of APP/PS1 transgenic mice. *Int. J. Dev. Neurosci.* **2006,** *24* (2-3), 195-201; (b) Poduslo, J. F.; Wengenack, T. M.; Curran, G. L.; Wisniewski, T.; Sigurdsson, E. M.; Macura, S. I.; Borowski, B. J.; Jack, C. R., Molecular targeting of Alzheimer's amyloid plaques for contrast-enhanced magnetic resonance imaging. *Neurobiol. Dis.* **2002,** *11* (2), 315-329; (c) Wadghiri, Y. Z.; Sigurdsson, E. M.; Sadowski, M.; Elliott, J. I.; Li, Y. S.; Scholtzova, H.; Tang, C. Y.; Aguinaldo, G.; Pappolla, M.; Duff, K.; Wisniewski, T.; Turnbull, D. H., Detection of Alzheimer's amyloid in transgenic mice using magnetic resonance microimaging. *Magnet. Reson. Med.* **2003,** *50* (2), 293-302; (d) Petiet, A.; Santina, M.; Bertrand, A.; Wiggins, C. J.; Petit, F.; Houitte, D.; Hantraye, P.; Benavides, J.; Debeir, T.; Rooney, T.; Dhenain, M., Gadolinium-staining reveals amyloid plaques in the brain of Alzheimer's transgenic mice. *Neurobiol. Aging* **2012,** *33*, 1533-1544; (e) Higuchi, M.; Iwata, N.; Matsuba, Y.; Sato, K.; Sasamoto, K.; Saido, T. C., ^{19}F and ^{1}H MRI detection of amyloid beta plaques in vivo. *Nat. Neurosci.* **2005,** *8* (4), 527-533.

64. Hintersteiner, M.; Enz, A.; Frey, P.; Jaton, A.-L.; Kinzy, W.; Kneuer, R.; Neumann, U.; Rudin, M.; Staufenbiel, M.; Stoeckli, M.; Wiederhold, K.-H.; Gremlich, H.-U., In vivo detection of amyloid-β deposits by near-infrared imaging using an oxazine-derivative probe. *Nat. Biotechnol.* **2005,** *23*, 577-583.

65. (a) Di Domizio, J.; Zhang, R.; Stagg, L. J.; Gagea, M.; Zhuo, M.; Ladbury, J. E.; Cao, W., Binding with nucleic acids or glycosaminoglycans converts soluble protein oligomers to amyloid. *J. Biol. Chem.* **2012,** *287*, 736-747; (b) Braun, S.; Humphreys, C.; Fraser, E.; Brancale, A.; Bochtler, M.; Dale, T. C., Amyloid-associated nucleic acid hybridisation. *Plos One* **2011,** *6*, e19125.

66. (a) Ariga, T.; Yu, R. K., GM1 inhibits amyloid beta-protein-induced cytokine release. *Neurochem. Res.* **1999,** *24* (2), 219-226; (b) Wakabayashi, M.; Okada, T.; Kozutsumi, Y.; Matsuzaki, K., GM1 ganglioside-mediated accumulation of amyloid beta-protein on cell membranes. *Biochem. Bioph. Res. Co.* **2005,** *328*, 1019-1023.

67. Williamson, M. P.; Suzuki, Y.; Bourne, N. T.; Asakura, T., Binding of amyloid beta-peptide to ganglioside micelles is dependent on Histidine-13. *Biochem. J.* **2006,** *397*, 483-490.

68. (a) Kakio, A.; Nishimoto, S.; Yanagisawa, K.; Kozutsumi, Y.; Matsuzaki, K., Cholesterol-dependent formation of GM1 ganglioside-bound amyloid beta-protein, an endogenous seed for Alzheimer amyloid. *J. Biol. Chem.* **2001,** *276* (27), 24985-24990; (b) Patel, D.; Henry, J.; Good, T., Attenuation of beta-amyloid induced toxicity by sialic acid-conjugated dendrimeric polymers. *BBA-Gen. Subjects* **2006,** *1760* (12), 1802-1809; (c) Patel, D. A.; Henry, J. E.; Good, T. A., Attenuation of beta-amyloid-induced toxicity by sialic-acid-conjugated dendrimers: Role of sialic acid attachment. *Brain Res.* **2007,** *1161*, 95-105.

69. (a) Barnham, K. J.; Kenche, V. B.; Ciccotosto, G. D.; Smith, D. P.; Tew, D. J.; Liu, X.; Perez, K.; Cranston, G. A.; Johanssen, T. J.; Volitakis, I.; Bush, A. I.; Masters, C. L.; White, A. R.; Smith, J. P.; Cherny, R. A.; Cappai, R., Platinum-based inhibitors of amyloid-beta as therapeutic agents for Alzheimer's disease. *P. Natl. Acad. Sci. U.S.A.* **2008,** *105* (19), 6813-6818; (b) Kim, J. E.; Lee, M., Fullerene inhibits beta-amyloid peptide aggregation. *Biochem. Bioph. Res. Co.* **2003,** *303* (2), 576-579; (c) Ikeda, K.; Okada, T.; Sawada, S.-i.; Akiyoshi, K.; Matsuzaki, K., Inhibition of the formation of amyloid beta-protein fibrils using biocompatible nanogels as artificial chaperones. *FEBS Lett.* **2006,** *580* (28-29), 6587-6595; (d) Geng, J.; Li, M.; Ren, J.; Wang, E.; Qu, X., Polyoxometalates as inhibitors of the aggregation of amyloid beta peptides associated with Alzheimer's disease. *Angew. Chem. Int. Ed.* **2011,** *50* (18), 4184-4188; (e) Saraiva, A. M.; Cardoso, I.; Carmo Pereira, M.; Coelho, M. A. N.; Joao Saraiva, M.; Moehwald, H.; Brezesinski, G., Controlling amyloid-beta peptide(1-42) oligomerization and toxicity by fluorinated nanoparticles. *ChemBioChem* **2010,** *11* (13), 1905-1913; (f) Zhang, D.; Neumann, O.; Wang, H.; Yuwono, V. M.; Barhoumi, A.; Perham, M.; Hartgerink, J. D.; Wittung-Stafshede, P.; Halas, N. J., Gold nanoparticles can induce the formation of protein-based aggregates at physiological pH. *Nano Lett.* **2009,** *9* (2), 666-671; (g) Rocha, S.; Thueneman, A. F.; Pereira, M. d. C.; Coelho, M.; Moehwald, H.; Brezesinski, G., Influence of fluorinated and hydrogenated nanoparticles on the structure and fibrillogenesis of amyloid beta-peptide. *Biophys. Chem.* **2008,** *137* (1), 35-42; (h) Bieschke, J.; Herbst, M.; Wiglenda, T.; Friedrich, R. P.; Boeddrich, A.; Schiele, F.; Kleckers, D.; del Amo, J. M. L.; Gruening, B. A.; Wang, Q.; Schmidt, M. R.; Lurz, R.; Anwyl, R.; Schnoegl, S.; Faendrich, M.; Frank, R. F.; Reif, B.; Guenther, S.; Walsh, D. M.; Wanker, E. E., Small-molecule conversion of toxic oligomers to nontoxic beta-sheet-rich amyloid fibrils. *Nat. Chem. Biol.* **2012,** *8* (1), 93-101; (i) Wu, W.-h.; Sun, X.; Yu, Y.-p.; Hu, J.; Zhao, L.; Liu, Q.; Zhao, Y.-f.; Li, Y.-m., TiO_2 nanoparticles promote beta-amyloid fibrillation in vitro. *Biochem. Bioph. Res. Co.* **2008,** *373* (2), 315-318; (j) Brambilla, D.; Verpillot, R.; Le Droumaguet, B.; Nicolas, J.; Taverna, M.; Kóňa, J.; Lettiero, B.; Hashemi, S. H.; De Kimpe, L.; Canovi, M.; Gobbi, M.; Nicolas, V.; Scheper, W.; Moghimi, S. M.; Tvaroška, I.; Couvreur, P.; Andrieux, K., Pegylated nanoparticles bind to and alter amyloid-beta peptide conformation: Toward engineering of functional nanomedicines for Alzheimer's disease. *ACS Nano* **2012,** *6*, 5897-5908.

70. (a) Palmacci, S.; Josephson, L.; Groman, E. Synthesis of polysaccharide covered superparamagnetic oxide colloids. 1995; (b) El-Dakdouki, M. H.; Zhu, D. C.; El-boubbou, K.; Kamat, M.; Chen, J.; Li, W.; Huang, X., Development of multifunctional hyaluronan-coated nanoparticles for imaging and drug delivery to cancer cells. *Biomacromolecules* **2012,** *13*, 1144-1151; (c) Kamat, M.; El-boubbou, K.; Zhu, D.; Lansdell, T.; Lu, X.; Li, W.; Huang, X.,

Hyaluronic acid immobilized magnetic nanoparticles for active targeting and imaging of macrophages. *Bioconjugate Chem.* **2010,** *21*, 2128-2135.

71. (a) El-Boubbou, K.; Zhu, D. C.; Vasileiou, C.; Borhan, B.; Prosperi, D.; Li, W.; Huang, X., Magnetic glyco-nanoparticles: A tool to detect, differentiate, and unlock the glyco-codes of cancer via magnetic resonance imaging. *J. Am. Chem. Soc.* **2010,** *132* (12), 4490-4499; (b) Wang, Y.; El-Boubbou, K.; Kouyoumdjian, H.; Sun, B.; Huang, X.; Zeng, X., Lipoic acid glyco-conjugates, a new class of agents for controlling nonspecific adsorption of blood serum at biointerfaces for biosensor and biomedical applications. *Langmuir* **2010,** *26*, 4119-4125.

72. Roher, A. E.; Lowenson, J. D.; Clarke, S.; Woods, A. S.; Cotter, R. J.; Gowing, E.; Ball, M. J., Beta-amyloid-(1-42) is a major component of cerebrovascular amyloid deposits: Implications for the pathology of Alzheimer disease. *Proc. Natl. Acad. Sci. U S A.* **1993,** *90* (22), 10836-10840.

73. (a) García-Matas, S.; de Vera, N.; Aznar, A. O.; Marimon, J. M.; Adell, A.; Planas, A. M.; Cristòfol, R.; Sanfeliu, C., In vitro and in vivo activation of astrocytes by amyloid-beta is potentiated by pro-oxidant agents. *J. Alzheimers Dis.* **2010,** *20*, 229-245; (b) Allaman, I.; Gavillet, M.; Bélanger, M.; Laroche, T.; Viertl, D.; Lashuel, H. A.; Magistretti, P. J., Amyloid-beta aggregates cause alterations of astrocytic metabolic phenotype: Impact on neuronal viability. *J. Neurosci.* **2010,** *30*, 3326-3338.

74. LeVine, H., Quantification of β-sheet amyloid fibril structures with Thioflavin T. *Meth. Enzymol.* **1999,** *309*, 274-284.

75. Khurana, R.; Coleman, C.; Ionescu-Zanetti, C.; Carter, S. A.; Krishna, V.; Grover, R. K.; Roy, R.; Singh, S., Mechanism of Thioflavin T binding to amyloid fibrils. *J. Struct. Biol.* **2005,** *151*, 229-238.

76. Moores, B.; Drolle, E.; Attwood, S. J.; Simons, J.; Leonenko, Z., Effect of surfaces on amyloid fibril formation. *PLoS One* **2011,** *6*, e25954.

77. (a) Inbar, P.; Bautista, M. R.; Takayama, S. A.; Yang, J., Assay to screen for molecules that associate with Alzheimer's related beta-amyloid fibrils. *Anal. Chem.* **2008,** *80* (9), 3502-3506; (b) Inbar, P.; Yang, J., Inhibiting protein-amyloid interactions with small molecules: A surface chemistry approach. *Bioorg. Med. Chem. Lett.* **2006,** *16* (4), 1076-1079; (c) Inbar, P.; Li, C. Q.; Takayama, S. A.; Bautista, M. R.; Yang, J., Oligo(ethylene glycol) derivatives of Thioflavin T as inhibitors of protein-amyloid interactions. *ChemBioChem* **2006,** *7* (10), 1563-1566.

78. Bohrmann, B.; Tjernberg, L.; Kuner, P.; Poli, S.; Levet-Trafit, B.; Naslund, J.; Richards, G.; Huber, W.; Dobeli, H.; Nordstedt, C., Endogenous proteins controlling amyloid beta-peptide polymerization - possible implications for beta-amyloid formation in the central nervous system and in peripheral tissues. *J. Biol. Chem.* **1999,** *274* (23), 15990-15995.

79. (a) Jun, Y. W.; Lee, J. H.; Cheon, J., Chemical design of nanoparticle probes for high-performance magnetic resonance imaging. *Angew. Chem. Int. Ed.* **2008,** *47*, 5122-5135; (b) Na, H. B.; Song, I. C.; Hyeon, T., Inorganic nanoparticles for MRI contrast agents. *Adv. Mater.* **2009,** *21*, 2133-2148.

80. (a) Roch, A.; Gossuin, Y.; Muller, R. N.; Gillis, P., Superparamagnetic colloid suspensions: Water magnetic relaxation and clustering. *J. Magn. Magn. Mater.* **2005,** *293* (1), 532-539; (b) Yung, K. T., Empirical models of transverse relaxation for spherical magnetic perturbers. *Magn. Reson. Imaging* **2003,** *21* (5), 451-463; (c) Lee, H.; Sun, E.; Ham, D.; Weissleder, R., CHIP-NMR biosensor for detection and molecular analysis of cells. *Nat. Med.* **2008,** *14* (8), 869-874; (d) Koh, I.; Hong, R.; Weissleder, R.; Josephson, L., Sensitive nmr sensors detect antibodies to influenza. *Angew. Chem. Int. Ed.* **2008,** *47* (22), 4119-4121.

81. (a) Bravo, R.; Arimon, M.; Valle-Delgado, J. J.; García, R.; Durany, N.; Castel, S.; Cruz, M.; Ventura, S.; Fernàndez-Busquets, X., Sulfated polysaccharides promote the assembly of amyloid beta(1-42) peptide into stable fibrils of reduced cytotoxicity. *J. Biol. Chem.* **2008,** *283*, 32471-32483; (b) Teplow, D. B., *Methods enzymol*. 2006; Vol. 413, p 20-33; (c) Bitan, G.; Vollers, S. S.; Teplow, D. B., Elucidation of primary structure elements controlling early amyloid beta-protein oligomerization. *J. Biol. Chem.* **2003,** *278* (37), 34882-34889; (d) Bitan, G.; Teplow, D. B., Preparation of aggregate-free, low molecular weight amyloid-beta for assembly and toxicity assays. *Methods Mol. Biol.* **2005,** *299*, 3-9; (e) Klein, W. L.; Krafft, G. A.; Finch, C. E., Targeting small abeta oligomers: The solution to an Alzheimer's disease conundrum? *Trends Neurosci.* **2001,** *24*, 219-224.

82. Temsamani, J.; Vidal, P., The use of cell-penetrating peptides for drug delivery. *Drug. Discov. Today* **2004,** *9*, 1012-1019.

83. Silva, G. A., Nanotechnology approaches to crossing the blood-brain barrier and drug delivery to the cns. *BMC Neurosci.* **2008,** *9(Suppl 3)*, S4.

84. Abbott, N. J.; Ronnback, L.; Hansson, E., Astrocyte-endothelial interactions at the blood-brain barrier. *Nat. Rev. Neurosci.* **2006,** *7* (1), 41-53.

85. Pardridge, W. M., Blood-brain barrier drug targeting: The future of brain drug development. *Mol. Interventions* **2003,** *3* (2), 90-51.

86. (a) Farokhzad, O. C.; Langer, R., Nanomedicine: Developing smarter therapeutic and diagnostic modalities. *Advanced Drug Delivery Reviews* **2006,** *58* (14), 1456-1459; (b) Veiseh, O.; Gunn, J. W.; Zhang, M., Design and fabrication of magnetic nanoparticles for targeted drug delivery and imaging. *Adv. Drug Delivery Rev.* **2010,** *62* (3), 284-304.

87. Pang, Z.; Gao, H.; Chen, J.; Shen, S.; Zhang, B.; Ren, J.; Guo, L.; Qian, Y.; Jiang, X.; Mei, H., Intracellular delivery mechanism and brain delivery kinetics of biodegradable cationic bovine serum albumin-conjugated polymersomes. *Int. J. Nanomed.* **2012,** *7*, 3421-3432.

88. (a) Qiao, R.; Yang, C.; Gao, M., Superparamagnetic iron oxide nanoparticles: From preparations to in vivo MRI applications. *J. Mater.Chem.* **2009,** *19* (35), 6274-6293; (b) Cheon, J.; Lee, J.-H., Synergistically integrated nanoparticles as multimodal probes for nanobiotechnology. *Acc. Chem. Res.* **2008,** *41* (12), 1630-1640; (c) Sun, C.; Lee, J. S. H.; Zhang, M., Magnetic nanoparticles in MR imaging and drug delivery. *Adv. Drug Delivery Rev.* **2008,** *60* (11), 1252-1265.

89. Kreuter, J.; Hekmatara, T.; Dreis, S.; Vogel, T.; Gelperina, S.; Langer, K., Covalent attachment of apolipoprotein A-i and apolipoprotein B-100 to albumin nanoparticles enables drug transport into the brain. *J. Controlled Release* **2007,** *118* (1), 54-58.

90. Gan, C. W.; Feng, S.-S., Transferrin-conjugated nanoparticles of poly(lactide)-d-alpha-tocopheryl polyethylene glycol succinate diblock copolymer for targeted drug delivery across the blood-brain barrier. *Biomaterials* **2010,** *31* (30), 7748-7757.

91. Ke, W.; Shao, K.; Huang, R.; Han, L.; Liu, Y.; Li, J.; Kuang, Y.; Ye, L.; Lou, J.; Jiang, C., Gene delivery targeted to the brain using an angiopep-conjugated polyethyleneglycol-modified polyamidoamine dendrimer. *Biomaterials* **2009,** *30* (36), 6976-6985.

92. Yim, Y. S.; Choi, J.-s.; Kim, G. T.; Kim, C. H.; Shin, T.-H.; Kim, D. G.; Cheon, J., A facile approach for the delivery of inorganic nanoparticles into the brain by passing through the blood-brain barrier (BBB). *Chem. Commun.* **2012,** *48* (1), 61-63.

93. Veiseh, O.; Sun, C.; Fang, C.; Bhattarai, N.; Gunn, J.; Kievit, F.; Du, K.; Pullar, B.; Lee, D.; Ellenbogen, R. G.; Olson, J.; Zhang, M., Specific targeting of brain tumors with an optical/magnetic resonance imaging nanoprobe across the blood-brain barrier. *Cancer Res.* **2009,** *69* (15), 6200-6207.

94. Ariga, T.; Yu, R. K., GM1 inhibits amyloid beta-protein-induced cytokine release. *Neurochem. Res.* **1999,** *24* (2), 219-226.

95. Kumagai, A. K.; Eisenberg, J. B.; Pardridge, W. M., Absorptive-mediated endocytosis of cationized albumin and a beta-endorphin-cationized albumin chimeric peptide by isolated brain capillaries. Model system of blood-brain barrier transport. *J. Biol. Chem.* **1987,** *262* (31), 15214-9.

96. Li, S.-D.; Huang, L., Pharmacokinetics and biodistribution of nanoparticles. *Molecular Pharmaceutics* **2008,** *5* (4), 496-504.

97. Alexis, F.; Pridgen, E.; Molnar, L. K.; Farokhzad, O. C., Factors affecting the clearance and biodistribution of polymeric nanoparticles. *Mol. Pharm.* **2008,** *5* (4), 505-515.

98. (a) Huwyler, J.; Wu, D. F.; Pardridge, W. M., Brain drug delivery of small molecules using immunoliposomes. *Proc. Natl. Acad. Sci. U. S. A.* **1996,** *93* (24), 14164-14169; (b) Massignani, M.; LoPresti, C.; Blanazs, A.; Madsen, J.; Armes, S. P.; Lewis, A. L.; Battaglia, G., Controlling cellular uptake by surface chemistry, size, and surface topology at the nanoscale. *Small* **2009,** *5* (21), 2424-2432.

99. Kumagai, A. K.; Eisenberg, J. B.; Pardridge, W. M., Absorptive-mediated endocytosis of cationized albumin and A beta-endorphin-cationized albumin chimeric peptide by isolated brain capillaries - model system of blood-brain-barrier transport. *J. Biol. Chem.* **1987,** *262* (31), 15214-15219.

100. Kellner, V.; Menkes-Caspi, N.; Beker, S.; Stern, E. A., Amyloid-beta alters ongoing neuronal activity and excitability in the frontal cortex. *Neurobiol. Aging* **2014,** *35* (9), 1982-91.

101. (a) Zhang, S.; Li, J.; Lykotrafitis, G.; Bao, G.; Suresh, S., Size-dependent endocytosis of nanoparticles. *Adv. Mater.* **2009,** *21* (4), 419-424; (b) Bareford, L. M.; Swaan, P. W., Endocytic mechanisms for targeted drug delivery. *Adv. Drug Delivery Rev.* **2007,** *59* (8), 748-758.

102. (a) Jiang, X.; Röcker, C.; Hafner, M.; Brandholt, S.; Dörlich, R. M.; Nienhaus, G. U., Endo- and exocytosis of zwitterionic quantum dot nanoparticles by live Hela cells. *ACS Nano* **2010,** *4* (11), 6787-6797; (b) Qiao, R.; Jia, Q.; Hüwel, S.; Xia, R.; Liu, T.; Gao, F.; Galla, H.-J.; Gao, M., Receptor-mediated delivery of magnetic nanoparticles across the blood–brain barrier. *ACS Nano* **2012,** *6* (4), 3304-3310; (c) Lu, W.; Xiong, C.; Zhang, R.; Shi, L.; Huang, M.; Zhang, G.; Song, S.; Huang, Q.; Liu, G.-y.; Li, C., Receptor-mediated transcytosis: A mechanism for active extravascular transport of nanoparticles in solid tumors. *J. Controlled Release* **2012,** *161* (3), 959-966; (d) Nam, J.; Won, N.; Jin, H.; Chung, H.; Kim, S., pH-induced aggregation of gold nanoparticles for photothermal cancer therapy. *J. Am. Chem. Soc.* **2009,** *131* (38), 13639-13645.

103. Nicolazzo, J. A.; Charman, S. A.; Charman, W. N., Methods to assess drug permeability across the blood-brain barrier. *J. Pharm. Pharmacol.* **2006,** *58* (3), 281-293.

104. Brown, R. C.; Morris, A. P.; O'Neil, R. G., Tight junction protein expression and barrier properties of immortalized mouse brain microvessel endothelial cells. *Brain Res.* **2007,** *1130* (0), 17-30.

105. Omidi, Y.; Campbell, L.; Barar, J.; Connell, D.; Akhtar, S.; Gumbleton, M., Evaluation of the immortalised mouse brain capillary endothelial cell line, b.End3, as an in vitro blood–brain barrier model for drug uptake and transport studies. *Brain Res.* **2003,** *990* (1–2), 95-112.

106. Koto, T.; Takubo, K.; Ishida, S.; Shinoda, H.; Inoue, M.; Tsubota, K.; Okada, Y.; Ikeda, E., Hypoxia disrupts the barrier function of neural blood vessels through changes in the expression of claudin-5 in endothelial cells. *Am. J. Pathol.* **2007,** *170* (4), 1389-1397.

107. Wang, Y.; El-Boubbou, K.; Kouyoumdjian, H.; Sun, B.; Huang, X.; Zeng, X., Lipoic acid glyco-conjugates, a new class of agents for controlling nonspecific adsorption of blood serum at biointerfaces for biosensor and biomedical applications. *Langmuir* **2010,** *26* (6), 4119-4125.

108. (a) Aminoff, D., Methods for the quantitative estimation of N-acetylneuraminic acid and their application to hydrolysates of sialomucoids. *Biochem. J.* **1961,** *81*, 384-392; (b) Santos-Lopez, G.; Flores, E.; Banos, R.; Herrera-Camacho, I.; Reyes-Leyva, J., Purification of the Porcine Rubulavirus attachment protein by liquid isoelectric focusing. *Protein Expression Purif.* **2004,** *35*, 120-125.